TEKST NR 358 1998

Modeling of Feedback Mechanisms which Control the Heart Function in a View to an Implementation in Cardiovascular Models

Ph.D. Thesis

by

Michael Danielsen

TEKSTER fra

IMFUFA ROSKILDE UNIVERSITETSCENTER
INSTITUT FOR STUDIET AF MATEMATIK OG FYSIK SAMT DERES FUNKTIONER I UNDERVISNING, FORSKNING OG ANVENDELSER

IMFUFA, Roskilde University, P.O.Box 260, 4000 Roskilde, Denmarl

Modeling of Feedback Mechanisms which Control the Heart Function in a View to an Implementation in Cardiovascular Models

Ph.D. Thesis by: Michael Danielsen (2nd ed)

IMFUFA text nr. 358/98 145 pages ISSN 01066242

We study the interaction between heart and vasculature by coupling a model of isovolumic ventricular pressure to a description of the vasculature. This approach allows separation between ventricular and vascular properties. The key element is a model of the isovolumic ventricular pressure as function of time and volume contained based on the Frank mechanism. This model exhibits the principal features of the pumping heart. In particular, the results reduce Starling' law to the Frank mechanism. Termed the ejection effect, we identify two phenomena, deactivation and hyperactivation, during ejection. We interpret the ejection effect as alterations in the contractile properties of the ventricle attributable to muscle shortening during ejection. We relate the two phenomena to detachment of bonds and formation of new crossbridge bonds, respectively. The results suggest that ventricular ejection directly changes the underlying muscle contraction process and that the ventricle is influenced by alterations in vascular properties. Inertia of blood movement and vascular reflects cannot alone explain the ejection effect which apparently consists of a number of small effects.

Also, we establish a lumped pulsatile human circulation model in which the two ventricles are guided by a pair of time-varying elastance functions. In addition, we develop two models of the baroreceptor mechanism. In particular, we adopt the unified model which embodies all the known non-linear phenomena exhibited by the firing rate of the carotid sinus baroreceptors in one of the models. Both models discriminate between sympathetic and parasympathetic activity and offer regulation of heart rate, cardiac contractility, peripheral resistance, venous compliance and venous unstressed volume. Also, the models include different time delays to each of the regulations. The computed results of the first model during an 10 % acute hemorrhage, heart pacing and different pulsatile carotid sinus pressures are compared with corresponding experiments. The results of the second model are compared with an 10 % acute hemorrhage.

Preface

A fundamental requirement in mathematical modeling of physiology is the ability to reduce a complex environment into a tractable form which contains the essential properties of the system under study. I will try to adopt this as the guiding line in my modeling efforts in this dissertation which is comprised of two distinct parts. The first part contains my research efforts into the interaction between the left ventricle and the receiving arterial system. The second part has a practical goal and contains the development of a human circulation model and a mathematical description of the baroreceptor mechanism of the intact human.

My Ph.D. study has been carried out at the Department of Mathematics and Physics (IMFUFA), Roskilde University, at Math-Tech (a private company involved in mathematical modeling) and at the Department of Cardiothoracic and Vascular Surgery, Aarhus University Hospital. My Ph.D. study has been organized as an industrial Ph.D. which has been supported by the Academy of Technical Sciences and the three institutions mentioned above. The results of my Ph.D. studies will be or have been published in (Danielsen, 1996; Danielsen and Ottesen, 1997; Danielsen, Palladino and Noodergraaf, 1998).

I wish to express my gratitude to the following people. My advisors Professor Stig Andur Pedersen, Departments of Philosophy and Mathematics, Roskilde University, his continuing support and encouragement have been essential, President, Ph.D., Jesper Larsen, Math-Tech, and M.D., Ph.D. Erik Morre Pedersen, Department of Cardiothoracic and Vascular Surgery, Aarhus University Hospital. I would also give my thanks to Associate Professor Johnny T. Ottesen, Department of Mathematics and Physics, Roskilde University for his supervision and discussions during my Ph.D. study. My sincere thanks to Dr. Abraham Noordergraaf, Cardiovascular Studies Unit, University of Pennsylvania, for his guidance and encouragement. His has teached me cardiovascular research and his criticism of my work have been fundamental. I am also greatful for his improvements of the manuscript. I would also like to thank Joseph L. Palladino, Department of Engineering, Trinity College, for our discussions about the ventricular modeling, Heine Larsen, Math-Tech for computing support, the BioMath group at Roskilde University for many lively discussions and Padmanabhan Krishnaswamy for his

reading of the dissertation. Finally, my sincere thanks to my family and my best friends.

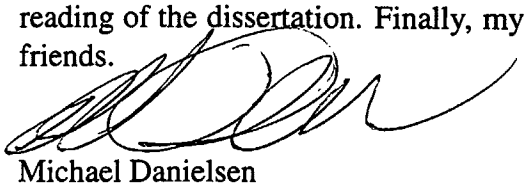

Michael Danielsen
Roskilde University, 13th July 1998

Contents

Chapter 1

Introduction

The historical fascination of the heart has lasted for many centuries and continues to attract considerable attention both theoretically and clinically. The first goal of our research is to obtain a better theoretical understanding of the physiological mechanisms involved in the interaction between the left ventricle and the receiving arterial system. A description of this interaction is not simple and involves not only the influence from the vasculature in terms of preload and afterload, but also the properties of the heart muscles and the neural and the hormonal influences.

Our approach is the following. We describe the ventricle and the arterial system independently and then the interaction between the two parts. The classical models of the left ventricle tend to lump this complex interaction such that the properties of the heart and of the arterial system are difficult to distinguish. The popular time-varying elastance concept is an explicit example of such a lumped approach.

The key element in our studies is an analytical description of the isovolumic ventricular pressure as a function of time and volume contained based on the Frank mechanism. This new mathematical model was established by (Mulier, 1994) and based on experiments in isolated dog hearts. The model gives an excellent description of the heart during isovolumic conditions. By allowing this model to eject we will examine carefully the interaction between the left ventricle and the arterial load and relate the events at the chamber level with those at the ultrastructural muscle level. During ejection, we will identify two phenomena, deactivation and hyperactivation, denoted the ejection effect. We interpret the ejection effect as alterations in the contractile properties of the ventricle attributable to muscle shortening. These two phenomena will be related to detachment of bonds and formation of new ones and cycling of crossbridge bonds, respectively. Furthermore, we will show that Starling's law is included in the new ventricular model and thus disqualify Starling's law as an independent law of the heart and merely state, that it follows from the Frank mechanism. This constitutes the first part of this research.

In the *second part* of the dissertation we shift the emphasis from basic physiological modeling to practical modeling aiming at the development of real time models. This project was initiated by the efforts to develop an anesthesia simulator of the intact human based on mathematical models. In addition to a physiologically founded model of the heart and the vasculature, it is essential for such a simulator to have a good model of the human short term pressure control represented by the baroreceptor mechanism. The human blood pressure control provides proper blood flow to the various organs of the human circulatory system. In essence, it promotes a normal distribution of fluids, hormones, electrolytes and other agents in the body. During influence of anesthesia, the nervous control of the baroreceptor mechanism may be unaffected, weaken or even absent[1]. In order to understand the behavior pattern during anesthesia, it is important to reduce the complexity to the normal situation. In fact, it is the normal situation we will consider in this study.

The second goal of this work is thus to develop a mathematical model of the baroreceptor mechanism and a model of the human circulatory system suitable for an anesthesia simulator. The strategy used to develop these models, consists of a reduction of the complexity of the physiological system down to the most simple view which still includes the principal properties necessary for solving the problems at hand.

In our model of the human cardiovascular system, the ventricular performance is specified by two time-varying elastance functions and the vasculature is described by lumped elements. The model generates root aortic pressure and ventricular outflow curves representative for the human as reported in the literature. The pressure and volume distribution and parameter values are based on literature data.

Two mathematical models of the baroreceptor mechanism will be proposed. The two models differ fundamentally in their description of the nervous activity. In the *first model*, the nervous activity will only be sensitive to the average arterial pressure. In contrast, the *second model* will adopt a thorough description of the firing rates of the carotid sinus receptors which includes all the known non-linear phenomena displayed by the firing rates. To our knowledge no previous model of the baroreceptor mechanism has included adaptation of the baroreceptors.

The description of the control on the human circulation is common to both models. The models offer a description of the sympathetic and the parasympathetic influence on the heart rate, the cardiac contractility, the peripheral resistance, the venous compliance and the venous unstressed volume. In addition, the model includes different time delays to each of the controls. The complex interaction between the baroreceptor mechanism and the human circulation will be

[1] Personal communications with different anesthesiologists.

illustrated during an acute hemorrhage, heart pacing and different pulsations of the carotid sinus pressure. The different controls in the baroreceptor mechanism are not equally important during an acute hemorrhage. In order to understand the impact exhibited by the controls we will carry out a sensitivity analysis by reducing the strength of the controls.

We divide the dissertation into two distinct parts. The first part contains our research into the interaction between the left ventricle and the arterial system. The second part describes our model of the human cardiovascular system and the two baroreceptor models.

Outline of the Dissertation

Chapter 1: Introduction. This chapter.

Part 1

The Interaction between the Left Ventricle and the Arterial Load

Chapter 2: The Pumping Heart. The chapter offers an overview of the basic physiology of the heart, both at the chamber level and at the muscle level. It introduces two main modeling principles in the mathematical description of the heart at the organ level along with a short critical historical review of earlier work. In addition, the chapter describes the goal of our research efforts into the interaction between the left ventricle and the arterial system.

Chapter 3: The Interaction between the Ventricle and the Arterial Load. The chapter describes the isovolumic ventricular model established by (Mulier, 1994) and identifies two ejection phenomena, deactivation and hyperactivation, which we define as the ejection effect. The chapter presents the first model of the ejection effect and shows that Starling's law is not a fundamental independent law of the ventricle.

Part 2

Modeling the Human Cardiovascular System and the Baroreceptor Mechanism with Reference to an Anesthesia Simulator

Chapter 4: A Cardiovascular Model. The chapter describes the human circulation model. It also offers an introduction to the basic physiology of the cardiovascular system and presents some of the different modeling approaches.

Chapter 5: The Baroreceptor Mechanism. The chapter gives an introduction to the physiology of the baroreceptor mechanism and a review of some of the recent and previous models of the baroreceptor mechanism and of the firing rates from the receptors. In addition, the chapter describes the goal of the modeling efforts into the baroreceptor mechanism.

Chapter 6: A Baroreceptor Model. The chapter establishes the two baroreceptor models. The chapter also describes the experimental open loop responses used to model the baroreceptor mechanism and presents the computed results from both models.

Chapter 7: Conclusion.

Appendix A: English Summary.

Appendix B: Dansk Resume. Summary in Danish.

Part I

Interaction between Left Ventricle and Arterial Load

Chapter 2

The Pumping Heart

In the ancient center of Mesopotamia (1600 BC) the heart was viewed as the place of intelligence (Noordergraaf, 1998). Others suggested that the heart is a respiratory organ. The contemporary view of the heart as a compression pump was advanced by William Harvey as late as in 1628. Until then, the commanding view was that of Galenos (Gladius Galenos, 131-201 AD). In his view, blood is produced in the liver and distributed by the veins. Some blood passes through invisible pores from the right to the left ventricle. Also, some blood is sucked into the right ventricle from which a part of it is carried to the left ventricle via the lungs. Blood in the left ventricle is sucked into the aorta (Acierno, 1994). The cardiovascular system as a circulatory system should also be credited to William Harvey who argued against the Galenic viewpoint. William Harvey's idea of the circulation arose before the capillaries were discovered by Malpighi in 1661 as the connection between arteries and veins. Thus the circulatory concept was not recognized by the Greeks and not contained in the famous Hippocrates of Corpus (460-370 BC) (Noordergraaf, 1998). The modern view of the heart, and its interaction with the surrounding environment, differs fundamentally from the ancient Mesopotamian and Egyptian view. Today the heart is considered as the only source of energy to the movement of the blood in the human circulatory system.

In addition to the brief summary of a very long history, this chapter will offer an overview of the basic physiology of the heart, both at the chamber level and at the muscle level. We will introduce two main modeling principles in the mathematical description of the heart at the organ level along with a short critical historical review of earlier work. Further historical details may be found in (Noordergraaf, 1978; Palladino, 1990; Acierno, 1994; Palladino, Mulier and Noordergraaf, 1998; Noordergraaf, 1998).

2.1 Physiology of the Heart

The function of the heart at the chamber level is the result of events in the muscle fibers or on an even lower hierarchic level. Muscle fibers receive energy from biochemical processes and develop force which manifests itself as increasing cavity pressure. This connection will become critical for the understanding of the following Chapter 3. Consideration of this relation may give impetus to the understanding of observations at the chamber level based on knowledge at the muscle level and vice versa. Therefore, we give an elementary introduction to the physiology of both the heart at the chamber level and at the muscle level in this section.

2.1.1 Physiology at Chamber Level

The heart consists of four chambers as shown in Figure 2.1. The left ventricle and left atrium constitute the two left chambers connected via the mitral valve which prevents flow into the atrium from the ventricle during normal conditions. The time course of a heart period can roughly be divided into an active and a relaxed phase. The heart is electrically activated causing ventricular muscles to contract. Consequently, ventricular pressure increases first isovolumically (i.e. non-ejecting), which ends when it equals arterial pressure and the aortic valve opens and blood flows into the arterial system. During *systole*, ventricular pressure rises and falls as dictated by muscle contraction and prevailing conditions in the vasculature. The aortic valve closes when ventricular pressure drops below arterial pressure and initiates the following isovolumical relaxation phase. When the ventricular pressure falls below the atrial pressure, the mitral valve opens and blood flows from the atrium into the ventricle. The maximum ventricular volume reached is the *end-diastolic volume* V_{ed}. This non-ejecting period is denoted *diastole*. The left atrium follows a similar track. The left atrium is filled from the pulmonary circulation during ventricular systole and supplies the ventricle actively with blood during ventricular diastole. The pumping heart repeats this course during each beat with a time period of approximately 0.8 s in resting humans. In Figure 2.2 we show ventricular pressure and flow curves, representative for a normal human left ventricle.

2.1.2 Muscle Physiology

The heart has a complex geometric structure with muscles lying in a complicated pattern which may be understood from the band concept recently introduced by (Guasp, 1980). The cardiac muscle itself consists of individual muscle fibers, or myocytes, which are the smallest functional units in the muscle structure. Each muscle fiber is approximately $40 - 100\mu$m long with a diameter of $10 - 20\mu$m.

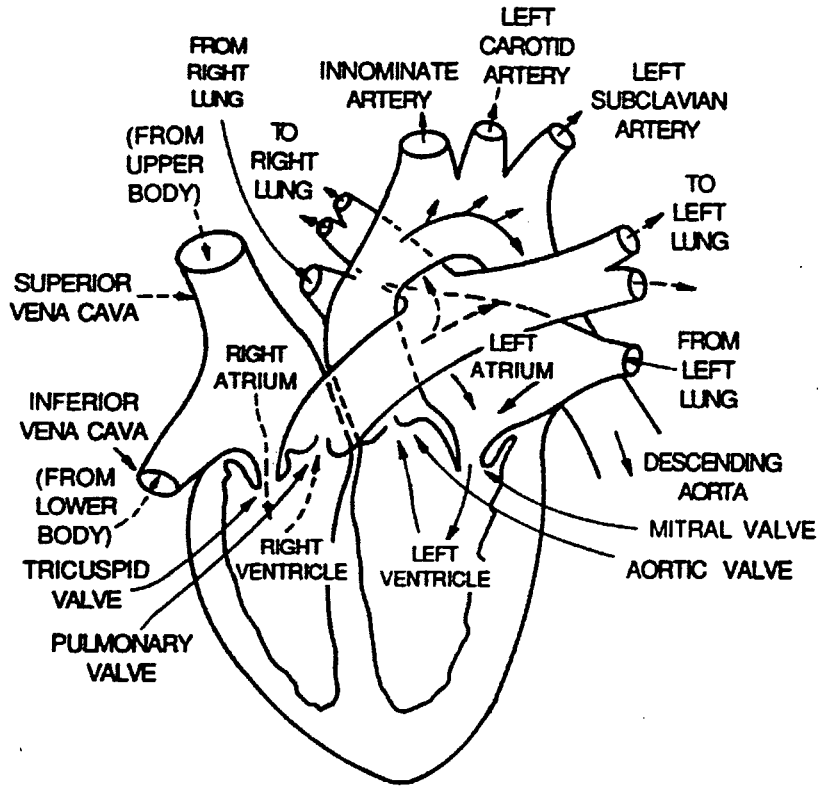

Figure 2.1: The four chambered heart is divided into two separated parts, the left and the right sides. Both parts consist of a ventricle and an atrium. The left side of the heart is anatomically larger than the right side. Adapted from (Rideout, 1991)

Muscle fibers contain a number of fibrils placed in parallel as shown in figure 2.3. The fibrils have a characteristic striped pattern. This pattern results from the parallel bundles of filaments, the interdigitating thick and thin filaments, lying between the Z-lines in Figure 2.4. Filaments lie along the fibrils divided into around 50 2μm blocks. A block is called a sarcomere and consists of approximately 1000 single thick-thin units of the type in Figure 2.4. Figure 2.5 shows the sarcoplasmic reticulum between the fibrils in the muscle fiber. The sarcoplasmic reticulum contains a Ca^{2+} reservoir which is essential during contraction. In addition, the muscle fibers contain the T-tubules vital for conduction of action potentials to the fibrils. The question is now how muscle contraction is accomplished. The sliding filament theory is the most widely embraced theory based on a mechanical concept though this theory is not the only one. Rather than mechanical descriptions, others propose a field theory approach (Spencer and Worthington, 1960; Elliott, Rome and Spencer, 1970), but this has not enjoyed the same popularity since evi-

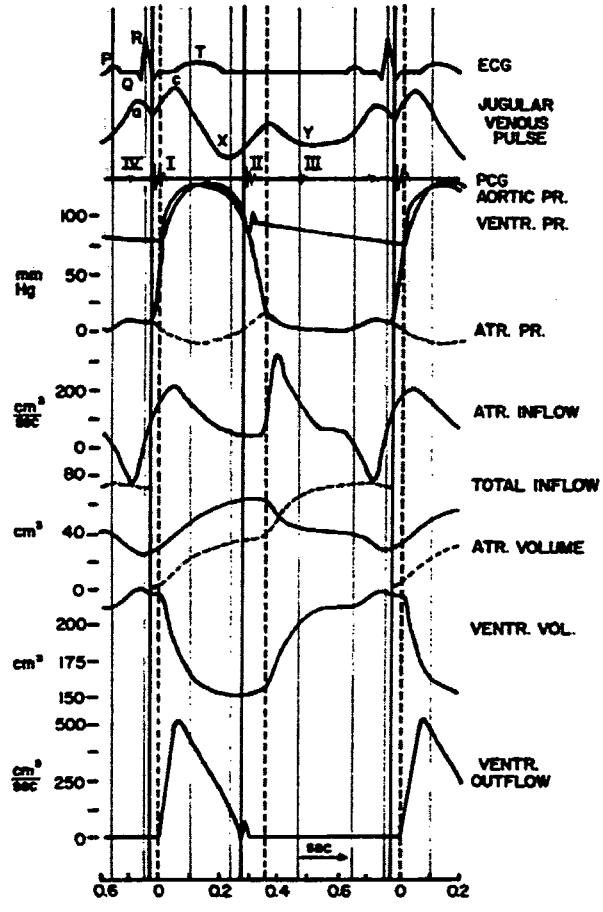

Figure 2.2: The electrocardiogram, venous pressure, phonocardiogram, root aortic pressure, ventricular pressure, atrial pressure, arterial inflow, total inflow to the heart, atrial volume, ventricular volume and ventricular outflow. The fully drawn lines and the dashed lines indicate valve closure and openings, respectively. Adapted from (Noordergraaf, 1978).

dence exists in favor of a mechanical type (Noordergraaf, 1978). Accordingly, we will give a description of the fundamental idea behind the sliding filament theory below.

The Sliding Filament Theory

It was observed in the 1950's that the thick filaments remained in a fixed position during contraction whereas the distance between neighboring Z-lines diminished. This led to the sliding filament theory. The main idea is that the thick and thin filaments slide during contraction, changing the overlap between them. Sliding is

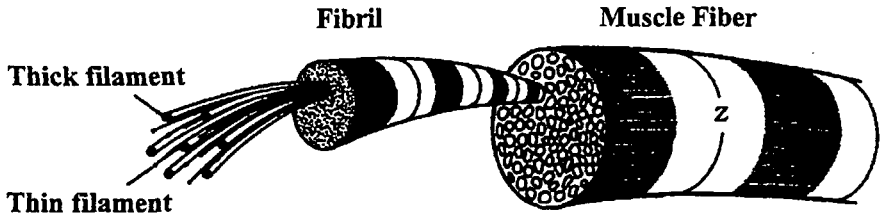

Figure 2.3: Muscle fibers contain approximately 100 fibrils in parallel. The fibrils have a characteristic striped pattern which stems from the filaments, the interdigitating thick and thin filaments as indicated. The striped pattern is also shown in Figure 2.4. Adapted from (Warberg, 1995).

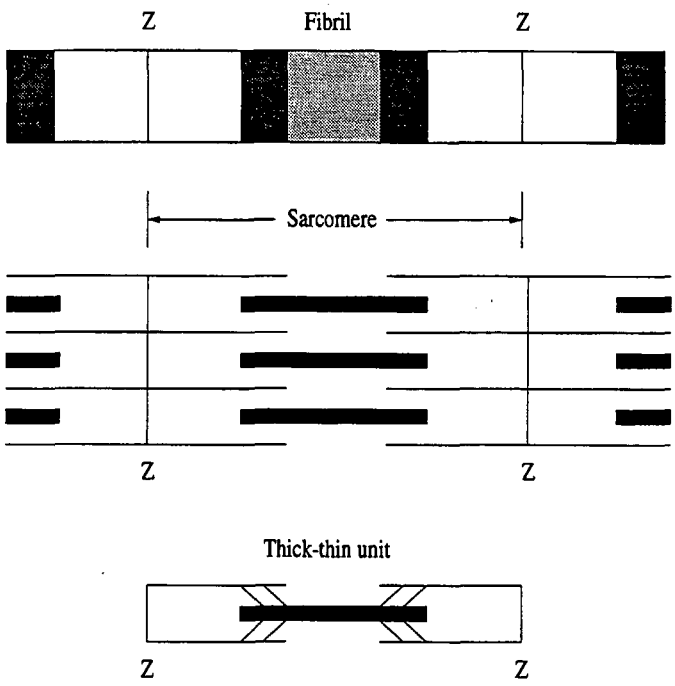

Figure 2.4: Top panel shows section of a fibril. The striped pattern follows from the bundles of filaments, the interdigitating thick and thin filaments, shown in the middle panel. A sarcomere is also indicated. The lower panel shows a single thick-thin unit with crossbridge bonds between thick and thin filaments.

accomplished by mechanical connections between thick and thin filaments which induce thin filaments to move with respect to thick filaments. The connections are called *crossbridges bonds* or *bonds*. During contraction, crossbridge bonds attach from the thick to thin filaments. As crossbridge bonds continue to attach, force is developing and the distances between neighboring Z-lines are diminished

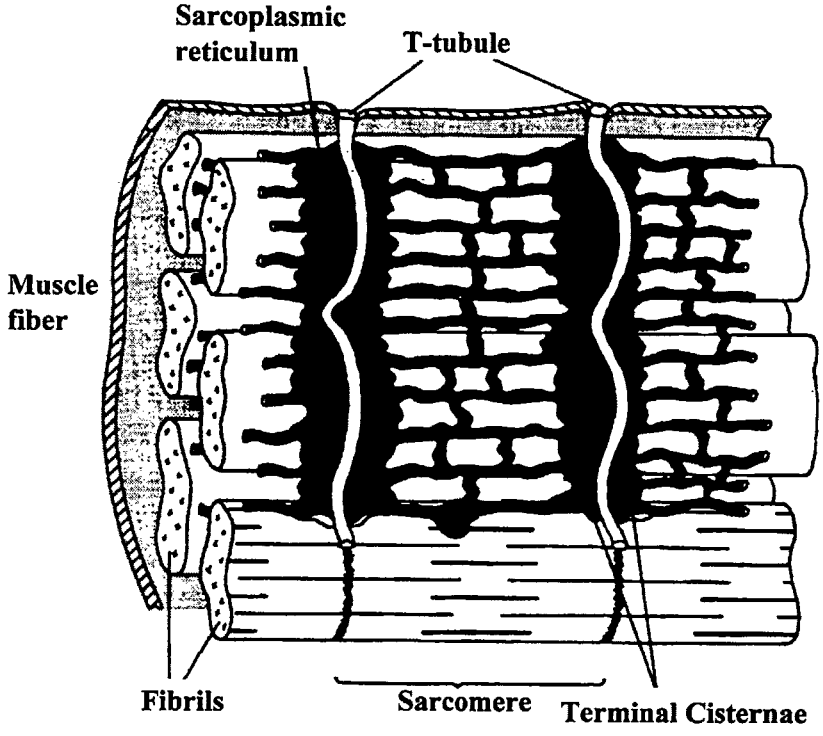

Figure 2.5: A part of a single muscle fiber with the sarcoplasmic reticulum. The T- tubule runs through the muscle fiber in a transverse direction through the fiber. Ca^{2+} is released from the terminal cisternae and diffuses into the fibrils. Adapted from (Warberg, 1995).

with a concomitant increased overlap between the filaments as shown in Figure 2.6. Consequently, force develops as allowed by the biochemical energy until crossbridges bonds detach in sufficiently high numbers and the force eventually decreases and the muscle relaxes. After a bond has detached it can attach again, *cycling of bonds*, during the same contraction.

Models based on the sliding filament theory disagree on the way bonds attach and detach (Noordergraaf, 1978; Palladino and Noordergraaf, 1998). Some models apply different functions to describe the rate of attachment and detachment of bonds. (Palladino, 1990) uses mechanical properties of the filaments (see Section 2.2). Thus a number of different model variations exit. Previous models seem to be designed to predict a particular muscle experiment but fail to describe a broader range of phenomena associated with other muscle experiments (Palladino and Noordergraaf, 1998). The experiments include quick stretch and release of the muscle fibers during contraction. In these experiments force increases and decreases, respectively, followed by a recovery. In addition, transient phenomena are observed in force development after perturbations. With few exceptions,

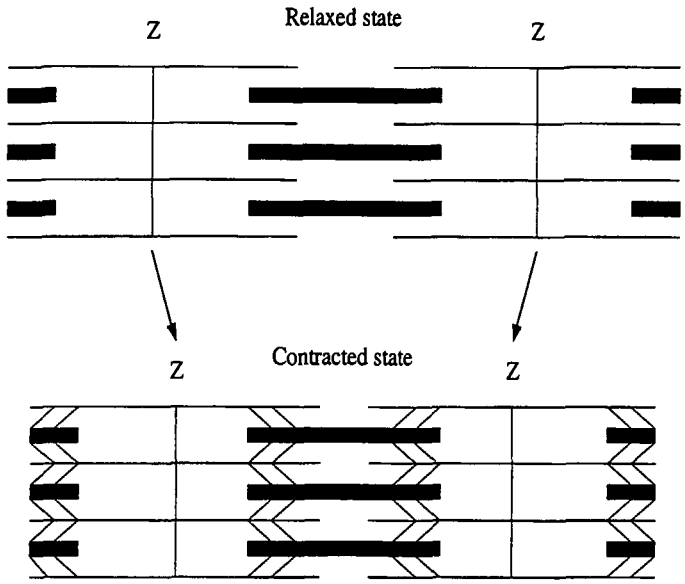

Figure 2.6: Top panel shows overlapping thick and thin filaments in the relaxed state. As crossbridge bonds attach between thick and thin filaments force develops with a concomitant increased overlap between the filament and diminished distance between neighboring Z-lines as indicated in the lower panel.

the models are such that they do not answer the question about the origin of the involved biochemical energy (Noordergraaf, 1978).

Biochemical Energy

In the sliding filament theory, force is assumed to develop from a combination of mechanical and biochemical processes. The available biochemical energy is closely related to the amount of Ca^{2+} while the actual release of energy stems from interaction between the proteins in the filaments. Thick filaments consist mainly of the protein myosin and thin filaments of the protein actin. During contraction the fibrils are electrically activated in direction of the axes, and in the radial direction by the T-tubule. This promotes release of Ca^{2+} near the Z-lines from the sarcoplasmic reticulum. After the release, Ca^{2+} binds to the protein troponin which lies around actin molecules in the thin filaments. Troponin inhibits reaction between myosin and actin but the Ca^{2+} binding promotes structural changes which release this inhibition. Subsequently, myosin interacts with actin via the crossbridge bonds and releases energy. Shortly after, Ca^{2+} is pumped back to the sarcoplasmic reticulum which also requires energy. This enhances inhibition of the actin-myosin interaction and thus formation of new bonds. Eventually force decreases and the muscles relax.

Relation between events at the sarcomere level and at the Chamber level

In summary, force generation in the muscle is considered to be the result of formation of crossbridge bonds between thick and thin filaments in the fibrils. The following detachment of bonds results in a decline in force and relaxation of the muscles. The amount of Ca^{2+} plays a key role in the availability of biochemical energy in this process. Thus energy is produced during the formation of crossbridge bonds between thick and thin filaments. At the chamber level ventricular pressure increases during formation of bonds between thick and thin elements and decreases during detachment of bonds.

2.2 A Model of Muscle Fibers

In this section we will illustrate one principle behind generation of force using the sliding filament theory. We introduce the only distributed model of a single muscle fiber proposed by (Palladino, 1990). The model describes the structure of a muscle fiber in a reduced form in order to have a manageable number of differential equations. A muscle fiber consists of approximately 100 fibrils. Each fibril is subdivided into 50 sarcomeres in series. A sarcomere consists of 1000 thick-thin units of the type as shown in Figure 2.4 each with 300 crossbridge bonds. The model consists of 50 sarcomeres each with one thick-thin unit. A half thick-thin unit consists of 50 crossbridge bonds, thus lumping three bonds, in order to a have manageable number of differential equations. The model is built up as follows:

- The mass of thick and thin filaments and the movement of filaments with respect to each other are included. The model is shown in Figure 2.7.
- Crossbridge bonds are assumed to have viscoelastic properties
- The sarcomeres are electrically activated with a current running from one end to the other of the fiber with a finite speed. The T-tubule leads the current in radial direction with no time-delay. As the thick-thin units are activated along the fiber, Ca^{2+} diffuses from the Z-lines and inwards. Bonds between thick and thin filaments are formed as Ca^{2+} diffuses inwards and are subsequently stretched. This asynchronous activation pattern is shown in Figure 2.8.
- Force develops depending on the degree of overlap between thick and thin filaments
- When the stress in a bond equals zero, it detaches and does not attach again. Thus during contraction, bonds are either attached or detached.

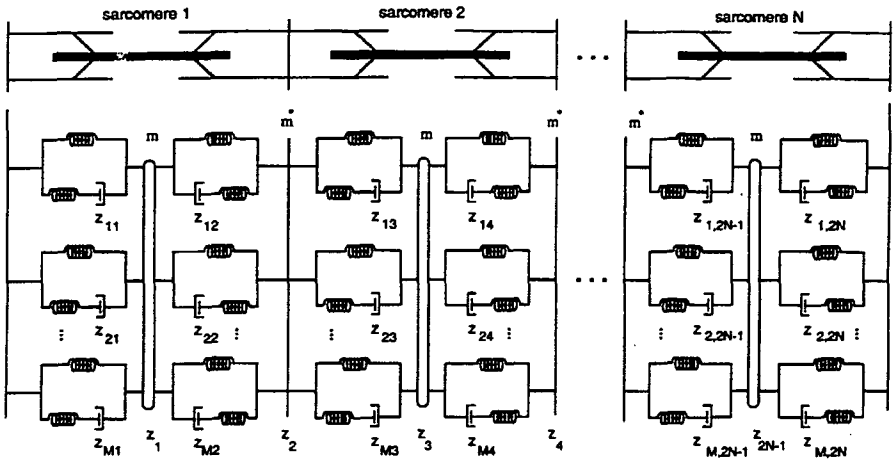

Figure 2.7: The figure shows a model of a muscle fiber consisting of N series sarcomeres with M parallel crossbridge bonds. A schematic picture is shown in the top panel. The mechanical model description is shown in the lower panel. Adapted from (Palladino, Mulier and Noordergraaf, 1998).

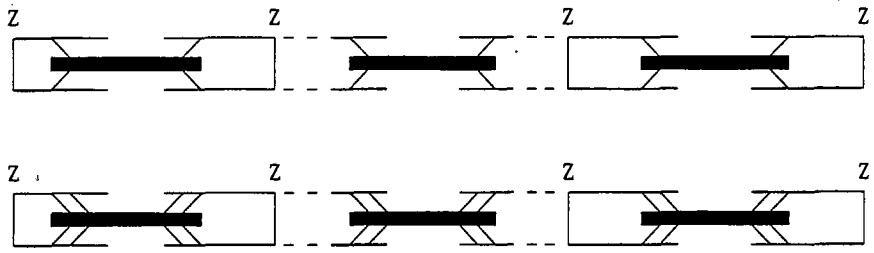

Figure 2.8: The muscle fiber is electrically stimulated from the left to the right and bonds attach as the thick-thin units are activated (upper panel). Subsequently Ca^{2+} is released from the terminal citernae and diffuses inwards from the Z-lines to the middle of the thick-thin units and bonds attach accordingly as shown in the lower panel.

The model predicts quick stretch and release experiments in good agreement with experimental data (Palladino, 1990). The model suggests that the significant drop in force, deactivation, observed during quick release of muscle length is caused by enhanced vibrations in the structure which tend to promote detachment. This mechanical approach to detachment is supported by ultrasound studies and x-ray diffraction studies (Palladino, 1990; Palladino and Noordergraaf, 1998). A more detailed study of this and other similar models can be found in (Palladino, 1990; Palladino and Noordergraaf, 1998). In the next Section 2.3 we return to the organ level, specifically the ventricle, and describe mathematical models of pressure and flow generation as functions of time.

2.3 Modeling the Ventricle

The mathematical descriptions of the heart have developed along a number of different avenues including muscle models, distributed models and lumped models. We focus on the latter type pursuing our interest in pressure, flow and volume as functions of time. Two types of lumped models have dominated the literature:

1. *Non-pulsatile models*, which describe the average values from beat to beat and exclude any details during an individual heart beat.
2. *Pulsatile models*, which describe the principal time varying features during each heart beat.

The principal concepts of the two types of models, along with a short historical review, are given in the following sections 2.3.1 and 2.3.3.

2.3.1 Pulsatile Models

In pulsatile models the pumping ventricle is typically viewed as an elastic bag which becomes stiffer during contraction, equivalent to a decrease in ventricular compliance C_v. The classical compliance

$$C_v = \frac{dV_v}{dp_v} \tag{2.1}$$

has been approximated by the linear relation

$$C_v = \frac{V_v}{p_v}, \tag{2.2}$$

where V_v is ventricular volume and p_v ventricular pressure. (Warner, 1959) seems be the first one who used the compliance concept (2.2). He applied a step function with a low systolic value and a high diastolic value to model the pumping ventricle. (De fares, Hara, Osborn and McLeod, 1963) applied the reciprocal of (2.2) also called the elastance. (De fares et al., 1963) made the obvious extension and used a continuous function of time. The time varying compliance was soon adopted in several pulsatile models to drive the ventricular function (Snyder and Rideout, 1969). Later (Suga and Sagawa, 1972) defined the elastance as

$$E_v(t) = \frac{p_v(t)}{V_v(t) - V_d}, \tag{2.3}$$

where V_d is a constant. The formulation (2.3) was claimed to be independent of alterations in end-diastolic volume and arterial load (Suga, 1969; Suga, 1970).

The maximum E_{max} of $E_v(t)$ was proposed as a measure of the heart's ability to pump in (Suga, Sagawa and Shoukas, 1973). These properties were later shown only to hold true for ejection fractions less or equal to 50 % which is low for humans.

The time varying elastance (2.3) is perhaps the most embraced description of the ventricle and a popular tool in pulsatile cardiovascular models. At least two main reasons can be advanced:

- A single time varying elastance captures the main features of the pumping human ventricle (Porter, Ryan, Melbin and Noordergraaf, 1982).

- The elastance is attractive because of its simplicity. The concept offers easy access for modeling changes in heart rate and modifications caused by neural effects.

Depending on the model, the single elastance function is complemented by a resistive term to include viscous effects. An inductive term may also be added to include inertia of blood movement. According to (Abutaleb, Melbin and Noordergraaf, 1986) the compliance is the most significant parameter, then follow resistance and inertia. The energy involved in the pumping ventricle, driving the time-varying elastance function, is assumed to be embodied by biochemical processes in the heart.

Serving as an example the elastance function (2.3) was adopted by (Stergiopulos, J. and Westerhof, 1996) and described by

$$E_v(t) = E_{max}\left[\frac{\left(\frac{t}{\alpha_1 t_h}\right)^{n_1}}{(1-\left(\frac{t}{\alpha_1 t_h}\right)^{n_1})(1+\left(\frac{t}{\alpha_2 t_h}\right)^{n_2})}\right] + E_{min}, \qquad (2.4)$$

where t is time, t_h heart period, n_1 and n_2 describe the steepness of the ascending and descending parts of the elastance curve whereas α_1 and α_2 are shape parameters. Figure 2.9 shows the ventricle, described by a elastance function, coupled to a 3-element modified Windkessel model and a constant pressure reservoir p_r. Similar types of time-varying elastance functions with or without resistive and inductive terms have been used in several models in recent years. A few of these models include (Martin, Schneider, Mandel, Prutow and Smith, 1986; Tham, 1988; Rideout, 1991; Neumann, 1996; Stergiopulos et al., 1996; Danielsen and Ottesen, 1997; Ursino, 1998). We include a ventricular model of this type in the SIMA simulator (Danielsen, 1996; Danielsen and Ottesen, 1997). This is more carefully described in Section 4.3.1 of Chapter 4.

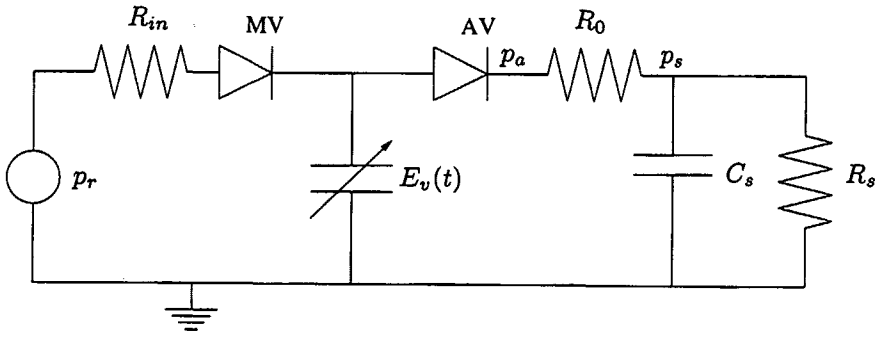

Figure 2.9: The left ventricle, described by an elastance function $E_v(t)$, coupled to a 3-element modified Windkessel arterial load and a constant venous pressure reservoir p_r. The mitral and the aortic valve are indicated.

2.3.2 Shortcomings of the Elastance Concept

The highly popular ventricular model (2.3) was previously thought to determine ventricular contraction uniquely. However, this widely embraced model is subject to limitations and discrepancies.

During an isovolumic contraction (i.e. non-ejecting), the model (2.3) predicts that ventricular cavity pressure increases linearly with end-diastolic volume, contradicting the non-linear behavior for high values of the ventricular volume V_v as measured by Frank in 1898 (Palladino, Mulier and Noordergraaf, 1998). The pumping heart exhibits a maximum ventricular work and stroke volume whereas the model predicts stroke volume and ventricular work to increase with end-diastolic volume. During ejection (2.3) predicts the ventricular pressure to equal $p_v(t_{max}) = (V_v(t_{max}) - V_d)E_{max}$ at time t_{max} for maximum elastance, E_{max}. Thus, peak pressure in an isovolumic ventricle with volume $V_v(t_{max})$ is equal to the ventricular pressure during ejection at time t_{max}. Experimentally, this is not always the case. Ventricular cavity pressure can be higher in late ejection, hyperactivation, than the isovolumic pressure for the same volume (Ducas, Schick, Girling and Prewitt, 1985; Hunter, 1989; Mulier, 1994). This contradicts directly the model (2.3) which predicts ventricular pressure to be consistently lower than or equal to the corresponding isovolumic pressure. The same prediction is obtained when a passive resistive term is included. Ventricular pressure decreases during ejection more than expected from the change in volume alone, deactivation. This depressive effect was studied by (Hunter, Janicki, Weber and Noordergraaf, 1983; Vaartjes and Herman, 1987) and is not included by a single time-varying elastance function. Deactivation is included when the single time-varying elastance is complemented by a passive resistive term or an inductive term.

A single time-varying elastance predicts that infusion of small volumes ΔV results in the same end-systolic pressure independent of the time of infusion since $p_v = E_v(t_{es})(V_v + \Delta V - V_d)$. According to (Hunter et al., 1983), the end-systolic pressure depends on the time of infusion or withdrawal of small volumes ΔV. In addition, a single time-varying elastance function cannot predict transient phenomena associated with quick withdrawal of small volumes ΔV during an otherwise isovolumic contraction (i.e. non-ejecting). In contrast to experiments, the model predicts a direct transition from the first isovolumic pressure curve with volume V_v to one with volume $V - \Delta V$. Similar behavior patterns are observed during quick infusion of small volumes (Palladino, 1990).

A variety of observations are not covered by the time-varying elastance concept and the question may be to ask how this should be embedded in ventricular modeling. A resistive term which depends on time was suggested by (Vaartjes and Herman, 1987). The physiological interpretation of the resistive term is unclear. It may be interpreted as viscous elastic properties of blood or effects due to muscle shortening. This type of repairs may not be the right solution. The entire elastance concept suffers from one significant shortcoming which is that it does not separate ventricular effects from vascular effects when the measured pressure p_v and volume V_v in (2.3) are taken during ejection. This makes it difficult to gain insight into the properties of the ventricle. In addition, a pre-defined elastance function $E(t)$ makes the formation of crossbridges immune to instantaneous changing arterial conditions. An a priori definition of the elastance function fixes the number of crossbridge bonds formed during each heart beat. A change in the number of crossbridge bonds formed would change the elastance $E_v(t)$. An increased filling results in a higher pressure and also in an increased number of crossbridges formed according to the force-length relation (Palladino, Mulier and Noordergraaf, 1998, submitted). The time-varying elastance function $E(t)$ predicts that the higher pressure results exclusively from an increased stretch of the existing number of bonds. The pre-defined elastance concept also contradicts the Fenn-effect (Palladino, 1990) which states that the energy during ejection is different from the energy during an isovolumic contraction. A new approach to ventricular modeling at the chamber level seems warranted.

2.3.3 Non-Pulsatile Models

The ventricle can perform more work W with higher end-diastolic volume V_{ed}. This is one formulation of Starling's law (1914) and constitutes a key element in non-pulsatile models. Within physiological limits, Starling's law implies that for nearly constant systemic pressure, higher end-diastolic volume results in greater amount of ejected blood. At the muscle level this corresponds to increased force of contraction when muscle fibers are stretched more due to enhanced filling. Star-

ling's law may be seen as a pure functional relation between ventricle and vasculature.

Starling's law is widely accepted as a fundamental mechanism of the heart and as an argument for validity of pulsatile models. In addition, it serves as an independent building block in non-pulsatile cardiovascular system models. (Guyton, 1955) related cardiac output[1] to venous return and also atria pressure to venous return in a closed cardiovascular model. He used these relations to compute the steady state graphically. (Grodins, 1959) expressed Starling's law by the linear relation

$$W = \alpha V_{ed}, \tag{2.5}$$

where the constant α is the strength of the ventricle. In a closed cardiovascular model by (Ursino, Antonucci and Belardinelli, 1994) the left and the right ventricle were modeled by

$$SV_l = k_1(p_{la} - p_{la0}), \tag{2.6}$$
$$SV_r = k_2(p_{ra} - p_{ra0}), \tag{2.7}$$

where SV_l and SV_r are stroke volumes for the left and right ventricle, respectively, p_{la} and p_{ra} left and right atrial pressures, k_1 and k_2 parameters characterizing the ventricles, p_{la0} and p_{ra0} constants. Ursino (Ursino et al., 1994) included modification of k_1 and k_2 in (2.6)-(2.7) due to neural effects. This modification of Starling's law is accentuated during exercise when increase in cardiac output cannot be ascribed to enhanced filling alone or change in heart rate (Noordergraaf, 1978; Palladino and Noordergraaf, 1997; Palladino, Mulier and Noordergraaf, 1998; Milnor, 1990; Kappel, Lafer and Peer, 1997). Thus the heart is not governed by Starling's law alone but affected by many factors. Starling's law is not disqualified by this but should be seen as a relation including hemeometric and heterometric effects as pointed out by (Palladino, Mulier and Noordergraaf, 1998).

2.4 Goal

Inasmuch as the pumping heart is considered as the central organ and the pump of the cardiovascular system, it is not an independent energy source but interacts strongly with the rest of the cardiovascular system. This constitutes one of our key interests, namely, the interaction between the heart and the receiving arterial system. Classical mathematical models of the ventricle based on the time-varying elastance function (Warner, 1959; De fares et al., 1963; Suga, 1969) tend to lump this complex interaction such that the properties of the heart and of the arterial

[1] Cardiac output is stroke volume times heart rate.

system are difficult to distinguish. My work is an attempt to highlight this interaction issue. Also, the time-varying elastance concept suffers from a number of shortcomings as discussed in Section 2.3.2.

A new approach to ventricular modeling is needed. This approach should carefully relate events at the chamber level with those at the ultrastructural muscle level, and allow the formation of crossbridges to depend on the instantaneous conditions during ejection also in ventricular models at the chamber level.

We adopt an approach fundamentally different from previous attempts by starting from an experimentally based analytical description of the isovolumic ventricular pressure as a function of time and volume contained. (Mulier, 1994) established this new mathematical model of the isovolumic ventricular cavity pressure as a function of time t and ventricular volume V_v based on experiments in isolated dog hearts. This new model casts information on the isovolumic heart and gives an excellent description of the heart during isovolumic conditions. We allow the new model to eject into the vasculature and examine carefully the interaction between the left ventricle and the arterial load. The arterial load is described independently by a modified Windkessel model. We relate attachment and detachment of crossbridge bonds to alterations in the contractile properties. During ejection, we identify two phenomena, deactivation and hyperactivation, and relate the phenomena to events at the ultrastructural muscle level (see Section 3.4). We denote the two phenomena the ejection effect. In addition, we disqualify Starling's Law as an independent law of the ventricle.

Chapter 3

Interaction between Ventricle and Arterial Load

3.1 Introduction

The peak developed pressure of the isovolumically contracting ventricle increases with end- diastolic pressure to an upper physiological limit. This is known as the Frank mechanism. The result was included in Otto Frank's first study on the heart 'On the dynamics of cardiac muscle' published in 'Zeitschrift fuer Biologie' in 1895. Otto Frank recognized in this publication that cardiac output depends on the conditions in the arterial system. Consequently he focused on the isolated heart (Palladino, Mulier and Noordergraaf, 1998). But Otto Frank was so interested in the properties of the arterial system that "he really did not return to analyzing mathematically his finding on the left ventricle" (Palladino, Mulier and Noordergraaf, 1996). Despite its simplicity, the Frank mechanism has never enjoyed the same popularity as Starling's law. In fact it has never been applied to ventricular modeling (Palladino, Mulier and Noordergraaf, 1998) until (Mulier, 1994) adopted it and established an analytical model of ventricular pressure as a function of time and volume contained. The model of (Mulier, 1994) constitutes the key element in our investigations of the interaction between the left ventricle and the arterial load. The approach taken, starting with an isolated heart, is fundamentally different from previous attempts and allows a more careful investigation of the ejecting phase. Based on experimental data from isolated dog hearts, the model casts information on the isovolumic ventricle into an analytical description. The model will be described in detail in Section 3.2. When coupled to a model of a vascular system, this ventricular model exhibits the main features of the pumping ventricle including diminished cavity pressures compared to isovolumic ones (Palladino, Rabbany, Mulier and Noordergraaf, 1997; Pal-

ladino, Mulier, Wu, Moser, Kenner, Baevsky and Noordergraaf, 1996; Palladino and Noordergraaf, 1997; Palladino, Ribeiro and Noordergraaf, 1998). In addition, we will show in Section 3.3 that Starling's law follows from the Frank mechanism. This disqualifies Starling's law as an independent law of the ventricle. In Section 3.4 we will uncover, upon more detailed analysis, that discrepancies exist between model predicted and experimentally obtained ventricular pressures during ejection. We will interpret these differences as alterations in ventricular contractile properties attributable to muscle shortening during ejection. We denote these differences the ejection effect. The ejection effect tends to lower cavity pressure during early ejection and raise it during late ejection compared to that predicted from applicable isovolumic conditions. Corresponding changes in the shape of the ejection curve and in the ventricular pressure curve will be observed. The lower cavity pressure is included in several models by a series resistance. (Hunter et al., 1983; Campell., Ringo, Knowlen, Kirkpatrick and Schmidt, 1986). The higher cavity pressure, although observed previously (Ducas et al., 1985; Hunter, 1989; Mulier, 1994) has not been appreciated to the same degree. In Section 3.4.2 we will give our first mathematical description of the ejection effect. The interaction between the left ventricle and the arterial load will subsequently be studied in Section 3.5. Section 3.6 will offer an alternative to the model proposed in Section 3.4.2. We will end the chapter with a summary and outlook in Section 3.7.

3.2 The Model of the Isovolumic Ventricle

The Frank mechanism is the key element in the experimentally based ventricular model by (Mulier, 1994) of the isovolumic ventricular pressure as a function of time and volume contained. In this section we will describe this analytical model in some detail.

The model assumes that ventricular isovolumic pressure p_v equals a passive (diastolic) $p_d(V_v)$ plus an active (systolic) $p_s(V_v)g(t)$ component

$$p_v(V_v, t) = p_d(V_v) + p_s(V_v)g(t). \tag{3.1}$$

where

$$g(t) = \begin{cases} (1 - e^{-(\frac{t}{\tau_c})^\alpha}) & 0 \le t \le t_d \\ (1 - e^{-(\frac{t}{\tau_c})^\alpha})e^{-(\frac{t-t_d}{\tau_r})^\alpha}, & t_d < t < t_h \end{cases} \tag{3.2}$$

The second term on the right hand side of (3.1) describes the active contractile processes in the systolic pressure generation. The time constants τ_c and τ_r in (3.2) characterize the contraction (pressure increase) and relaxation (pressure decrease)

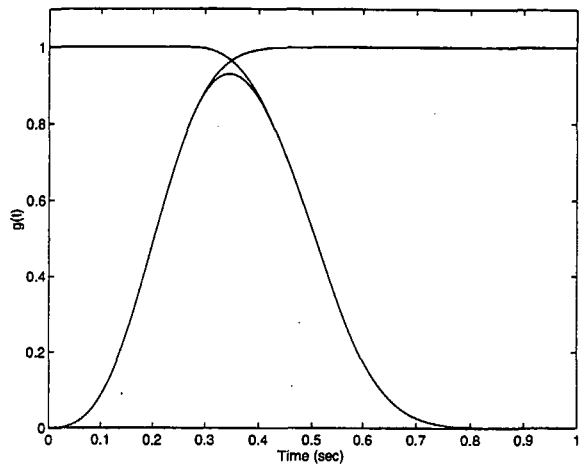

Figure 3.1: The g function consists of two factors. The first factor describes the build-up of ventricular pressure during contraction via muscle crossbridge bond attachment. The second factor describes the relaxation following bond detachment.

processes, respectively, while α is a measure of the overall rate of onset of these processes. The constant t_h denotes the heart period and t_d is the time when the relaxation process begins to evolve, and is directly related to τ_c, τ_r and α, and to the time of peak generated pressure, t_p, by

$$t_d = t_p \left\{ 1 - \left(\frac{\tau_r}{\tau_c}\right)^{\frac{\alpha}{\alpha-1}} \left[\frac{e^{-(\frac{t_p}{\tau_r})^\alpha}}{1 - e^{-(\frac{t_p}{\tau_c})^\alpha}} \right]^{\frac{1}{\alpha-1}} \right\} \tag{3.3}$$

since $\dot{p}_v(t_p) = 0$. The function g is the product of two factors as shown in Figure 3.1. The first describes the build-up of pressure attendant upon crossbridge formation in the constituent muscle fibers comprising the ventricle. The second describes the relaxation of pressure resulting from bond detachment. From experiments (Mulier, 1994), the peak developed pressure is described by

$$p_s(V_v)g(t_p) = p_v(V_v, t_p) - p_d(V_v) = cV_v - d, \tag{3.4}$$

where c and d are directly related to the volume dependent and volume independent components of developed pressure, respectively.

Experiments also show that the passive component $p_d(V_v)$ of (3.1) is best described by

$$p_d(V_v) = a(V_v - b)^2, \tag{3.5}$$

where a is a measure of diastolic ventricular elastance and b corresponds to diastolic volume for zero diastolic pressure (Mulier, 1994). In summary, using (3.1)-

(3.5), ventricular pressure in an isovolumic beat, as it depends on ventricular volume and time, can be described by an analytical model based on experiments on isolated dog hearts (Mulier, 1994) by

$$p_v(V_v, t) = a(V_v - b)^2 + (cV_v - d)f(t), \tag{3.6}$$

where f is the normalization of g

$$f(t) = \begin{cases} \frac{(1-e^{-(\frac{t}{\tau_c})^\alpha})}{(1-e^{-(\frac{t_p}{\tau_c})^\alpha})e^{-(\frac{t_p-t_d}{\tau_r})^\alpha}}, & 0 \le t \le t_d \\ \\ \frac{(1-e^{-(\frac{t}{\tau_c})^\alpha})e^{-(\frac{t-t_d}{\tau_r})^\alpha}}{(1-e^{-(\frac{t_p}{\tau_c})^\alpha})e^{-(\frac{t_p-t_d}{\tau_r})^\alpha}}, & t_d < t < t_h \end{cases} \tag{3.7}$$

This model (3.6)-(3.7) thus contains eight parameters a, b, c, d, t_p, τ_c, τ_r and α which follow from experimental data with the last three from a curve-fitting procedure and all parameters have a physiological interpretation. Simplicity is a key element in the functional description of the active and the passive components of the isovolumic pressure. More complex functional descriptions can give higher accuracy of the fit of experimental data. But independence among the parameters and a clear physiological interpretation may be lost. Higher order polynomials can fit the experimental data arbitrarily well but the coefficients offer no clear physiological interpretations as do the time constants τ_c and τ_r in (3.7). In contrast to the functional descriptions of the volume dependencies in the model (3.6) no alternatives to the function g seem to have been pursued except for polynomials and fourier expansions. Thus the exponential functions in g may be seen as a convenient but not as the only possible description. In addition, the time constants τ_c and τ_r seem to depend on volume. Moreover, the isovolumic ventricle has not been examined for other heart rates than 1 Hz. The latter may limit the range of applications of this ventricular model.

3.3 The Ventricular Model and the Arterial Load

For the purpose of permitting the ventricle to eject, the model of the isovolumic ventricle is coupled to a 3-element modified Windkessel arterial load. The ventricle is given a constant end-diastolic volume as shown in Figure 3.2. The input impedance of the Windkessel then relates arterial pressure p_a to ventricular volume V_v as

$$\dot{p_s} = -\frac{R_s + R_0}{R_0 R_s C_s} p_s + \frac{1}{R_0 C_s} p_v(t, V_v), \tag{3.8}$$

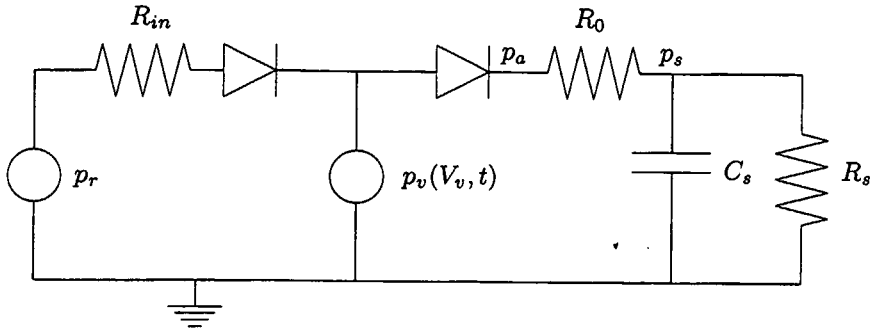

Figure 3.2: The ventricular model $p_v(V_v, t)$ coupled to a 3-element modified Windkessel arterial load and a venous pressure source. The mitral and the aortic valve are indicated. End-diastolic volume $V_{ed} = 125$ ml (filling pressure $p_r = 10$ mmHg). Parameter values for the arterial load and the constant pressure reservoir p_r can be found in Table 3.2.

$$\dot{V}_v = \frac{1}{R_0}p_s - \frac{1}{R_0}p_v(t, V_v), \tag{3.9}$$

$$p_a = p_s - R_0\dot{V}_v, \tag{3.10}$$

where R_o is the characteristic aortic impedance, R_s is the total peripheral resistance and C_s is the total arterial compliance. The simultaneous solution of (3.6)-(3.10) permits the computation of ventricular pressure for the ejecting (*i.e* non-isovolumic) ventricle, root aortic pressure, and ejection flow. Representative computed pressure p_v and flow Q_v $(= -\frac{dV_v}{dt})$ curves for the human left ventricle for an ejecting heart beat are shown in Figure 3.3 together with the isovolumic pressure p_{iso} for the same end-diastolic volume. The pressure difference between p_v and p_{iso} is caused by the changing volume during ejection. The computed curves exhibit all the major features of the standard experimental pressure and flow curves (Palladino, Ribeiro and Noordergraaf, 1998). In addition, the model embodies Starling's two observations as shown in Figure 3.4 which implies that ventricular work increases with end-diastolic volume. Consequently, Starling's law follows from the Frank mechanism. In this sense, Starling's law is reduced to the Frank mechanism and thus disqualified as an independent law of the ventricle. The difference between the model results and Starling's law is the absence of a maximum ventricular work (equivalent to maximum stroke volume in Figure 3.4). The experimental isovolumic peak pressure reaches an upper physiological limit for a finite end-diastolic volume. The muscular equivalent is the force-length relation where the developed force is maximum for a specific optimal length and lower for all other lengths. The reason for the difference is that this feature is not included in the model.

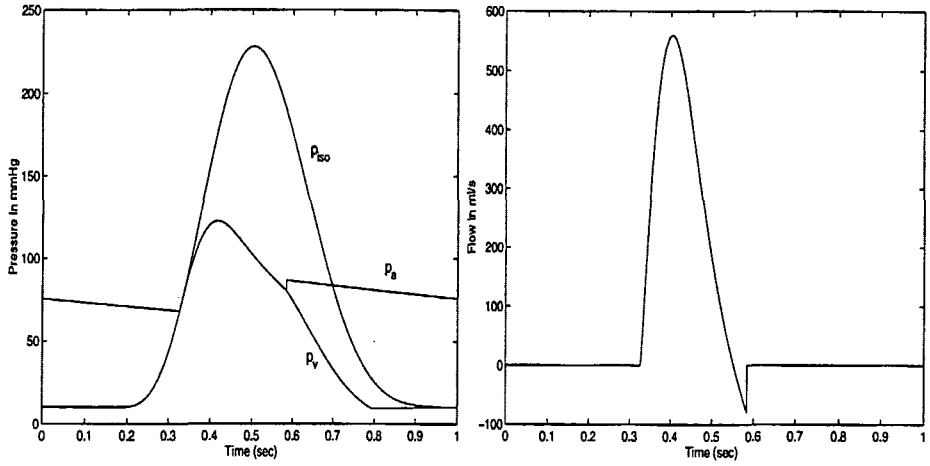

Figure 3.3: The left panel shows isovolumic pressure p_{iso}, arterial and ventricular pressures, p_a and p_v, respectively. The panel on the right shows the ventricular outflow Q_v. All curves are computed for a normal human ventricle ejecting into the arterial load given in Figure 3.2. End-diastolic volume (filling) $V_{ed} = 125$ ml., stroke volume $SV = 70$ ml, ejection fraction $EF = 0.56$ and heart rate $H = 1$ Hz. Ventricular parameters are given in table 3.3.

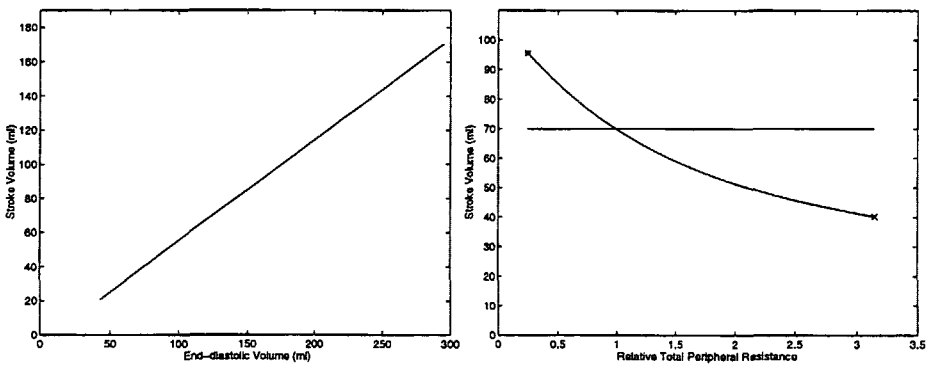

Figure 3.4: Starling's two observations are shown in the left and right panels, respectively. The left panel shows that the stroke volume is proportional to the end-diastolic volume and the right panel that stroke volume is inversely proportional to the total peripheral resistance for a constant end-diastolic volume 125 ml (along the axis is the total peripheral resistance relative to R_s of table 3.2). In addition, the right panel indicates that stroke volume can be held constant by adjusting the end-diastolic volume. The stroke volume in point (*) and (x) can be changed to 70 ml if the end-diastolic volume is altered to 93.7 ml and 141 ml respectively. In both figures the ventricular pressure increases while the heart rate is held constant, $H = 1$ Hz, giving Starling's law that the ventricular work increases with increasing end-diastolic volume.

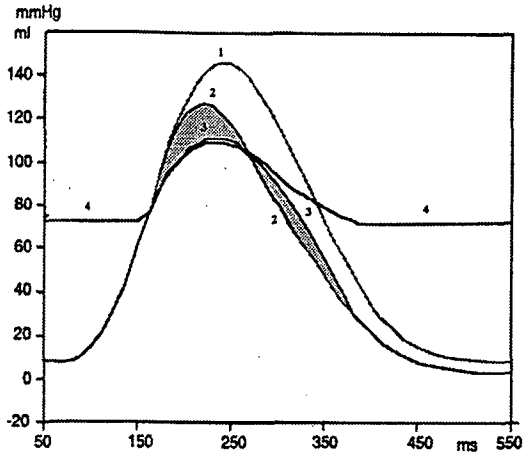

Figure 3.5: Ventricular pressures measured on one isolated dog heart. Curve 1 is isovolumic pressure at fixed end-diastolic volume and curve 2 is the calculated pressure p_{cal} computed from (3.6). Curve 3 is measured pressure for an ejecting beat. Comparing curve 2 and 3, ventricular pressure is lower in early systole (deactivation) and higher in late systole (hyperactivation). The first shaded area from the left represents deactivation and the second shaded area represents hyperactivation. Adapted from (Mulier, 1994).

3.4 The Ejection Effect

In the preceding section it was shown that the major differences between an isovolumically contracting ventricle and an ejection ventricle are displayed by the model. Closer inspection reveals discrepancies when ventricular pressure p_{mes} and volume V_{mes} measured on an isolated canine left ventricle for an ejecting beat are compared to the model predicted pressure computed using (3.6) with the measured volume V_{mes}. This computed pressure is denoted the *calculated pressure* $p_{cal}(t)$ (i.e. $p_{cal} = p_v(V_{mes}(t), t)$,) and would equal the measured ventricular pressure p_{mes} if this results from the Frank mechanism alone. But the measured pressure p_{mes} differs from the calculated pressure as shown in Figure 3.5. Measured ventricular pressure p_{mes} in the early phase of ejection, when ventricular outflow is large, is lower than the calculated pressure p_{cal}, termed pressure *deactivation*. Later in systole the pressure is somewhat higher, termed pressure *hyperactivation*, not always observed (Burkhoff, DeTombe and Hunter, 1993; De Tombe and Little, 1994). In addition, the waveforms of the pressure and flow curves differ from the profiles reported in (Guyton, 1991; Noordergraaf, 1978). The descending part of the computed flow curve (see Figure 3.3) tends to be concave instead of convex. We denote these differences the *ejection effect* which amounts to a correction term for this ventricular model and is due to effects different from the Frank mechanism.

At the muscle level, deactivation may be qualitatively related to *Hill's force-velocity relation* stating that the force of muscle contraction is more reduced the higher the velocity of muscle shortening. Muscle shortening forces cross-bridge bonds to detach and results in diminished force. On the chamber level this is equivalent to a reduction in ventricular pressure with increased early flow (Palladino, 1990; Mulier, 1994). Hyperactivation follows deactivation and is manifested as an increase in ventricular pressure above the calculated pressure. Hyperactivation may be related to the formation of new crossbridge bonds between thick and thin filaments. The strength of the hyperactivation is subsequently conditioned by available biochemical energy. In support of the above (De Tombe and Little, 1994) concluded on experimental grounds that these positive and negative inotropic effects of ejection are myocardial properties.

Hyperactivation has not been given a precise definition. This may be related to the absence of an isovolumic ventricular model. (Ducas et al., 1985) seems to be the first who observed hyperactivation by lowering of the resistive afterload. (Hunter, 1989) measured that end-systolic ventricular pressure exceeded the isovolumic pressure in the ventricle when volume was equal to the end-systolic volume from the previous ejecting beat. This was observed during a small ejection fraction, 0.3, with hyperactivation varying between $1 - 17$ mmHg. Hyperactivation was shown to disappear during even lower or higher ejection fractions. He related hyperactivation to underlying cardiac properties. (Baan, 1992) concluded that hyperactivation and homeometric autoregulation stems from the same mechanism. Thus he relates hyperactivation to biochemical processes. Hyperactivation may be a ventricular response to reflected waves from the vascular periphery under certain conditions. According to experiments hyperactivation can disappear in reflection free afterloads (Mulier, 1994).

3.4.1 The Inertial Effect of Ventricular Blood

The inertial effect of blood in the ventricle tends to lower the arterial pressure in early systole (similar to deactivation) and increase the pressure in late systole (akin to hyperactivation). Moreover, it may improve the bending of the outflow curves. In order to test if the inertial effect can explain the ejection effect, the model of the isovolumic ventricle (3.6) was coupled to the arterial load in Figure 3.2 with an L_v placed before the aortic valve. Thus the arterial pressure p_a and the ventricular outflow Q_v are then related as

$$\dot{p}_s = -\frac{1}{R_s C_s} p_s + \frac{1}{C_s} Q_v, \tag{3.11}$$

$$\dot{Q}_v = -\frac{1}{L_v} p_s - \frac{R_0}{L_v} Q_v + \frac{1}{L_v} p_v(t, V), \tag{3.12}$$

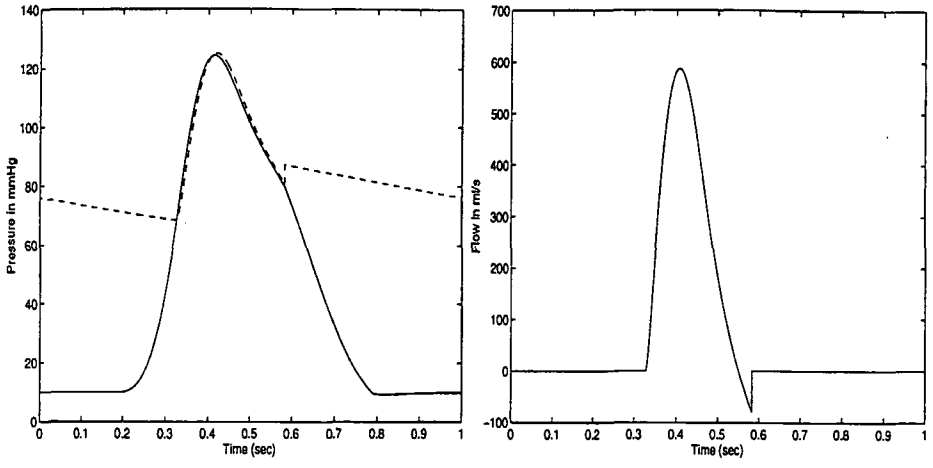

Figure 3.6: The left panel shows ventricular pressure p_v (full line), arterial pressure p_a (dashed line) when the ventricle ejects into the modified Windkessel load of Figure 3.2 obtained by using (3.12) -(3.13) with an inductance $L_v = 0.000416$ mmHg s^2/ml. The right hand panel shows the corresponding flow curve. Vascular parameters are given in table 3.3.

$$p_a = p_s + R_0 Q_v. \tag{3.13}$$

The inertial effect of ventricular blood contributes slightly to the shape of pressure and flow curves, as shown in Figure 3.6 and provides a phase shift between ventricular and aortic pressure as observed experimentally (Pasipoularides, Murgo, Miller and Craig, 1987). However, the model shows no worthwhile improvement in the shape for physiological values of the inductance calculated by assuming a cylindrical geometry of the ventricle.

Also, the interaction with reflected waves was eliminated by making the compliance equal to $100C_s$ (Berger, Li, Lasky and Noordergraaf, 1993). The computations showed that reflected waves play only a minor role in the profiles of the curve both in the case with the inertial effect of ventricular blood and in the case with the modified Windkessel model of Figure 3.2. Although the inertial effect of ventricular blood contributes in the right direction, it, and reflection, cannot alone explain the ejection effect. Apparently the ejection effect consists of a number of small components.

3.4.2 A model of the Ejection Effect

As a first, rough, approximation, the ejection effect: deactivation, hyperactivation and the shape of the computed ejection curves, may be described by modification

of the parameter c in (3.6), to $c(x)$, via

$$c(x) = c - \bar{c}(x), \quad x = \frac{V_{ed}}{V_v(t)}, \tag{3.14}$$

where V_{ed} is the end-diastolic volume and

$$\bar{c}(x) = \gamma \left[\frac{1}{(1 + e^{\beta_1(1-x)})(1 + e^{\beta_2(x-1)})} - \frac{1}{4} \right]. \tag{3.15}$$

The positive parameter γ represent the strength of the ejection effect whereas β_1 and β_2 represent the rates of the effect. Thus (3.6) is rewritten as

$$p_v(V_v, t) = a(V_v - b)^2 + [(c - \bar{c}(x))V_v - d)]\, f(t) \tag{3.16}$$

during ejection. The parameter c is directly related to the ventricle's contractile state. During isovolumic contractions $\bar{c}(x) = 0$ and (3.16) reduces to (3.6).

3.5 The Ejection Effect and the Arterial Load

The left ventricle was filled from a constant pressure reservoir p_r and coupled to a 3-element modified Windkessel arterial load as in Figure 3.2 with the parameters given in tables 3.2 and 3.4. The computed arterial and ventricular pressures, including the ejection effect, and the corresponding ventricular outflow are shown in Figure 3.7. In both pressure and flow curves the ejection effect correction yields curve shapes far more representative of the normal human ventricle and are in close agreement with curves in Figure 2.2 and in (Guyton, 1991). In particular the flow curve in Figure 3.7 shows a clearly convex shape. Table 3.1 compares model results with typical normal values of the human ventricle adopted from (Noordergraaf, 1978). The model computed values arise from the parameters given in table 3.4. In particular, the time constraints in table 3.1 result mainly from lowering the parameters τ_c and τ_r. Figure 3.8 demonstrates that both deactivation and hyperactivation are introduced by the ejection effect which follow directly from $c(x)$ in (3.14). The time course of $c(x)$ during one heart beat is also shown in Figure 3.8. The value of $c(x)$ falls below c in early systole, followed by an increase above c, thereby introducing deactivation and hyperactivation, respectively. The inertial effect of ventricular blood is only of minor importance in the normal situation as shown in Figure 3.9. This is also reflected in the vascular parameters γ, β_1 and β_2 which are adjusted to the needs as shown by the different parameter values listed in table 3.5.

Both deactivation and hyperactivation are influenced by the interaction with the vasculature. According to (Mulier, 1994) deactivation increases with higher

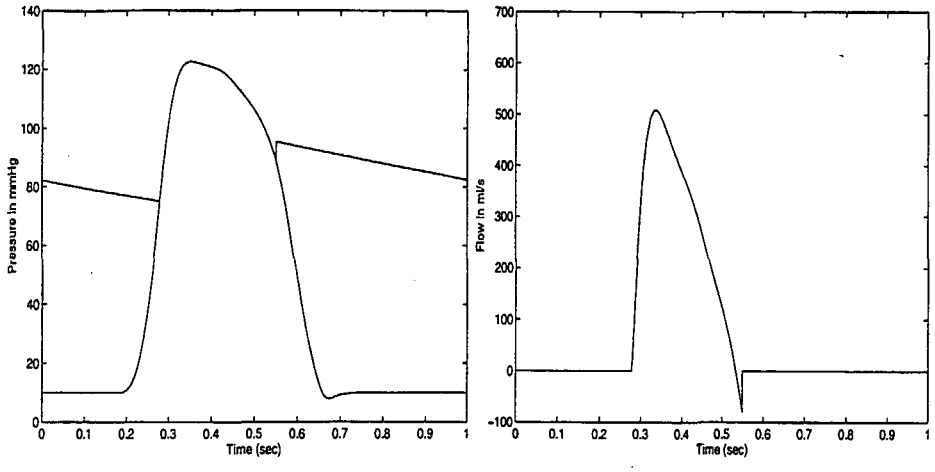

Figure 3.7: The left panel shows arterial and ventricular pressures, p_a and p_v computed for a normal human ventricle with the ejection effect (3.14) and the arterial load of Figure 3.2. The right panel shows the corresponding ventricular outflow. The parameter values of the ejection effect and the ventricle can be found in table 3.4. End-diastolic volume $V_{ed} = 125$ ml, stroke volume is $SV = 77$ ml, the ejection fraction $EF = 0.62$ and heart rate $H = 1$ Hz.

Table 3.1: Typical values of the human ventricle (Noordergraaf, 1978) and model computed values are shown in central columns, respectively. The time interval Δt_{pres} is measured between the 20 mmHg levels of the ventricular pressure during ejection. The duration of the systole is Δt_s, Δt_p the time to develop peak flow, p_s peak systolic pressure and p_d is the end-diastolic pressure.

Type	*Human Values*	*Model Values*	*Units*
Δt_{pres}	400	407	ms
Δt_s	275	272	ms
Δt_p	70	52	ms
p_s	120	123	mmHg
p_d	80	75	mmHg

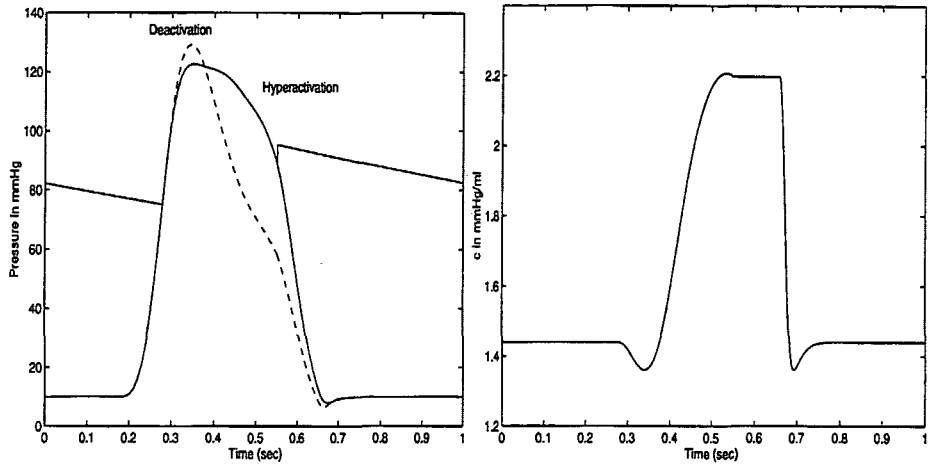

Figure 3.8: The left panel shows arterial and ventricular pressures with the ejection effect (full line) and without ($\bar{c}(x) = 0$ in (3.16), shown by dashed line). The time course of $c(x)$ during one heart beat is shown in the right panel for the parameters given in table 3.4.

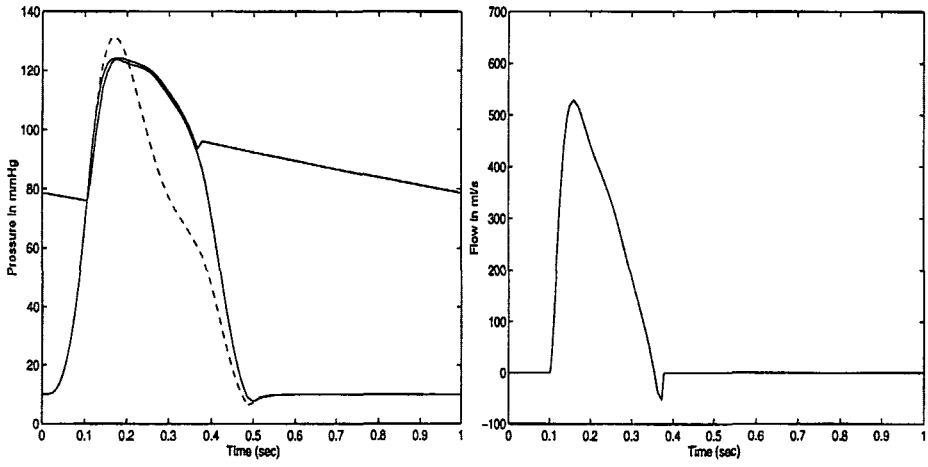

Figure 3.9: The left panel shows arterial pressure p_a and ventricular pressure p_v obtained using (3.12)-(3.13) with the inductance $L_v = 0.000416$ (fully drawn lines). The computed pressure without the ejection effect is shown with dashed lines. The right panel shows the corresponding flow Q_v. The parameters of the ejection effect can be found in table 3.5.

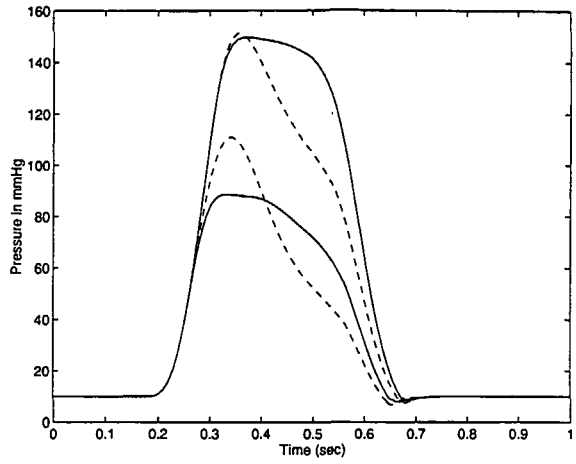

Figure 3.10: The upper and lower curves show the ventricular pressures with (full lines) and without the ejection effect (dashed lines) when the peripheral resistance is $2R_s$ and $\frac{R_s}{2}$, respectively. Deactivation is only slightly present whereas hyperactivation is present most of the systole when the peripheral resistance is $2R_s$. Deactivation is accentuated and hyperactivation diminished when the peripheral resistance is $\frac{R_s}{2}$ compared to the situation in Figure 3.7.

ventricular flow Q_v. This is shown in Figure 3.10 where deactivation is accentuated by high ventricular outflow when peripheral resistance equals $\frac{R_s}{2}$, and diminished by low ventricular outflow, peripheral resistance $2R_s$. The hyperactivation follows the opposite track and is more pronounced when the peripheral resistance equals $2R_s$ and vice versa. Figure 3.11 shows that hyperactivation is diminished compared to the normal situation in Figure 3.10 when the ventricle ejects into a reflection free afterload. But hyperactivation is still significantly present and the computations show that physiological curves cannot be obtained without hyperactivation.

Any perturbation of the vasculature or the ventricle implies changes in the parameters of the ejection effect. Perturbations can be manifested by non-physiolo/-gical pressure curves as shown in the left hand side of Figure 3.12 where the peripheral resistance R_s is changed to $2R_s$ and $\frac{R_s}{2}$ respectively with no alterations in the parameters of the ejection effect. On the right hand side of Figure 3.12 the parameters γ, β_1 and β_2 of the ejection effect are adapted and the curves are clearly more representative for the human ventricle. These alterations in the parameters may be guided by neural, hormonal and other effects affecting the interaction between ventricle and vasculature. The ventricular model (3.6) offers a separation between ventricle and vasculature whereas the complex interaction between the heart and the vasculature is addressed by the ejection effect.

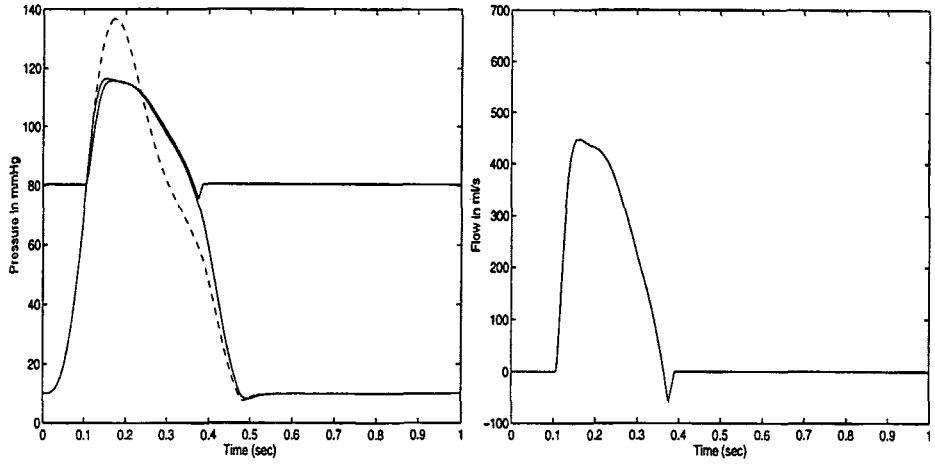

Figure 3.11: The left panel shows the ventricular pressure p_v and the arterial pressure p_a (full lines) when the ventricle ejects into a reflection free afterload (compliance equals $100C_s$). The calculated pressure p_{cal} is shown by dashed lines. The solution is obtained using (3.12)-(3.13) with $L_v = 0.000416$ mmHg s^2/ml. All other parameters can be found in table 3.2. The parameters of the ejection effect are listed in table 3.5. The case with $L = 0$ shows increased hyperactivation.

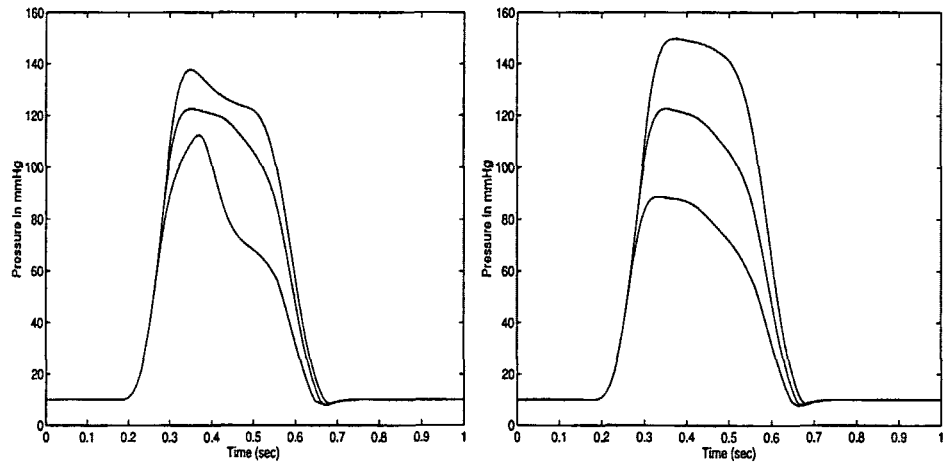

Figure 3.12: The left panel shows the ventricular pressure for different values of the peripheral resistance $2R_s$, R_s and $\frac{R_s}{2}$ when the parameters of ejection effect are unaltered. The right panel shows the same case but when the parameters of the ejection effect are adjusted to the new arterial load. The parameter value for γ, β_1 and β_2 are given in table 3.5.

3.6 Alternative Models of the Ejection Effect

(Mulier, 1994) offered the first attempt to include deactivation mathematically in the model (3.6). (Mulier, 1994) considered deactivation as an independent mechanism modeled by

$$p_d = \alpha_d(\dot{V}_v)^2 \tag{3.17}$$

such that ventricular pressure is given by

$$p_v(V_v, Q_v, t) = p_v(V_v, t) - \alpha_d Q_v^2,$$

where the constant α_d represents the strength of deactivation. Hyperactivation was assumed to be caused by reflections. According to (Mulier, 1994) deactivation is then related to flow alone and claimed not to alter the fundamental parameters of the model (3.6). We model the ejection effect above by relating the parameter c, which is directly connected to the contractile properties of the ventricle, to volume V_v by using (3.14). As (3.17) holds, the difference between the predicted pressure during ejection and its measured counterpart should be related to the cumulative effect of measured flow Q_v $(= -\frac{dV_v}{dt})$, since correction for ventricular volume $V_v(t)$ itself is incorporated by the Frank mechanism in the ventricular model (3.6). Regarding the ejection effect we can thus emphasize that:

- Deactivation should be related to ventricular outflow via Hill's force-velocity relation (or pressure-flow relation).
- Hyperactivation should be related to the formation of new bonds and cycling of bonds.

As an alternative to the volume based model (3.14), following the strategy above, the ejection effect can be related to outflow Q_v $(= -\frac{dV_v}{dt})$ during ejection and volume V_v during diastole by modification of the parameter c in (3.6) according to

$$c(Q_v, x) = \begin{cases} c - \alpha_1 Q_v, & 0 < t \leq t_{Q_{max}} \\ c - \alpha_1 Q_v + \alpha_2(Q_{max} - Q_v), & t_{Q_{max}} < t \leq t_{es} \\ c - [\alpha_1 Q_{min} + \alpha_2(Q_{max} - Q_{min})]\cos(\frac{x - x_{es}}{a}), & t_{es} < t \leq t_h, \end{cases}$$

where t_{es} is time for end of systole and $x_{es} = \frac{V_{ed}}{V_{es}}$ with V_{es} as end-systolic volume. The terms Q_{max} and Q_{min} are maximum and minimum of ventricular outflow Q_v during ejection, respectively. The computed root aortic pressure and ventricular outflow are shown in Figure 3.13 when the model (3.6), including the ejection description above, is coupled to the modified Windkessel model in Figure 3.2. Both pressure and flow curves are clearly representative for the normal human ventricle and in close agreement with curves found in (Guyton, 1991; Noordergraaf, 1978).

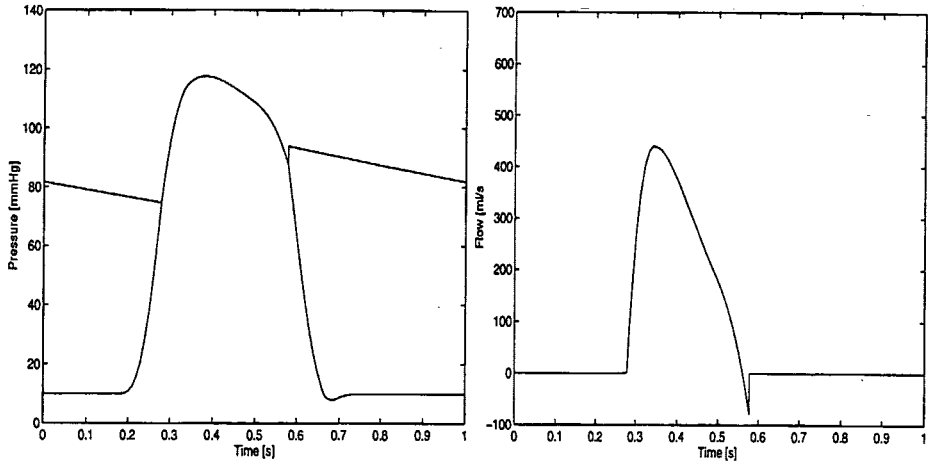

Figure 3.13: The left panel shows the ventricular pressure p_v and root aortic pressure p_a for a normal human ventricle with the ejection effect correction (3.18) and the arterial load of Figure 3.2. The right panel shows the corresponding ventricular outflow Q_v. The parameter values of the ejection effect and the ventricle can be found in Table 3.6. End-diastolic volume V_{ed} is 125 ml, stroke volume is $SV = 76$ ml, the ejection effect $EF = 0.61$ and heart rate $H = 1$Hz.

Another approach to the modeling of the ejection effect, which is attractive from the point of view of identification of physiological mechanisms, may be to return to the functions on which the isovolumic pressure function was built. The second term on the right hand side of (3.1) corresponds to systolic pressure generation. The generating function g is shown in Figure 3.1 and includes the product of two exponential functions. The first

$$(1 - e^{-(\frac{t}{\tau_c})^\alpha})$$

describes the pressure increase resulting from crossbridge bond formation. The second

$$e^{-(\frac{t-t_d}{\tau_r})^\alpha}$$

describes the pressure decrease resulting from crossbridge bond detachment. The hypothesis is that the two sigmoidal functions of Figure 3.2 are modified by both pressure deactivation and hyperactivation. Consequently, the function g and the relevant parameters would be somewhat different from the isovolumic ones as is the case for the parameter c via (3.14). This will be the topic of the work in the near future. A fundamental different modeling approach to the ejection effect will be taken, based on shifting of energy along the time axis. The approach takes the effect of flow into account and can briefly be described as follows. The ventricular pressure drops due to ejection compared with a non-ejecting ventricle. A recover

of the energy here will then start. The recovery will follow the pattern of the isovolumic pressure curve. The entire recovery will be represented by a complex sum of isovolumic pressure curves each representing a small amount of volume ejected. The approach in this chapter fails to describe the observed recovery of pressure after quick withdrawals of volume during an otherwise isovolumic contraction. This is due to the fact that model of the ejection effect only allows c to vary when the ventricular volume varies. The new approach may be tested against these experiments.

3.7 Summary

The ventricular model (3.6), based on the Frank mechanism, was shown to include Starling's two observations and thus disqualifies Starling's law as an independent mechanism. The addition of the ejection effect to the model (3.6) by expanding the model parameter c, directly related to the ventricle's contractile state, from a fixed value to a function of instantaneous ventricular volume broadens the range of the description of the left ventricle. The results suggest that ventricular ejection directly changes the underlying muscle contraction process and that the ventricle is influenced by alterations in the vascular parameters. The ejection effect cannot be explained by smaller effects alone, as inertial effects of ventricular blood and vascular reflections, though they contribute in the right direction.

Alternative approaches to the modeling of the ejection effect should be related to the ventricular outflow Q_v since the correction for volume is incorporated by the Frank mechanism. Deactivation should be modeled as detachments of bonds via Hill's force-velocity relation and hyperactivation as formation of new and cycling of crossbridge bonds.

The model (3.6) shows the principal features when coupled to a closed model of the human cardiovascular system including expected response to preload and afterload changes (Palladino, Ribeiro and Noordergraaf, 1998). Gratifying as this may be, we encounter at least two practical problems if we extend the model to real world applications. Firstly, the heart rate is not easily changed due to the exponential functions in (3.1). Secondly, the pressure and flow curves differ from the normal human curve profiles without the ejection effect. The ejection effect can correct these deficiencies but the parameters depend on the prevailing conditions in the vasculature and on neural effects. This dependence is not mathematically formulated. But this practical view has not been the purpose with the modeling. The modeling interest is directed towards the physiological mechanisms behind the ejection effect. Identification of the mechanisms involved may emerge in the future from new animal experiments.

3.8 Tables with parameter values

Table 3.2: The parameters for the constant pressure reservoir p_r and the 3-element modified Windkessel model in Figure 3.2.

Parameter	*Value*	Units
p_r	10	mmHg
R_0	0.08	mmHg s/ml
C_s	2.75	ml/mmHg
R_s	1.125	mmHg s/ml
R_{in}	0.001	mmHg s/ml

Table 3.3: Parameters for the model (3.6). Figure 3.3 shows the corresponding pressure and flow curves when the model is coupled to the arterial load in Figure 3.2.

Parameter	*Value*	Units
a	0.0007	mmHg/ml
b	5	ml
c	1.6	mmHg/ml
d	1	mmHg
τ_c	0.225	s
τ_r	0.285	s
t_p	0.375	s

Table 3.4: The parameters for the ventricular model (3.16) with the ejection effect. Figure 3.7 shows the corresponding pressure and flow curves when the ventricular model is coupled to the Windkessel model in Figure 3.2.

Parameter	*Value*	*Units*
a	0.0007	mmHg/ml
b	5	ml
c	1.44	mmHg/ml
d	1	mmHg
τ_c	0.13	s
τ_r	0.13	s
t_p	0.3	s
α	2.88	
γ	3.8	mmHg/ml
β_1	3.3	
β_2	1.8	

Table 3.5: The parameters for the ejection effect for varying peripheral resistances $\frac{R_s}{2}$, R_s, $2R_s$ produce the curves given on the right hand side of Figure 3.12. The parameters in the case of the inductance L give the curves in Figure 3.6. The case of no reflection (L & $100C_s$) are shown in Figure 3.11.

Value	γ	β_1	β_2
$\frac{R_s}{2}$	3.2	4.5	1
R_s	3.8	3.3	1.8
$2R_s$	3.1	4.6	3.175
L	3.7	3.5	1.85
L & $100C_s$	2	10	1.7

Table 3.6: The parameters for the ventricular model (3.16) with the ejection effect (3.18). Figure 3.13 shows the corresponding pressure and flow curves when the ventricular model is coupled to the Windkessel model in Figure 3.2.

Parameter	*Value*	*Units*
a	0.0007	mmHg/ml
b	5	ml
c	1.44	mmHg/ml
d	1	mmHg
τ_c	0.13	s
τ_r	0.13	s
t_p	0.3	s
α	2.88	
α_1	0.0005.3	mmHg s/ml^2
α_2	0.003	mmHg s/ml^2

Part II

Modeling the Human Cardiovascular System and the Baroreceptor Mechanism with Reference to an Anesthesia Simulator

Chapter 4

A Cardiovascular Model

"The blood current flows continuously in a circle and never stops . . . The blood cannot but flow continuously like current of a river, or the sun and moon in their orbits. It may be compared to a circle without beginning or end . . . The blood travels a distance of three inches during inhalation and another three inches during exhalation, making six inches with one respiration.". This can be found in *Neiching* from ancient China 1000 BC which is thought to be written by the Yellow Emperor, Huang Ti (Acierno, 1994). In addition, the *Neiching* consider the heart as repository for the pulse and energy that stems from the lungs.

The blood flows in the human cardiovascular system with the pumping heart as the driving force as explained by William Harvey in 1628. The heart was studied in the previous Chapters 2 and 3. The goal of this chapter is to present our model of the human cardiovascular system. We establish a lumped pulsatile cardiovascular model which embraces the principal features of the human circulation and is based on available physiological data found in the literature. The model is partially based on the human circulatory model by (Rideout, 1991). The major differences between the two models are outlined in Section 4.3.5. The model provides

- ventricular pressure, root aortic pressure and ventricular outflow curves which closely resemble the corresponding human ones found in the literature.

- three arterial and two venous pressure and volume levels in both the systemic and the pulmonary circuit of the human circulation.

Preceding the description of the cardiovascular model, Section 4.1 gives an elementary introduction to the physiology of the cardiovascular system. We focus on the cardiovascular system as a transport system and conclude with an overview of the pressure and volume distribution in the system. Section 4.2 introduces the major modeling approaches used to describe the impedance of the arterial tree

and the overall function of the cardiovascular system in terms of pressure and flow. The human circulation model is established in Section 4.3. The heart and the vasculature is described in Sections 4.3.1 and 4.3.2. The vascular pressure and volume distribution are given in Section 4.3.3 which also reveals the strategy used to determine the parameter values in the cardiovascular model. Computed results are given in Section 4.3.4 and a summary is found in Section 4.4. The differential equations comprising the cardiovascular model are quantified in Section 4.5. All the parameter values are stated in Section 4.6.

The cardiovascular model is an integrated part of the SIMA project. We have developed two cardiovascular models. One of the models is used in a commercial anesthetic simulator developed by the SIMA group. Thus, the cardiovascular model is a part of a complex environment in which the model interacts with a number of other models describing different physiological processes. This imposes a range of requirements on the model. In addition to the principal features listed above, the simulator has to run in real time which generates concerns about computational speed and, in turn, adds restrictions to the complexity of the model. Hence, the cardiovascular model in the simulator must be simple. In essence, a lumped or Windkessel type of model of the cardiovascular system is perfectly suitable. The requirement to the computational speed is related to the variety of different models in the simulator which are shown in Figure 4.1. The simulator contains a *pharmacokinetic model* which contains information about the concentration of anesthetic drugs in the blood, tissue and major organs. The *pharmacodynamic model* contains a statistically based model of the correlation between drug concentrations and alterations in e.g. heart and brain. In addition, the simulator contains a *respiratory* as well as a *metabolic model.* The former describes transport of oxygen and carbon dioxide in the body and the latter computes carbon dioxide concentrations and controls production of heat. A fluid and electrolyte balance model accounts for the volumes of plasma, protein, electrolytes and distribution of body fluids. The simulator contains also an *EKG model* and a *temperature model.* Moreover, a *baroreceptor model* is integrated in the simulator. This model accounts for the short term nervous control by the central nervous system. We will present this model as a whole in Chapter 6.

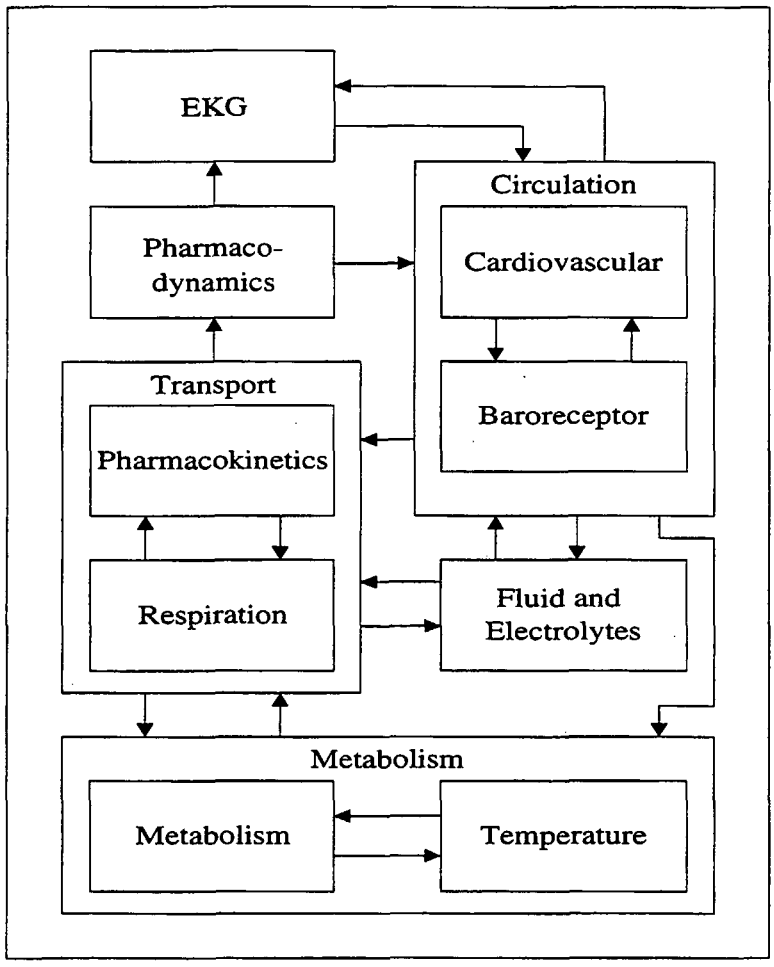

Figure 4.1: The different models in the SIMA simulator. Adopted from (Olufsen et al., 1998).

4.1 The Cardiovascular System

The human cardiovascular system with its complex branching exhibits major changes along the closed circulation path as shown in Figure 4.2. The system consists of two separate parts, the systemic and the pulmonary circuit, which are connected via the left and right heart chambers as shown in Figure 4.3. The cardiovascular

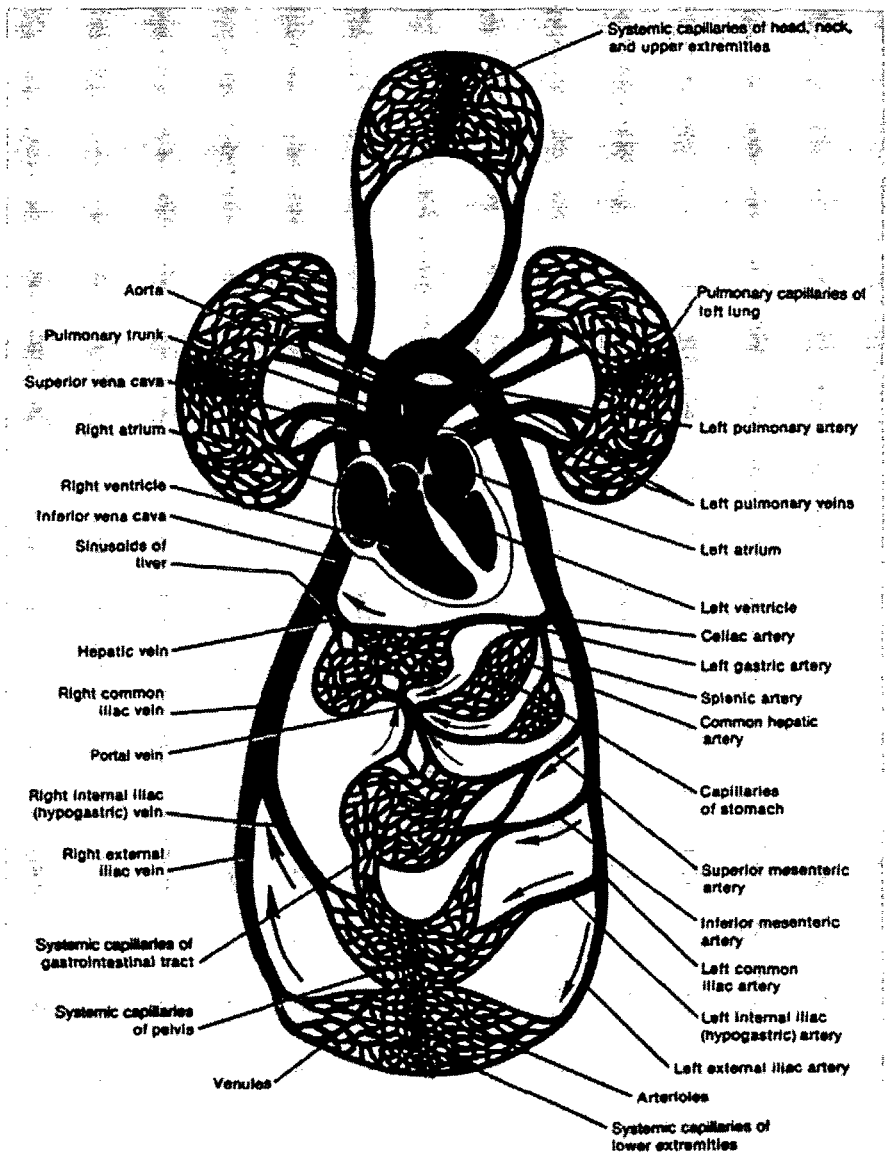

Figure 4.2: The human cardiovascular model. Adapted from (Tortora and Anagnostakos, 1990).

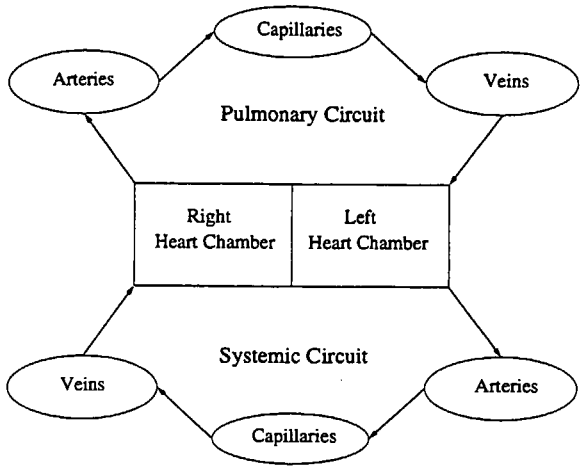

Figure 4.3: The cardiovascular circuit consists of a systemic and a pulmonary system which are separated by the heart. Both circuits are divided into an arterial and a venous part connected via the capillaries.

system is primarily a transport system. Oxygen, carbon dioxide and nutrients to the various tissues are carried by the blood which circulates in the closed human cardiovascular system. Oxygenated blood is transported from the lungs through the left heart chamber to the tissues in the systemic circuits. Simultaneously, carbon dioxide is returned from the tissues and transported via the right heart chamber to the pulmonary circulation where carbon dioxide leaves the blood and the partly deoxygenated blood receives oxygen from the alveolar air. The nearly fully oxygenated blood is then carried to the left heart chamber and thus makes a full circle when blood is ejected into the systemic circuit. In addition, blood carries fluids, hormones, nutrients, electrolytes and other agents. By diffusion, these substances are exchanged between blood and fluid in the tissue cells, mediated by the extracellular fluids. Moreover, the circulation participates in control of the temperature by transporting heat to the body surface.

The left ventricle pumps blood into the high pressure areas constituted by the aorta and the arteries of the systemic system. The aorta and its main branches have highly elastic properties. These areas are followed by the arterioles which have less elastic tissue and cause blood pressure to drop. The walls of the arterioles contain more smooth muscle than the walls of the aorta and its primary branches. The blood flow encounters considerable resistance to flow in the arterioles controlled by the degree of muscle constriction which can be significant. This muscular region is followed by the capillaries which contain no muscles. The capillaries are the area where nutrients are exchanged between blood and tissue cells. The level of branching of the vessels reaches its maximum in the capillaries

and the region has a very high surface area as indicated in Figure 4.2. The capillary vessels discharge their blood into the venules and larger veins. The veins are low pressure vessels and their vessel walls have low elastic properties. The latter makes the veins ideal for the storage of blood. Large volume alterations are archived without significant pressure changes in the veins. The veins contain muscles which allow mobilization of volume to other parts of the cardiovascular system. From the systemic veins the blood is returned to the right heart chamber from which it enters the pulmonary circuit. The pulmonary circuit manifests the same organization as described above and will not be discussed in greater detail.

The systemic and pulmonary circuits exhibit significant differences in terms of pressure levels and the amount of blood volume contained. The pressure level in both circuits are shown in Figure 4.4. In addition, the figure shows the approximate peak to peak pressures and average pressures in different locations of the cardiovascular system. The maximum and minimum pressures in the systemic aorta are approximately 120 and 80 mmHg, respectively. The corresponding pressures in the pulmonary arteries are 30 and 10 mmHg. The veins exhibit low pressures. The pressure in the venules tends to be 10 mmHg with very small oscillations. The oscillations in the pulmonary veins is shown to be more profound with a maximum pressure around 15 mmHg. The amount of volume in the pulmonary circuit is approximately 15 % of the total amount whereas the same figure is 75 % for the systemic circuit as shown in Table 4.1. The systemic veins alone contain around 55 % (Guyton, 1991; Ganong, 1975).

Table 4.1: The volume distribution in the cardiovascular system relative to the total amount (Ganong, 1975; Noordergraaf, 1978) left column. The computed values using the cardiovascular model is given in the right column.

Location	*Volume*	*Computed*
Systemic Arterial	20	25.4
Systemic Venous	54	58.8
Pulmonary Vasculature	14	8.4
Heart	12	7.4

4.2 Architecture of Cardiovascular Models

The mathematical formulations of the cardiovascular system may be divided into two classes of models, distributed and lumped. In the former, arterial pressure and flows may be described by use of partial differential equations or by spatial

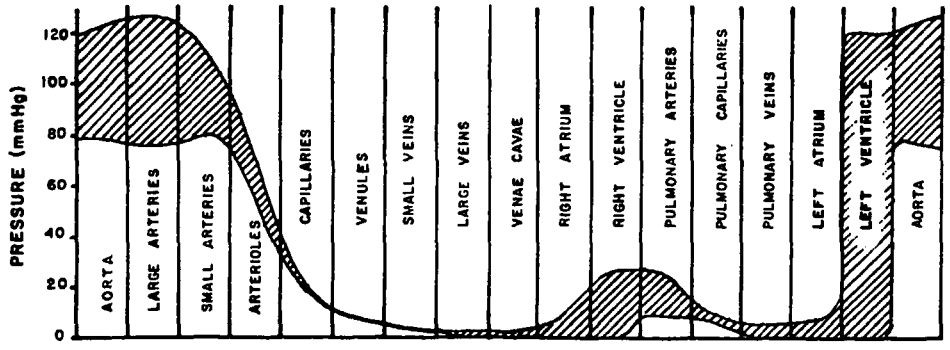

Figure 4.4: The pressure distribution in the human cardiovascular system. Adapted from (Noordergraaf, 1978).

models based on ordinary differential equations. Both approaches account for the detailed geometry of the vessels. In distributed models, the arterial tree may be divided into a number of segments. The viscous and inertial effects of blood in each segment are represented by a resistance R and an inductance L, respectively. The parameters are computed according to the corresponding vessel radius, viscosity and density of the blood and length of the segment. Calculation of the elastic properties may in addition require Young's modulus of elasticity. The elasticity is represented by the compliance C which is the reciprocal of the elastance. This class of models can be used to study the input impedance as seen by the heart, wave travel and wave reflections (Olufsen, 1998; Westerhof and Stergiopulos, 1998). Models based on random length distribution of the segments, and thus not on the real anatomy, have been shown to exhibit the same wave travel and impedance features as distributed models (Noordergraaf, 1978; Westerhof and Stergiopulos, 1998). Further details of these three types of models may be found in (Noordergraaf, 1978; Peskin, 1976; Pedley, 1980; Rideout, 1991; Olufsen, 1998; Westerhof and Stergiopulos, 1998).

Along another avenue we find the lumped models where the anatomical details are abandoned. An example is the modified Windkessel model in Figure 4.5. Although strikingly simple, the model gives a very good description of the input impedance of the arterial system (Toy, Melbin and Noordergraaf, 1985; Westerhof and Stergiopulos, 1998). Thus, ventricular models may be coupled to a modified Windkessel model to obtain a description of the arterial load as we did in Chapter 3. The entire human cardiovascular system may be described by a network of compliances, resistances and inductances not reflecting anatomical properties. These types of models exhibit the major features of their real counterpart as higher pressure in response to vessel constrictions, root aortic pressure and ventricular outflow curves representative for the human. In addition, phenomena with low

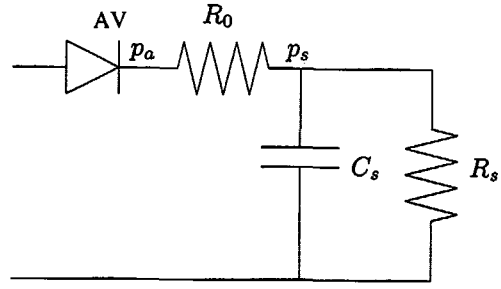

Figure 4.5: The 3-element modified Windkessel arterial load. This model is characterized by a characteristic aortic impedance R_0, a total peripheral resistance R_s and a total arterial compliance C_s. The aortic valve is indicated (AV).

frequency content, as Mayer waves, may also be studied (Ottesen, 1997a; Ursino, 1998). The cardiovascular models can be coupled to mathematical descriptions of nervous control to study effects of the central nervous system on the human circulation. In this case lumped models may be used to study the impact of the venous reservoir during hemorrhages (Ursino et al., 1994; Danielsen and Ottesen, 1997) or the effect of halothane on nervous regulation (Tham, 1988). Our knowledge of the complex impact of the central nervous system on the overall performance of the cardiovascular system is still limited and thus lumped models may be perfectly suitable. Lumped cardiovascular models may be roughly divided into two classes. The first class contains the non-pulsatile models where the heart is described by some variant of "Starling's law" as (2.5)-(2.7) in Section 2.3.3 of Chapter 2. The second class contains the pulsatile models. When pulsatility is included the heart is typically guided by a time-varying elastance function as described in Section 2.3.1 of Chapter 2. One exception is (Palladino, Ribeiro and Noordergraaf, 1998) where the ventricular model by (Mulier, 1994) is applied to a closed human circulation. Otherwise, models following the above lines of thinking include (Warner, 1958; Warner, 1959; Grodins, 1959; Beneken, 1965; Leaning, Pullen, Carson and Finkelstein, 1983; Leaning, Pullen, Carson, Al-Dahan, Rajkumart and Finkelstein, 1983; Martin et al., 1986; Tham, 1988; Rideout, 1991; Jin and Qin, 1993; Neumann, 1996; Sun, Beshara, Lucariello and Chiaramida, 1997; Danielsen and Ottesen, 1997; Ursino, 1998; Palladino, Ribeiro and Noordergraaf, 1998; Ottesen, 1998). Selection of the modeling approach is dictated by the problem at hand. The human circulatory model will be coupled to a model of the nervous control in Section 6.4 of Chapter 6. This accentuates the use of a simple approach considering the limited knowledge of the explicit interaction between the central nervous system and the cardiovascular system. Section 4.3 below introduces the cardiovascular model of the human circulation.

4.3 Cardiovascular Model

The pulsatile human circulation model is shown in Figure 4.6 which is partially based on the model by (Rideout, 1991). The model consist of a pumping heart

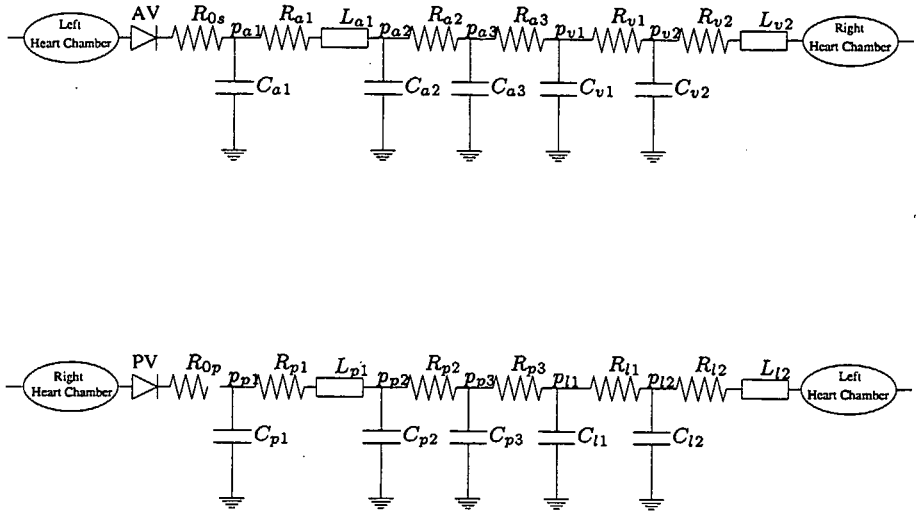

Figure 4.6: The human circulation model. The cardiovascular model consists of a pumping heart, a systemic (top part) and a pulmonary circuit (lower part). The left and right heart chambers are shown in Figure 4.7. The systemic arterial system is described by three sections and the systemic venous consists of two sections. The pulmonary circulation follows the same architecture. Variables and parameters are explained in the text. Parameter values can be found in tables 4.5 and 4.7. Pressure and volume distributions are given in Table 4.2.

coupled to a lumped description of the systemic and the pulmonary circulation. The ventricles are described by a pair of time-varying elastance functions whereas the two atrias are purely passive chambers as shown in Figure 4.7. The four heart valves are indicated in the figure. The aortic and pulmonary valves are designed to allow a small amount of volume to flow back into the left and right ventricles from the vasculature before closure is completed. When the left ventricular pressure exceeds root aortic systemic pressure p_{as} the aortic valve (AV) opens and blood flows through the characteristic systemic resistance R_{0s} into the arterial systemic consisting of three sections. The pressures in the arterial system include the root aortic pressure p_{as} and three pressures p_{a1}, p_{a2} and p_{a3}. The veins are described by two sections with the pressures p_{v1} and p_{v2}. The veins return the blood to the passive right atria. When right atrial pressure p_{ra} exceeds right ventricular cavity pressure p_{rv} the tricuspid valve (TV) opens and the right ventricle is filled through the filling resistance R_{ra}. Subsequently, blood is ejected into the pulmonary cir-

cuit through the pulmonary valve (PV) and characteristic pulmonary resistance R_{0p}. The architecture of the pulmonary circuit is a replica of the systemic one. The pressure and volume levels in each section and the corresponding physiological locations of the sections, determined by the average pressures, can be found in Table 4.2.

4.3.1 Heart

The model of the pumping heart is shown in Figure 4.7. The cardiac contractile

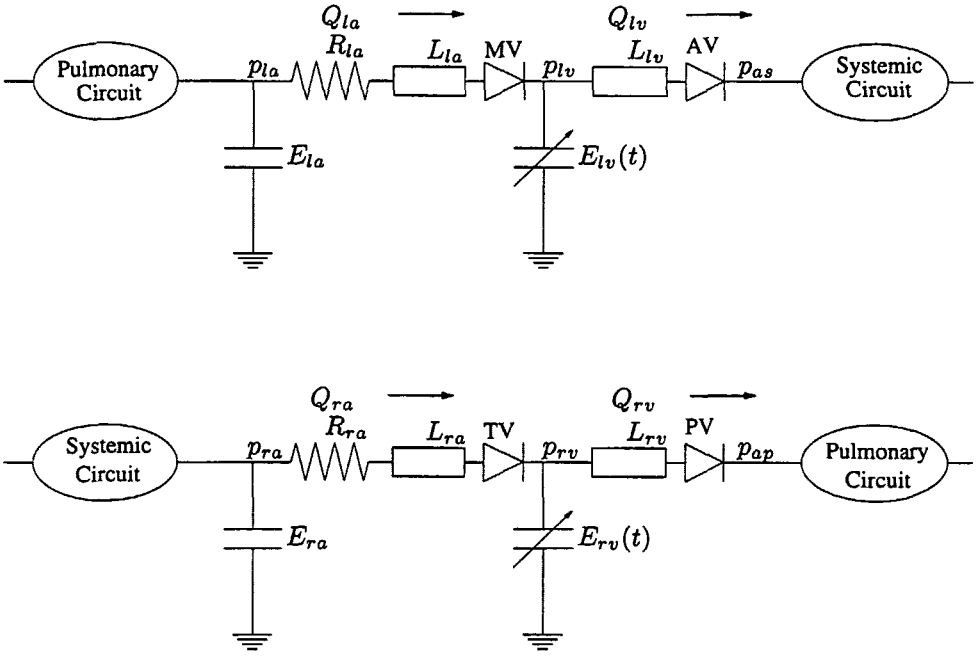

Figure 4.7: The upper and lower panels show the left and the right heart chambers of the cardiovascular model in Figure 4.6, respectively. Each side of the heart consists of a passive atria and an active ventricle. The left atrium is modeled by a constant elastance E_{la} while the performance of the left ventricle is described by a time-varying ventricular elastance function $E_{lv}(t)$ given by (4.2). The inertial properties of the blood are included by inductances L_{lv} and L_{la}. The viscous properties of blood are included by the left atria filling resistance R_{la}. The right heart is described in a similar fashion. The mitral and aortic valves are denoted by MV and AV, respectively. The tricuspid valve and pulmonary valve are denoted by TV and PV, respectively.

properties of the two ventricles are assumed to be defined by a pair of time-varying elastance functions. The inertia of blood movements in the ventricles are included by inductances which introduce a phase shift between ventricular pressure and the root aortic pressure. The viscous properties of blood in the two atrias are included

by ventricular filling resistances, R_{la} and R_{ra}, respectively. The relation between left ventricular cavity pressure p_{lv} and ventricular volume V_{lv} is described by

$$p_{lv} = E_{lv}(t)(V_{lv} - V_{d,lv}), \tag{4.1}$$

where $V_{d,lv}$ is left ventricular volume at zero pressure. The elastance function $E_{lv}(t)$ in (4.1) is given by

$$E_{lv}(t) = E_{min,lv}(1 - \phi(t)) + E_{max,lv}\phi(t), \tag{4.2}$$

where

$$\phi(t) = \begin{cases} a_\phi \sin\left(\frac{\pi t}{t_{ce}}\right) - b_\phi \sin\left(\frac{2\pi t}{t_{ce}}\right) & \text{for } 0 \leq t < t_{ce} \\ 0 & \text{for } t_{ce} \leq t \leq t_h \end{cases} \tag{4.3}$$

The parameters $E_{min,lv}$ and $E_{max,lv}$ are minimal diastolic and maximal systolic values of the left ventricular elastance function, respectively, t_h heart period and t_{ce} time for onset of constant elastance.
The relation between heart period t_h and t_{ce} is given by

$$t_{ce} = \kappa_0 + \kappa_1 t_h, \tag{4.4}$$

where κ_0 and κ_1 are constant parameters (Rideout, 1991).

When the aortic valve is open, the root aortic systemic pressure p_{as} then relates to ventricular outflow Q_{lv}, left ventricular cavity pressure p_{lv} and ventricular volume V_{lv} by

$$\begin{aligned} \frac{dQ_{lv}}{dt} &= \frac{1}{L_{lv}}(p_{lv} - p_{as}), \\ \frac{dV_{lv}}{dt} &= -Q_{lv}. \end{aligned}$$

When the aortic valve is closed

$$Q_{lv} = 0.$$

We allow an amount of volume $V_{lv,b}$ to flow back into the left ventricle before complete closure of the aortic valve. The maximum volume we allow to flow back into the left ventricle is denoted by $\tilde{V}_{lv,b}$. When $V_{lv,b}$ exceeds the volume $\tilde{V}_{lv,b}$, the valve closes. The right ventricle is given by a similar description. Both the left and right atria follow the architecture above. However, the atria are passive and described by constant elastances, E_{la} and E_{ra}, respectively. In addition, ventricular volume cannot flow in direction from the ventricle to the atria. The mathematical formulations are given in Section 4.5. Parameter values for both heart chambers can be found in tables 4.4 and 4.6.

4.3.2 Vasculature

The structural pattern of the cardiovascular model of Figure 4.6 follows the architecture of many previous cardiovascular descriptions and may only differ by the number of sections used to characterize the systemic and the pulmonary circuits. The model in Figure 4.6 is divided into ten sections with different pressure and flow levels. The systemic arteries are described by three sections and the systemic veins are characterized by two. The pulmonary circuit follows the same architecture. Each section may contain three components, a viscous loss term R_j, an inertial term L_j and a term describing the elastic vessel properties represented by the compliance C_j which is the inverse to the elastance. The index j denotes the particular section. The mathematical relation between vascular pressure and volume in each section amounts to three equations characterizing motion, conservation of mass and state of the system. Hence, the arterial pressure p_{a1}, flow Q_{a1} and volume V_{a1} in the first section of the cardiovascular model in Figure 4.6 are being described by the following three equations which follow the pattern by (Warner, 1959):

1. An equation of motion

$$p_{a1} - p_{a2} = R_{a1}Q_{a1} + L_{a1}\frac{dQ_{a1}}{dt}. \tag{4.5}$$

2. An equation for the conservation of mass

$$\frac{dV_{a1}}{dt} = Q_{lv} - Q_{a1}, \tag{4.6}$$

   where Q_{lv} is left ventricular outflow

3. A state equation

$$p_{a1} = \frac{1}{C_{a1}}(V_{a1} - V_{un,a1}). \tag{4.7}$$

By (4.7) we assume that the elastic vessel properties are independent of the vascular pressure levels in each section. Thus, we have adopted a linear relation between pressure and volume. This may be justified for the arteries but the relation is non-linear in the veins (Ganong, 1975; Noordergraaf, 1978). The parameter $V_{un,a1}$ in (4.7) is the unstressed volume which is defined as the volume at zero pressure. The vessels collapse when the volume falls below the unstressed volume and the elastic vessels exhibit highly non-linear properties (Ganong, 1975; Noordergraaf, 1978; Guyton, 1991).

The entire system of ordinary differential equations which comprises the human circulation model is given in Section 4.5. Parameter values of compliance, resistances and inductances can be found in tables 4.5 and 4.7.

4.3.3 Determination of Parameter Values

The selection of cardiovascular parameter values in the human circulation model is guided by data available in the literature. The goal is to obtain realistic average pressure levels and volume distribution in the system. In addition, computed ventricular pressure, root aortic pressure and outflow curves should closely resemble the corresponding human ones.

The strategy we use to achieve the goals may be comprised into two steps:

1. The desired average pressure and volume distribution and cardiac output determine the parameter values of compliances and resistances.

2. Inductances and elastance functions are subsequently assigned values that produce representative pressure and flow pulses.

Iterations between the two items are inevitable in determining the final parameter values.

We follow this strategy by first determining the pressure and volume distribution in the model. To this end, pressure and volume average levels for each section are shown in Table 4.2. The volume in each section is divided into a stressed and an unstressed component. The fraction between the unstressed and the stressed components is called n. The separation between the two types of volume is guided by pressure-volume curves for the vasculature. Since the number of sections in the cardiovascular model is not chosen in accordance with anatomical divisions, it is not surprising that the values of n vary among different lumped cardiovascular models (Beneken, 1965; Tham, 1988; Ursino et al., 1994). We have adopted a set of average values of n based on pressure-volume curves found in (Schmidt and Thews, 1976; Guyton, 1991).

Parameters values of compliances, resistances and inductances for the systemic and pulmonary circuits of the cardiovascular model of Figure 4.6 are given in tables 4.5 and 4.7, respectively.

The parameters of the left ventricle are κ_0, κ_1, $E_{min,l}$, a_ϕ, b_ϕ, $E_{max,l}$ and L_{lv}. The values for κ_0 and κ_1 in (4.11) of the elastance function are chosen in order to obtain systolic and diastolic time periods in close agreement with standard human pressure and flow profiles found in (Noordergraaf, 1978; Guyton, 1991). Minimal elastance $E_{min,l}$ provides ventricular filling, and maximal elastance $E_{max,l}$, constants a_ϕ and b_ϕ and inductance L_{lv} are chosen in order to obtain proper pressure and flow curves. The left ventricular elastance function (4.2) is shown in Figure 4.8.

Table 4.2: Average pressure and volume distribution among the vascular sections in the cardiovascular model. The first column specifies each section by its corresponding pressure as defined in the figures 4.6 and 4.7. The fraction between unstressed and stressed volume is denoted by n. The approximate physiological location is shown in the last column. The total volume is 5139 ml.

Section	*Pressure (mmHg)*	*Volume (ml)*	n	*Location*
				Systemic
p_{a1}	91.6	276	2.9	Large arteries
p_{a2}	84	507	2.7	Small arteries
p_{a3}	67.9	524	3.3	Arterioles
p_{v1}	7.3	693	6.2	Venules
p_{v2}	5.3	2328	5.0	Small veins
				Pulmonary
p_{p1}	18.7	91.4	1.2	Arteries
p_{p2}	16.6	55	1.2	Arteries
p_{p3}	11.8	74	2.6	Capillaries
p_{l1}	8.3	105.4	2.5	Veins
p_{l2}	6.0	105	2.5	Veins
				Heart
p_{ra}	2.9	78	0.6	Right atrium
p_{la}	4.9	95	0.5	Left atrium
p_{rv}	18.8	99	0.1	Right ventricle
p_{lv}	50.8	109	0.1	Left ventricle

4.3.4 Computed Results

In this section we will present some of the computed pressure and flow shapes of the cardiovascular model. The purpose is to show that the computed pressure and flow profiles are in agreement with corresponding human data found in the literature.

Computed left ventricular pressure p_{lv} and root aortic pressure p_{as} during ejection are given in the left panel of Figure 4.9[1]. Figure 4.9 shows also right ventricular pressure p_{rv} and pulmonary trunk pressure p_{ap} in the pulmonary circuit. Both pressures elegantly approximate curve shapes representative for the normal human ventricles as found in (Noordergraaf, 1978; Guyton, 1991). Representative outflow curves from right and left ventricle are given in Figure 4.10. Root aortic

[1]The computed curves in this section are shifted in time in order to obtain a better impression of the curves.

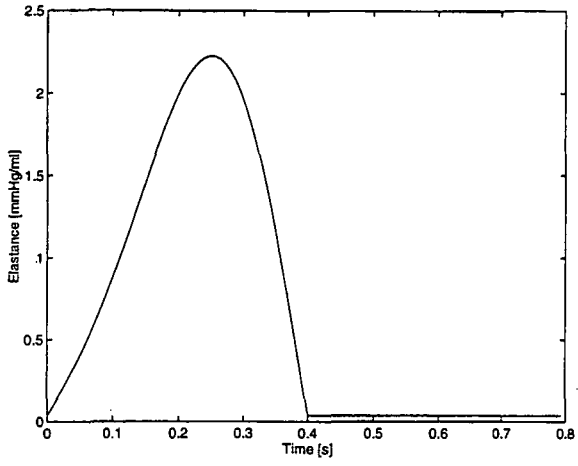

Figure 4.8: The left ventricular time-varying elastance function $E_{lv}(t)$ given by (4.2). Parameter values for both the left and right ventricular elastance functions can be found in tables 4.4 and 4.6. The heart period t_h is equal to 0.80 s.

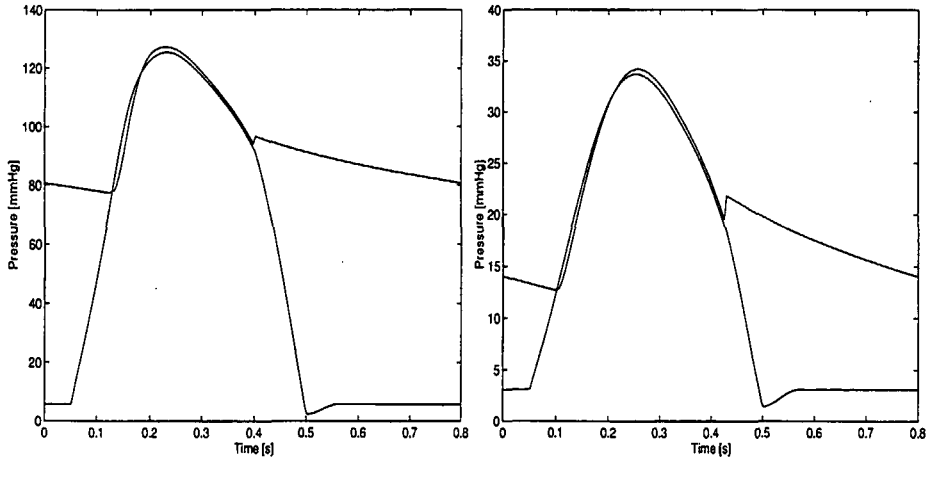

Figure 4.9: Left panel shows left ventricular pressure p_{lv} and root aortic systemic pressure p_{as}. Right panel shows right ventricular pressure p_{rv} and root pulmonary pressure p_{ap}.

systemic and pulmonary pressures are 127/78 mmHg and 34/13 mmHg, respectively. The corresponding changes in left and right ventricular volumes are shown in Figure 4.11. As a consequence of the lumped approach, the pressures in each section p_{a1}, p_{a2}, p_{a3}, p_{v1}, p_{v2}, p_{p1}, p_{p2}, p_{p3}, p_{l1}, p_{l2}, p_{la}, p_{ra} are not real physiological pressures but mathematical abstractions. The classic pressure-volume loops are also shown in Figure 4.11. The stroke volume V_s is 72.7 ml, heart rate H is 1.25 Hz resulting in a cardiac output CO equal to 90.9 ml/s. The left ventricular

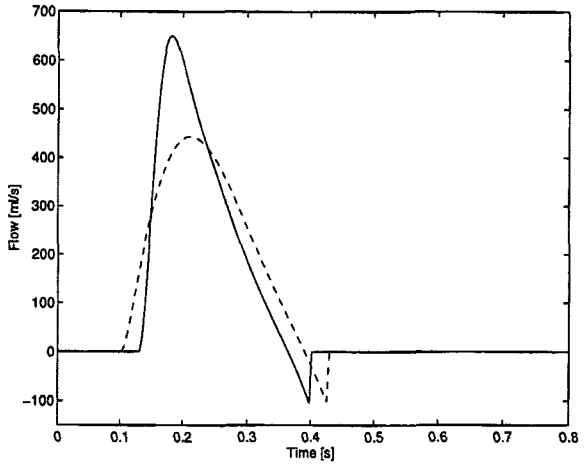

Figure 4.10: Left ventricular outflow Q_{lv} (full line) and right ventricular outflow Q_{rv} (dotted line). The negative outflows are accomplished by allowing volume to flow into the ventricles before the valves close.

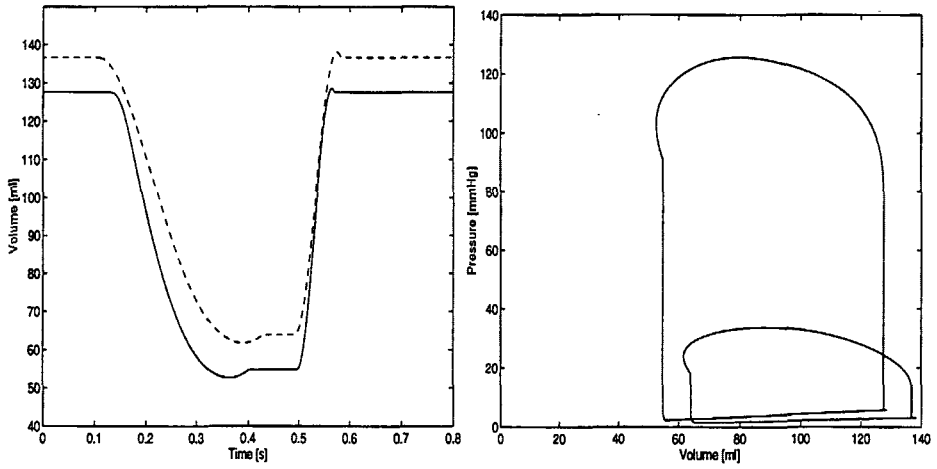

Figure 4.11: Left ventricular volume V_{lv} (full line) and right ventricular volume V_{rv} (dotted lines) during a cardiac cycle are shown in the left panel. The right panel shows pressure-volume work loops for the left and right ventricles, respectively. The area encompassed by the work loops denote left and right ventricular work, respectively.

ejection fraction EF[2] is 0.57. The results resemble data for a normal human found in (Guyton, 1991; Despopoulos and Silbernagl, 1991). The computed results are summarized in Table 4.3.

[2]The ejection fraction EF is defined as SV/V_{ed}, i.e. stroke volume divided by end-diastolic volume.

Table 4.3: Summary of the cardiovascular performance given by maximum systolic over end-diastolic pressures, end-diastolic volume V_{ed}, stroke volume V_s and ejection fraction EF.

Ventricle	*Pressure (mmHg)*	V_{ed} ml	V_s ml	EF
Left	127/78	127.6	72.7	0.57
Right	34/13	136.7	72.7	0.53

Hypertension and weak hearts can be studied by this model. Hypertension may be obtained by doubling the resistances in the systemic arterial. A weak heart may be simulated by taking the maximum elastance of the left ventricle equal to $E_{lv}/2$. As another example impaired filling of the right heart can be simulated by changing the filling resistance R_{ra} of the right heart. However, one important feature is obviously missing in these studies and that is the response from the nervous system. This will be the topic of Chapter 5.

4.3.5 The Cardiovascular Model in the SIMA Simulator

We have also developed the human circulation model in the SIMA simulator. The architecture of the SIMA simulator resembles the model of (Rideout, 1991) and the circulation model established in this chapter. The major differences between the model in this chapter and the model in the SIMA simulator amount to two items. In the model established in this chapter, the first part of the arterial systemic system and the pulmonary arterial system are defined by the left part of Figure 4.12. The first part in the SIMA simulator is described by the right panel of

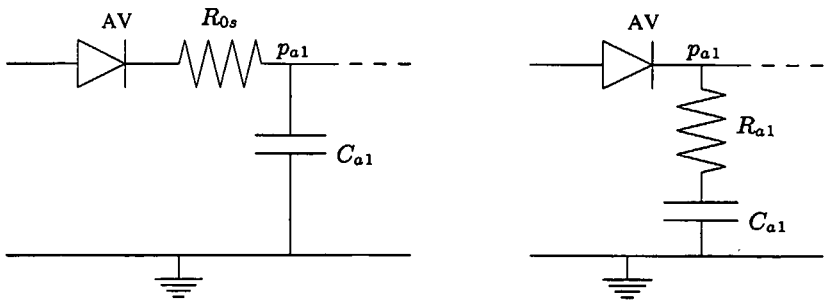

Figure 4.12: The left part shows the first section of the systemic arterial system in the model established in this chapter. It consists of a modified Windkessel model. The right part show the first section of the systemic arterial system in the SIMA simulator which is described by an alternate version of the modified Windkessel model.

Figure 4.12. The SIMA simulator includes a viscous resistance in the left and the right ventricles upstream of the inductance in Figure 4.7. We consider this contribution as less essential. The differences between the SIMA simulator and the model of (Rideout, 1991) are related to the heart valves and to the atrias. The heart valves are redevelopement such that the aortic and pulmonary valves allow a small backflow before complete closure of the valves. In addition, the two atrias are designed to be active in order to illustrate their pumping nature[3].

We deemed it necessary to determine an entirely new set of parameter values in order to obtain a physiologically founded model. The model by (Rideout, 1991) predicts more than 2000 ml of blood in the right atrium. Moreover, his total circulation volume amounts to 8600 ml. We used approximately the same relative volume and pressure distribution as given in Table 4.2 to estimate the new set of parameter values.

4.4 Summary

A human cardiovascular model is established with ventricular performance specified by two time varying elastance functions and the vasculature described by lumped elements based partially on the architecture of (Rideout, 1991). Three arterial and two venous pressures can be found in both systemic and pulmonary circulation. The model generates root aortic pressure and ventricular outflow curves representative for the human as reported in the literature. The pressure and volume distribution and parameter values are based on literature data. In addition, we described plus applied a strategy for the numerical determination of parameter values in lumped cardiovascular models.

The experimentally based ventricular model by (Mulier, 1994) exhibits the principal features when coupled to a closed lumped model of the human cardiovascular system including expected response to preload and afterload changes (Palladino, Ribeiro and Noordergraaf, 1998). However, this new model has not ripened to a stage where it can be used in the simulator. We encounter at least two practical problems when coupling the model to a cardiovascular model. Firstly, the heart rate is not easily changed. This is related to the two curves in generating function g in (3.2) of Chapter 3.2. Secondly, the root aortic pressure and ventricular outflow curves differ from the normal human curve profiles without the ejection effect. The ejection effect can correct these deficiencies but the parameters depend on the prevailing conditions in the vasculature and on neural effects. This dependence has not yet been formulated mathematically.

[3]We redeveloped the heart valves in co-operation with Heine Larsen, Math-Tech. We have not participated in estimating the parameters of the active atria.

4.5 The Cardiovascular Model in Equations

The cardiovascular model is comprised by a system of differential equations. In this Section we state all the equations involved. The parameter values are listed in Section 4.6.

Left Heart Chamber

$$\begin{aligned}
\frac{dQ_{la}}{dt} &= \frac{1}{L_{la}}(p_{la} - p_{lv}) - \frac{R_{la}}{L_{la}}Q_{la}, && \text{when the mitral valve is open,}\\
Q_{la} &= 0 && \text{when the mitral valve is closed,}\\
\frac{dV_{la}}{dt} &= Q_{l2} - Q_{la},\\
p_{la} &= E_{la}(V_{la} - V_{un,la}),\\
\frac{dQ_{lv}}{dt} &= \frac{1}{L_{lv}}(p_{lv} - p_{as}) && \text{when the aortic valve is open,}\\
Q_{lv} &= 0 && \text{when the aortic valve is closed,}\\
\frac{dV_{lv}}{dt} &= Q_{la} - Q_{lv},
\end{aligned}$$

where p_{as} is root aortic pressure and given by

$$p_{as} = R_{0s}Q_{lv} + p_{a1}.$$

We allow an amount of volume $V_{lv,b}$ to flow back into the left ventricle before complete closure of the aortic valve. The maximum volume we allow to flow back into the left ventricle is denoted by $\tilde{V}_{lv,b}$. When $V_{lv,b}$ exceeds the volume $\tilde{V}_{lv,b}$, the valve closes.

The relation between left ventricular cavity pressure p_{lv} and ventricular volume V_{lv} is described by

$$p_{lv} = E_{lv}(t)(V_{lv} - V_{l,lv}), \tag{4.8}$$

where $V_{d,lv}$ is left ventricular volume at zero pressure. The elastance function $E_{lv}(t)$ in (4.8) is given by

$$E_{lv}(t) = E_{min,lv}(1 - \phi(t)) + E_{max,lv}\phi(t),$$

where

$$\phi(t) = \begin{cases} a_\phi \sin\left(\frac{\pi t}{t_{ce}}\right) - b_\phi \sin\left(\frac{2\pi t}{t_{ce}}\right) & \text{for } 0 \le t < t_{ce} \\ 0 & \text{for } t_{ce} \le t \le t_h \end{cases} \tag{4.9}$$

The parameters $E_{min,lv}$ and $E_{max,lv}$ are minimal left diastolic and left maximal systolic elastance, respectively, t_h heart period and t_{ce} time for onset of constant elastance.

Right Heart Chamber

$$\begin{aligned}
\frac{dQ_{ra}}{dt} &= \frac{1}{L_{ra}}(p_{ra} - p_{rv}) - \frac{R_{ra}}{L_{ra}}Q_{ra}, && \text{when the tricuspid valve is open,}\\
Q_{ra} &= 0 && \text{when the tricuspid valve is closed,}\\
\frac{dV_{ra}}{dt} &= Q_{v2} - Q_{ra},\\
p_{ra} &= E_{ra}(V_{ra} - V_{un,ra}),\\
\frac{dQ_{lv}}{dt} &= \frac{1}{L_{rv}}(p_{rv} - p_{ap}) && \text{when the pulmonary valve is open,}\\
Q_{rv} &= 0 && \text{when the pulmonary valve is closed,}\\
\frac{dV_{rv}}{dt} &= Q_{ra} - Q_{rv}.
\end{aligned}$$

where p_{ap} is root aortic pressure and given by

$$p_{ap} = R_{0p}Q_{rv} + p_{p1}.$$

We allow an amount of volume $V_{rv,b}$ to flow back into the left ventricle before complete closure of the aortic valve. The maximum volume we allow to flow back into the left ventricle is denoted by $\tilde{V}_{rv,b}$. When $V_{rv,b}$ exceeds the volume $\tilde{V}_{rv,b}$, the valve closes.

The relation between right ventricular cavity pressure p_{rv} and ventricular volume V_{rv} is described by

$$p_{rv} = E_{rv}(t)(V_{rv} - V_{d,rv}), \tag{4.10}$$

where $V_{d,rv}$ is right ventricular volume at zero pressure. The elastance function $E_{rv}(t)$ in (4.10) is given by

$$E_{rv}(t) = E_{min,rv}(1 - \phi(t)) + E_{max,rv}\phi(t),$$

where the function ϕ is defined by (4.3) The parameters $E_{min,rv}$ and $E_{max,rv}$ are minimal right diastolic and right maximal systolic elastance, respectively, t_h heart period and t_{ce} time for onset of constant elastance.
The relation between heart period t_h and t_{ce} is given by

$$t_{ce} = \kappa_0 + \kappa_1 t_h, \tag{4.11}$$

where κ_0 and κ_1 are constant parameters (Rideout, 1991).

Systemic Arterial System

1. arterial section

$$\begin{aligned} \frac{dQ_{a1}}{dt} &= \frac{1}{L_{a1}}(p_{a1} - p_{a2}) - \frac{R_{a1}}{L_{a1}}Q_{a1}, \\ \frac{dV_{a1}}{dt} &= Q_{lv} - Q_{a1}, \\ p_{a1} &= \frac{1}{C_{a1}}(V_{a1} - V_{un,a1}). \end{aligned}$$

2. arterial section

$$\begin{aligned} \frac{dV_{a2}}{dt} &= Q_{a1} - Q_{a2}, \\ p_{a2} &= \frac{1}{C_{a2}}(V_{a2} - V_{un,a2}). \end{aligned}$$

3. arterial section

$$\begin{aligned} \frac{dV_{a3}}{dt} &= Q_{a2} - Q_{a3}, \\ p_{a3} &= \frac{1}{C_{a3}}(V_{a3} - V_{un,a3}) \end{aligned}$$

Systemic Veins

1. venous section

$$\begin{aligned} \frac{dV_{v1}}{dt} &= Q_{a3} - Q_{v1}, \\ p_{v1} &= \frac{1}{C_{v1}}(V_{v1} - V_{un,v1}). \end{aligned} \tag{4.12}$$

2. venous section

$$\begin{aligned} \frac{dQ_{v2}}{dt} &= \frac{1}{L_{v2}}(p_{v2} - p_{ra}) - \frac{R_{v2}}{L_{v2}}Q_{v2}, \\ \frac{dV_{v2}}{dt} &= Q_{v1} - Q_{v2}, \\ p_{v2} &= \frac{1}{C_{v2}}(V_{v2} - V_{un,v2}). \end{aligned} \tag{4.13}$$

Pulmonary Arterial System

1. arterial section

$$\begin{aligned} \frac{dQ_{p1}}{dt} &= \frac{1}{L_{p1}}(p_{p1} - p_{p2}) - \frac{R_{p1}}{L_{p1}}Q_{p1}, \\ \frac{dV_{p1}}{dt} &= Q_{rv} - Q_{p1}, \\ p_{p1} &= \frac{1}{C_{p1}}(V_{p1} - V_{un,p1}). \end{aligned}$$

2. arterial section

$$\begin{aligned} \frac{dV_{p2}}{dt} &= Q_{p1} - Q_{p2}, \\ p_{p2} &= \frac{1}{C_{p2}}(V_{p2} - V_{un,p2}). \end{aligned}$$

3. arterial section

$$\begin{aligned} \frac{dV_{p3}}{dt} &= Q_{p2} - Q_{p3}, \\ p_{p3} &= \frac{1}{C_{p3}}(V_{p3} - V_{un,p3}). \end{aligned}$$

Pulmonary Veins

1. venous section

$$\begin{aligned} \frac{dV_{l1}}{dt} &= Q_{p3} - Q_{l1}, \\ p_{l1} &= \frac{1}{C_{l1}}(V_{l1} - V_{un,l1}). \end{aligned}$$

2. venous section

$$\begin{aligned} \frac{dQ_{l2}}{dt} &= \frac{1}{L_{l2}}(p_{l2} - p_{la}) - \frac{R_{l2}}{L_{l2}}Q_{l2}, \\ \frac{dV_{l2}}{dt} &= Q_{l1} - Q_{12}, \\ p_{l2} &= \frac{1}{C_{l2}}(V_{l2} - V_{un,12}). \end{aligned}$$

4.6 Parameter Values

Table 4.4: The parameter values of the left heart chamber of Figure 4.7. The parameter $\tilde{V}_{lv,b}$ denotes the maximum volume we allow to flow back into the left ventricle before complete closure of the valve.

Parameter	*Value*	Units
H	1.25	Hz
$E_{max,lv}$	2.49	mmHg/ml
$E_{min,lv}$	0.049	mmHg/ml
E_{la}	0.075	mmHg/ml
$V_{d,lv}$	10	ml
$V_{d,la}$	30	ml
$\tilde{V}_{lv,b}$	2	ml
R_{la}	0.000089	mmHg · s/ml
L_{lv}	0.000416	mmHg · s^2/ml
L_{la}	0.00005	mmHg · s^2/ml

Table 4.5: Systemic parameter values of resistances, compliances, inductances and unstressed volumes of the cardiovascular model of Figure 4.6.

Parameter	*Value*	*Units*
R_{0s}	0.0334	mmHg · s/ml
R_{a1}	0.0824	mmHg · s/ml
R_{a2}	0.178	mmHg · s/ml
R_{a3}	0.667	mmHg · s/ml
R_{v1}	0.0223	mmHg · s/ml
R_{v2}	0.0267	mmHg · s/ml
C_{a1}	0.777	ml/mmHg
C_{a2}	1.64	ml/mmHg
C_{a3}	1.81	ml/mmHg
C_{v1}	13.24	ml/mmHg
C_{v2}	73.88	ml/mmHg
L_{a1}	0.00005	mmHg · s^2/ml
L_{v2}	0.00005	mmHg · s^2/ml
$V_{un,a1}$	205	ml
$V_{un,a2}$	370	ml
$V_{un,a3}$	401	ml
$V_{un,v1}$	596	ml
$V_{un,v2}$	1938	ml

Table 4.6: The parameter values of the right heart chamber of Figure 4.7. The parameter $\tilde{V}_{rv,b}$ denotes the maximum volume we allow to flow back into the left ventricle before complete closure of the valve.

Parameter	*Value*	*Units*
$E_{max,rv}$	0.523	mmHg/ml
$E_{min,rv}$	0.0283	mmHg/ml
E_{ra}	0.06	mmHg/ml
$V_{d,rv}$	10	ml
$V_{d,ra}$	30	ml
$\tilde{V}_{rv,b}$	2	ml
R_{ra}	0.0000594	mmHg · s/ml
L_{rv}	0.000216	mmHg · s^2/ml
L_{ra}	0.00005	mmHg · s^2/ml

Table 4.7: Pulmonary parameter values of resistances, compliances, inductances and unstressed volumes for the cardiovascular model of Figure 4.6.

Parameter	*Value*	*Units*
R_{0p}	0.0251	mmHg · s/ml
R_{p1}	0.0227	mmHg · s/ml
R_{p2}	0.0530	mmHg · s/ml
R_{p3}	0.0379	mmHg · s/ml
R_{l1}	0.0252	mmHg · s/ml
R_{l2}	0.0126	mmHg · s/ml
C_{p1}	2.222	ml/mmHg
C_{p2}	1.481	ml/mmHg
C_{p3}	1.778	ml/mmHg
C_{l1}	6.666	ml/mmHg
C_{l2}	5	ml/mmHg
L_{p1}	0.00005	mmHg · s^2/ml
L_{l2}	0.00005	mmHg · s^2/ml
$V_{un,p1}$	50	ml
$V_{un,p2}$	30	ml
$V_{un,p3}$	53	ml
$V_{un,l1}$	75	ml
$V_{un,l2}$	75	ml

Table 4.8: Summary of the parameters describing the function ϕ given in (4.3) and the division between the active and passive phase of the heart period in (4.11).

Parameter	*Value*
a_ϕ	0.9
b_ϕ	0.25
κ_0	0.29
κ_1	0.2

Chapter 5

The Baroreceptors Mechanism

The goal of this chapter is to offer an introduction to the basic physiology of the baroreceptors and the overall performance of the arterial blood pressure control provided by the baroreceptor mechanism. Section 5.1 offers an overview of the various control mechanisms of the human circulatory system. A brief introduction to the baroreceptor mechanism is given in Section 5.2. The individual components of the mechanism are quantified in Sections 5.3 and 5.4. Sections 5.3.1 and 5.3.2 provide also a critical historical review of some of the recent and previous models of the baroreceptors nerve activity. The historical review is continued in Section 5.5. In addition, Section 5.5 offers a presentation of some of the recent baroreceptor models. Further physiological and historical details can be found in (Ganong, 1975; Noordergraaf, 1978; Tortora and Anagnostakos, 1990; Guyton, 1991; Acierno, 1994).

5.1 Control Mechanisms of Human Circulatory System

It is needless to say that the entire regulation of the human blood pressure is complex and involves a manifold of control mechanisms. The principal philosophy of blood pressure control is to provide proper blood flow to the various organs of the human circulatory system. In essence, the pressure control promotes a normal distribution of fluids, hormones, electrolytes and other agents. The regulatory system consists roughly of two types of control mechanisms, a long term and a short term control mechanism. The long term control mechanism provides stabilization of blood pressure over longer periods (i.e. minutes, hours and days) whereas the short term controls are concerned with the immediate and acute circulatory perturbations (i.e. seconds and minutes).

The *long term control* operates mainly via the renal and homoral activities.

The kidneys increase the output of water and salt in response to an enhanced arterial pressure. This decreases blood volume and thus cardiac output. The net effect is a decline in the arterial pressure. A drop in the arterial pressure promotes secretion of renin from the kidneys. This forms for instance the hormone angiotensin II which enhances vessel constriction and thus increases arterial pressure.

The *short term regulation* is mainly mediated by the central nervous system (CNS) and involves the baroreceptors, the mechanoreceptors and the chemoreceptors (Guyton, 1981; Guyton, 1991). The overall goal of neural control is to redistribute blood flow to the different areas of the body by innervating the heart and the vessels. The nervous activity from the CNS modifies the heart rate, the cardiac contractility and the state of vessel constrictions. The chemoreceptors are sensitive to chemicals in the blood and react to alterations in the concentrations of oxygen, carbon dioxide, and hydrogen ions. A drop in the arterial pressure may decrease the concentration of oxygen. The chemoreceptors answer by increasing the cardiac strength and the vessel constriction. The baroreceptors are stretch receptors which are sensitive to pressure alterations. The most important receptors are located in the high pressure regions such as the carotid sinus and the aortic arch. The mechanoreceptors (or low pressure receptors) are located in the low pressure areas as the atria and the pulmonary veins. The mechanoreceptors are also stretch receptors and provide arterial pressure control by combating alterations in the venous volume. The baroreceptors are the best known and easily accessible receptors, consequently they have been investigated extensively. The mechanoreceptors are less studied and quantitative experimental data of these receptors are very sparse.

The phenomenon of *autoregulation* is a local control mechanism independent of the CNS. The local tissues can control blood flow in response to moderate changes in cardiac output and arterial pressure by dilation or contraction of the vessels (Guyton, 1981; Tortora and Anagnostakos, 1990). This may be due to a contractile response by the smooth muscles when stretched (Ganong, 1975).

5.2 The Baroreceptor Mechanism

The baroreceptor mechanism demands our key interest since this mechanism is believed to play the main role in short term pressure control. The baroreceptor mechanism provides a rapid negative feedback control which operates to control arterial blood pressure. An instantaneous drop in the arterial pressure is sensed by the baroreceptors. This starts a chain of events which leads to an increase in heart rate and cardiac contractility. It also stimulates the contraction of the vessels. In essence, this tends to alter the arterial pressure towards its previous value.

The baroreceptor mechanism has no long term regulation properties. An in-

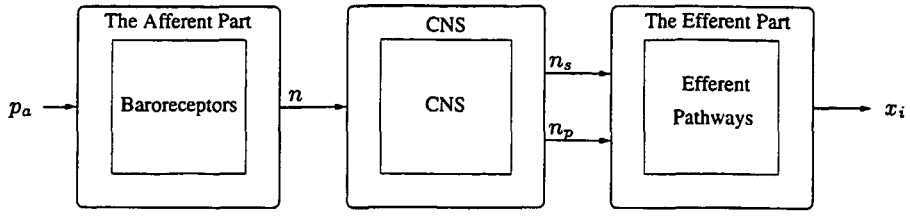

Figure 5.1: The complete baroreceptor mechanism divided into three components, an afferent component, the central nervous system (CNS) and an efferent component. Alterations in the arterial pressure p_a generate the firing rate n in the afferent part. From the CNS the sympathetic n_s and the parasympathetic n_p nervous activity are transmitted via the efferent pathways to modify the heart and the vasculature x_i.

stantaneous step increase in the carotid sinus pressure is followed by an enhanced firing activity in the baroreceptor nerves themselves which declines significantly the first few seconds and then decays more slowly. The decay continues and the time it takes the firing rate n to reach the previous value can take around $1-3$ days (Guyton, 1991; Taher, Cecchini, Allen, Gobran, Gorman, Guthrie, Lingenfelter, Rabbany, Rolchigo, Melbin and Noordergraaf, 1988). In hypertensive humans, for instance, the baroreceptors are adapted to the elevated arterial pressure. The baroreceptor mechanism operates to control this hypertensive pressure.

The baroreceptor mechanism may be divided into three components as shown in Figure 5.1. The first component is the *afferent part* which contains the receptors. The nerve activity n of the receptors is generated by alterations in the arterial pressure p_a. The second component is the central nervous system (CNS) which generates two nervous activities, the sympathetic n_s and the parasympathetic n_p activity. The third component is called the efferent part and consists of the efferent pathways to the individual organs in the cardiovascular system. From the CNS the two nervous activities are transmitted by the efferent pathways to alter heart rate, cardiac contractility and the state of the vessel constrictions denoted by x_i, where i designates the particular organ.

The following Sections 5.3 and 5.4 quantify the two components in Figure 5.1 more carefully.

5.3 The Afferent Part

The baroreceptors are stretch receptors located in the vessel walls. The most accessible receptors are located in the carotid sinus and in the aortic arch. The carotid sinus baroreceptors are located in a distinctive part of the two common carotid sinus arteries as shown in Figure 5.2. The aortic arch baroreceptors are

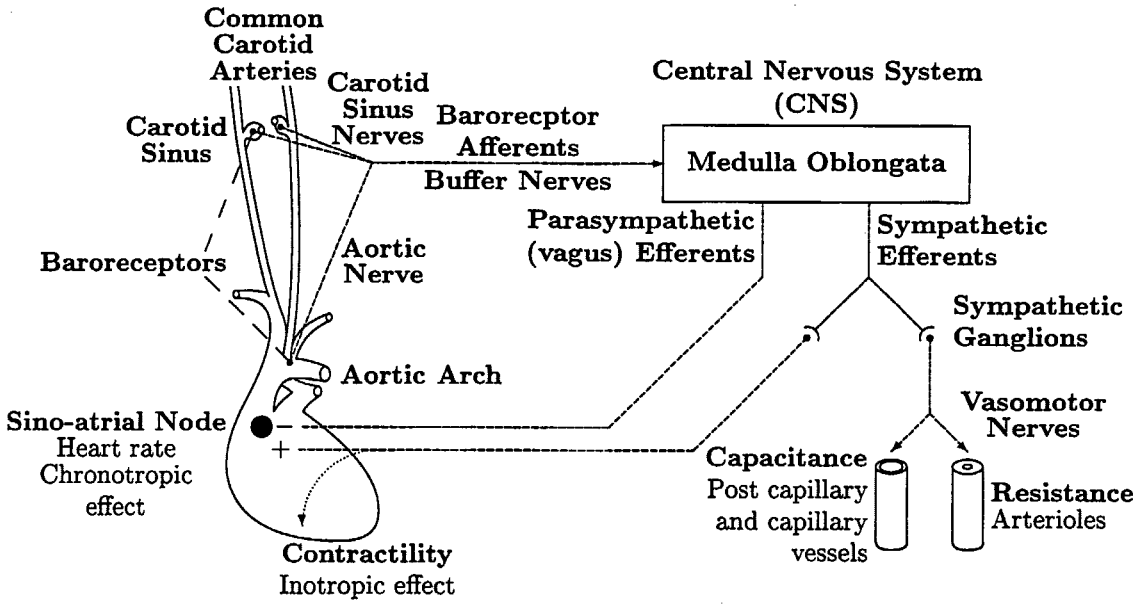

Figure 5.2: The complete baroreceptor mechanism. The baroreceptors are located in the vessel walls of the carotid sinus and the aortic arch. Alterations in the arterial pressure generates wall deformation which initiates the firing rate n from the receptors. The firing rate are pipelined by buffer nerves to the central nervous system (CNS). The CNS generates the sympathetic and the parasympathetic nerve activities. The sympathetic activity plays a vital role by innervating most of the effector organs in the cardiovascular system. The parasympathetic activity modifies mainly the heart rate. Adapted with permission from (Ottesen, 1997b).

located in the walls of the aortic arch. The carotid sinus receptors are the most studied whereas the aortic arch baroreceptors have received less attention. But the aortic arch and the carotid sinus receptors are believed to be functionally equal, except that the aortic arch receptors operate at a higher pressure level (Ganong, 1975).

The baroreceptors are nerve endings and respond to deformations in the vessel walls (Ganong, 1975; Brown, 1980; Guyton, 1991). The nerve activity evolves from two components, a pressure-mechanical and a mechanical-electrical one (Brown, 1980). The baroreceptors react to deformations in the vessel walls by a pressure-mechanical mechanism. Pressure alterations may cause changes in the cross-sectional areas of the vessels and thus deformations. The second component generates the nerve activity of the receptors by a mechanical-electrical mechanism within the receptors. We call this nerve activity from the carotid sinus receptors, *the firing rate*, denoted by n. The carotid sinus and the aortic arch nerve impulses are transmitted from the receptors via the glossopharyngeal nerve and the vagus nerve, respectively. The two nerves are joined in the so-called *buffer nerves* which direct the impulses to the central nervous system.

The firing rate n of the carotid sinus receptors vary with varying arterial pressure. This was first documented by (Bronk and Stella, 1932; Bronk and Stella, 1935). Since then various experiments have revealed that the firing rate n exhibit a number of non-linear phenomena associated with alterations in the carotid sinus pressure p_{cs}. These non-linear phenomena include

- *Threshold and saturation.* The firing rate n exhibit a threshold N which they can be forced below. In addition, the firing rate n increase with increasing carotid sinus pressure and display both low and high saturation.
- *Asymmetric response.* The firing rate n display a sigmoidal response as a function of carotid sinus pressure (Landgren, 1952). The response exhibits a hysteresis phenomenon or asymmetric response.
- *Step response.* A step change in the carotid sinus pressure results in a step change in the firing rate followed by a resetting phenomenon (Brown, 1980).
- *Adaptation.* The firing rate n increase when carotid sinus pressure rises. As the pressure is maintained at this higher level, the firing rate return to the threshold value N. This is called adaptation or resetting.

A more detailed discussion of the non-linear phenomena can be found in (Taher et al., 1988; Ottesen, 1997b).

5.3.1 Models of the Firing rate

Several efforts have been pursued to formulate the relation between the firing rate n and the carotid sinus pressure. (Robinson and Sleight, 1980) modeled the baroreceptor response to a step change in the pressure by a simple function of time

$$n = c_1 e^{-\frac{t}{\tau_1}} + c_2 e^{-\frac{t}{\tau_2}} + c_3,$$

where c_1, c_2 and c_3 are weighting parameters and τ_1 and τ_2 time constants describing the resetting.

The first mathematical description of the relation between pressure and firing rate, $n - N$, was advanced by (Warner, 1958). (Warner, 1958) proposed a differential approach given by

$$n = k_1(p - p_0) + k_2\frac{dp}{dt} + N, \tag{5.1}$$

where p is the pressure, k_1 and k_2 constant parameters, p_o the threshold pressure (i.e. the adapted pressure level which generates the threshold value N). Low and high saturation, the asymmetric response and the step response are not embodied

in the model. In (Warner, 1958) (5.1) was extended to include the asymmetric response.

A number of other models based on ordinary differential equations include (Scher and Young, 1973; Spickler and Kezdi, 1967; Franz, 1969; Srinivasan and Nudelman, 1972). The previous models embody some, and in few cases all, the non-linear phenomena (Taher et al., 1988; Ottesen, 1997b).

5.3.2 The Unified Models

Along another avenue we find two recent models which embody all the non-linear phenomena listed in Section 5.3 bred by adaptation, saturation and threshold. (Taher et al., 1988) proposed a so-called unified model described by

$$\Delta n = \Delta p \left(k_1 e^{-\frac{t}{\tau_1}} + k_2 e^{-\frac{t}{\tau_2}} + k_3 e^{-\frac{t}{\tau_3}} \right) \sin^{\frac{1}{2}}\left(\frac{n}{M}\pi\right), \tag{5.2}$$

where Δn is the change in the firing rate to a step change Δp in the pressure. The parameter M is the high saturation level of the firing rate. The parameters k_1, k_2 and k_3 are weighting factors and τ_1, τ_2 and τ_3 time constants which characterize the decay rate of Δn in response to Δp. Computation of a continuos firing rate n, using (5.2), requires a tremendous amount of bookkeeping. (Ottesen, 1997b) refined this model. He suggests the firing rate n described by

$$n = N + \int_{-\infty}^{t} \dot{p}_{cs} \left(k_1 e^{-\frac{t-s}{\tau_1}} + k_2 e^{-\frac{t-s}{\tau_2}} + k_3 e^{-\frac{t-s}{\tau_3}} \right) \left[\frac{n(M-n)}{(M/2)^2} \right] ds, \tag{5.3}$$

where p_{cs} is the carotid sinus pressure. This is equivalent to a system of three non-linear coupled differential equations given by

$$\begin{aligned} \dot{\Delta n_1} &= k_1 \dot{p}_{cs} \frac{n(M-n)}{(M/2)^2} - \frac{1}{\tau_1} \Delta n_1, \\ \dot{\Delta n_2} &= k_2 \dot{p}_{cs} \frac{n(M-n)}{(M/2)^2} - \frac{1}{\tau_2} \Delta n_2, \\ \dot{\Delta n_3} &= k_3 \dot{p}_{cs} \frac{n(M-n)}{(M/2)^2} - \frac{1}{\tau_3} \Delta n_3, \end{aligned} \tag{5.4}$$

where $n = \Delta n_1 + \Delta n_2 + \Delta n_3 - N$. The parameters k_1, k_2 and k_3 are weighting factors, τ_1, τ_2 and τ_3 time constants describing the resetting phenomenon, M the high saturation level of the firing rate and N the threshold value of the firing rate. The model contains 8 parameters k_1, k_2, k_3, τ_1, τ_2, τ_3, M and N found from data in the literature and through curve fitting procedures. Typical values of the parameters are found in Table 5.1. The parameter values of the weighting factors

Table 5.1: Typical parameter values for the unified model (5.4)

Type	*Values*	*Units*
τ_1	0.5	s
τ_2	5.0	s
τ_3	500	s
k_1	0.5	Hz/mmHg
k_2	0.5	Hz/mmHg
k_3	1.0	Hz/mmHg
N	30	Hz
M	120	Hz

and the time constants vary significantly in the literature (Taher et al., 1988). The time constant τ_3 may be assigned values in minutes, hours or days. In addition, (Ottesen, 1997b) uses different sets of parameter values to compute the non-linear phenomena. The parameters may vary due to the physiological processes involved in each of the non-linear phenomena.

By (5.4), the firing rate n vary linearly with the instantaneous time derivative of the carotid sinus pressure p_{cs}. The history of the carotid sinus pressure is included by integration of $\dot{p}_{cs}$ via the three exponentials. The physiological interpretation of the three components Δn_1, Δn_2 and Δn_3 in (5.4) is that they are sensitive to different types of changes in the carotid sinus pressure. The component Δn_1 with the smallest time constant is sensitive to quick changes in $\dot{p}_{cs}$. The component Δn_3 with the highest time constant τ_3 is sensitive to more slow phenomena. It depends not only on the instantaneous value of $\dot{p}_{cs}$ but on its integrated value. The component Δn_3 follows closely the behavior pattern of the carotid sinus pressure p_{cs}. The intermediate responses are captured by Δn_2. (Ottesen, 1997b) hypothesizes that the three components denote different baroreceptor types, A, B and C, characterized by different transmission speeds. The parameters k_1, k_2 and k_3 are the corresponding weighting factors which may be influenced by nervous control or other external conditions. Three components are included and are the smallest number which can capture the non-linear phenomena (Ottesen, 1997b).

The model covers the range of non-linear phenomena listed in Section 5.3. Examples of the results are shown in Figure 5.3 and Figure 5.4. Figure 5.3 shows the computed firing rate response to a step increase and decrease in the pressure. The computed results agree well with data reported by (Brown, 1980). The only discrepancy is the absence of the postexcitatory depression gap. This may be related to the assumption that the parameters k_1, k_2 and k_3 are independent of the

Na^+ concentration. Figure 5.4 shows the asymmetric response. The asymmetric

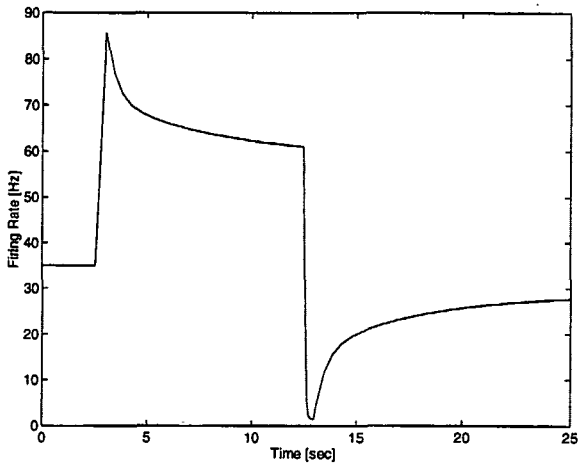

Figure 5.3: The firing rate response n to a step increase in the pressure computed from (5.4). The pressure increases from 170 mmHg to 178 mmHg at time 2.5 s. At time 12.5 s the pressure is forced back to 170 mmHg. The computed response agrees well with the data found in (Brown, 1980). The only difference is the absence of the postexcitatory depression gap. Adapted by permission from (Ottesen, 1997b).

response arises from the second term on the right hand sides of (5.4), the resetting terms. A more careful discussion of this model can be found in (Ottesen, 1997b).

5.4 The CNS and the Efferent Part

The CNS and the various pathways to each of the effector organs are shown in the figures 5.1 and 5.2. The firings rate n enter the central nervous system via the buffer nerves. The information is then processed in the medulla oblongata of the CNS. Subsequently, the cardioinhibitory center and the vasomotor center of the medulla oblongata generate sympathetic n_s and parasympathetic n_p nerve activity, respectively. An enhanced firing rate n excites the cardioinhibitory center and inhibits stimulation of the vasomotor center. The net effect is an enhanced parasympathetic activity and diminished sympathetic activity. The efferent pathways transmit the two nervous impulses to the various parts of the cardiovascular system. The sympathetic nerve fibers innervate most of the cardiovascular system whereas the parasympathetic nerve fibers are restricted to influence the heart. In summary:

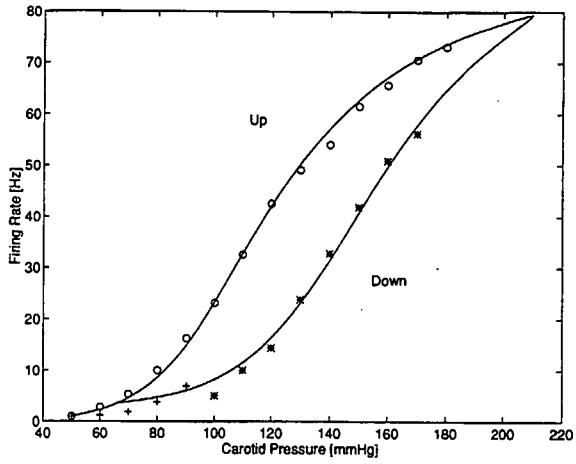

Figure 5.4: Computed asymmetric response (full line) based on (5.4) superimposed on experimental data found in the literature. Open circles denote measurements during increase of pressure. Stars indicate pressure lowered from 170 mmHg ($n = 56$ Hz) to 100 mmHg ($n = 5$ Hz). Plus-signs denote pressure lowered from 100 mmHg ($n = 23$ Hz) to 50 mmHg ($n = 1$ Hz). Data adapted from (Cecchini et al., 1982). The pressure increases by 1.37mmHg/s and decreases by -1.37mmHg/s. The parameter M is 103. Figure is adapted by permission from (Ottesen, 1997b).

Enhanced sympathetic activity

- stimulates the heart rate and improves cardiac contractility.
- stimulates vessel constriction in the arteries, arterioles and veins (Ganong, 1975; Guyton, 1991).

Enhanced parasympathetic activity

- decreases heart rate whereas modification of cardiac contractility and vessel constriction are insignificant (Guyton, 1991).

The entire mode of operation of the afferent, the CNS and the efferent part may be illustrated by an example. An infusion of volume into the human circulatory system increases the arterial pressure which in turn stimulates the carotid sinus baroreceptors. The increased firing rate n are then transmitted to the medulla oblongata via the buffer nerves. In the medulla oblongata, the firing rate excite the cardioinhibitory center and inhibit stimulation of the vasomotor center. The result is a counteraction which decreases the heart rate, the cardiac contractility and stimulates the arterial and the venous vessel dilation. The latter enables, for instance, blood to be stored in a venous reservoir. The net effect is a decreasing arterial pressure. The regulation is delayed by various mechanical and

biochemical processes within the events listed above. Stimulation of the heart is a quick process which amounts to a few seconds while regulation of the veins can take approximately one minute. Arterial vessel constriction is intermediate at around $10 - 15$ seconds (Donald and Edis, 1970; Rothe, 1983; Shoukas and Sagawa, 1973; Guyton, 1991) (see also Section 6.2.5).

5.5 Some Baroreceptor Models

The literature contains a variety of different models of the baroreceptor mechanism coupled to human circulatory models. Some of these models are based on experimental studies whereas others mainly simulate the qualitative behavior and hardly appreciate the physiological processes. The experimentally based approaches suffer from the fact, that many of the physiological mechanisms are poorly understood and that the literature tends to provide only qualitative relations of the baroreceptor mechanism. The effector regulation may, for instance, only be presented as a relation between changes in the effector organs and the average carotid sinus pressure taken in a very few discrete points.

In general, the baroreceptor models may be characterized by two gross classes of modeling.

1. Models where the description of the underlying physiological processes are hidden behind different mathematical and physical principles.

2. Models where the mathematical formulations of the physiological processes are directly accessible

The first class contains models by (Noldus, 1976; Ono, Uozumi, Yoshimoto and Kenner, 1982; Kappel and Peer, 1993; Kappel et al., 1997). (Noldus, 1976) uses optimal control theory and applies the principle of minimization of energy consumption. (Ono et al., 1982) and (Kappel and Peer, 1993) apply optimal control theory based on minimal deviation from set-points. Common for these particular models are that they make it difficult to access all the mathematical formulations of the physiological processes.

The second class contains models by (Warner and Cox, 1962; Leaning, Pullen, Carson and Finkelstein, 1983; Leaning, Pullen, Carson, Al-Dahan, Rajkumart and Finkelstein, 1983; Tham, 1988; Rideout, 1991; Ursino et al., 1994; Neumann, 1996; Ottesen, 1997b; Danielsen, 1996; Danielsen and Ottesen, 1997; Ursino, 1998). In this class, all the mathematical formulations of the physiological processes are directly accessible. This encourages the use of physiological knowledge and facilitates discussions of all the mathematical formulations.

The baroreceptor model by (Tham, 1988) controls the five main effect organs in a closed pulsatile cardiovascular model. The model is used to study the effects of halothane on the baroreceptor mechanism. The model distinguishes between sympathetic and parasympathetic activities but the model is only sparsely based on experimental studies.

Modeling the baroreceptor mechanism, (Rideout, 1991) applied linear control theory to the, by nature, non-linear problem. His model is established in two steps. The first step consists of a first order transfer function which is used to compute a distributed average pressure $\tilde{p}_{a3}$ according to

$$\frac{d\tilde{p}_{a3}}{dt} = \frac{1}{\tau}(p_{a3} - \tilde{p}_{a3}), \tag{5.5}$$

where p_{a3} is the arterial pressure in the third section of a cardiovascular model similar to Figure 4.6 in Chapter 4, τ a time constant which characterizes a time delay. (Rideout, 1991) does not explain why p_{a3} is used in (5.5). We suspect the reason to be the smaller oscillations in this pressure. The second step generates a control variable u

$$u = 1 + k(\tilde{p}_{a3} - p_0), \;\; u_{min} < u < u_{max},$$

where p_0 is the adapted pressure by the baroreceptors and the constants u_{min} and u_{max} are minimum and maximum of the control variable u. The control variable u is used to control the heart period t_h and the cardiac contractility s_l & s_r of the left and the right ventricle, respectively, according to

$$\begin{aligned} t_h &= a_1 + a_2 u, \\ s_l &= \frac{2s_{max,l}}{u+1}, \\ s_r &= \frac{2s_{max,r}}{u+1}, \end{aligned}$$

where $s_{max,l}$ and $s_{max,r}$ are maximum of the left and the right ventricular elastance functions and a_1 and a_2 constants. The model tends to stabilize arterial pressure but the parameter values and the mathematical formulations are not, whatsoever, based on experimental facts.

(Ursino et al., 1994) appears to be the first to assign individual time delays to each effector regulation based on values found in the literature. (Ursino et al., 1994) examined the importance of the venous reservoir during acute hemorrhages. The studies were based on a non-linear baroreceptor model coupled to a non-pulsatile human cardiovascular model. The model controls the main effector organs, except the cardiac contractility. Different time delays were assigned to the control of the heart rate, the peripheral resistance, the venous compliance and

the venous unstressed volume. All parameter values were based on physiological knowledge found in the literature. However, no efforts were made to distinguish between sympathetic and parasympathetic activities. The two nervous activities and the control of the cardiac contractility are included in a new version of the model (Ursino, 1998). The new baroreceptor model is coupled to a pulsatile human cardiovascular model. The model is used to examine the effect of the high pressure and the low pressure receptors during moderate hemorrhages and ventricular pacing. The baroreceptor nerve activity is generated from the carotid sinus pressure through a high-pass filter in series with a sigmoidal static relation. The sympathetic n_s and parasympathetic n_p activities, generated by the high pressure receptors, are given by

$$n_s = n_{min,s} + (n_{max,s} - n_{min,s})e^{-k_s n}, \tag{5.6}$$

$$n_p = \frac{n_{max,p}}{1 + e^{n_0 - n}}, \tag{5.7}$$

where $n_{min,s}$ and $n_{max,s}$ are the minimum and the maximum of the sympathetic activity, respectively, $n_{max,p}$ the maximum parasympathetic activity and n_0 a constant parameter. The formulation (5.6) is inspired by the experimental studies by (Wang, Brandle and Zucker, 1993) who show that n_s decreases exponentially with the average of the firing rate n. The parasympathetic activity n_s is assumed to have a similar behavior given by (5.7). In this model, the change Δx_i in the hemodynamical variables x_i (i.e. heart rate, cardiac contractility, arterial and venous vessel constriction), caused by the sympathetic influence, is given by

$$\tilde{x}_i = \begin{cases} c_i \ln(n_s(t - D_i) - n_{s,0} + 1) & , n_s \geq n_{s,0} \\ 0 & , n_s < n_{s,0} \end{cases}$$

$$\frac{d\Delta x_i}{dt} = \frac{1}{\tau_i}(-\Delta x_i + \tilde{x}_i).$$

Finally, the control is accomplished by

$$x_i = \Delta x_i + x_0. \tag{5.8}$$

The time constant τ_i denotes the distributed time delay required for completion of a regulation, D_i is the pure latency of each of the controls, $n_{s,0}$ a threshold value for the sympathetic influence and c_i a gain factor. The parasympathetic influence is modeled in a similar fashion. The use of the natural logarithm ln in (5.8) is not based on experimental evidence but merely included to obtain a favorable agreement with data of the intact human. The model is a good example of how various physiological knowledge can be compressed into a mathematical setting and how mathematical modeling can be used to examine the interaction between several mechanisms.

(Neumann, 1996) studied hemorrhages more thoroughly. Her baroreceptor model affects all cardiovascular compliances and resistances in a pulsating human cardiovascular model. The baroreceptor model is based on the approach by (Ursino et al., 1994) but each effector regulation is given the same time delay.

5.6 Goal

Inasmuch as the baroreceptor mechanism is believed to be the main factor in the short term pressure control, is it not the only mechanism involved. The mechanoreceptors, the chemoreceptors and the local controls contribute to the regulation. The approach taken here is to consider a simplified version of reality. We will only consider the baroreceptor mechanism in the short term pressure control.

The *primary goal* is to establish a model of the baroreceptor mechanism which can be applied to the human circulation model established in Chapter 4 and which is built on experimental data and physiological arguments. This model is intended to be used in the SIMA simulator. The model

- should exhibit the principal features of the short term nervous control when coupled to the human circulation model established in Chapter 4.
- should discriminate between the sympathetic and the parasympathetic activities. This may provide a platform for studying e.g. infusion of drugs which stimulate vessel constriction and cardiac performance.
- must be based on experimental observations found in the literature whenever possible.
- must be simple in order to accommodate the computational limitations of the SIMA simulator.

Previous models of the baroreceptor mechanisms tend to describe the afferent part by ordinary differential equations which embody some but not all the non-linear phenomena listed in Section 5.3 (Leaning, Pullen, Carson and Finkelstein, 1983; Leaning, Pullen, Carson, Al-Dahan, Rajkumart and Finkelstein, 1983; Tham, 1988; Ursino, 1997; Ursino, 1998). In these models, the firing rate of the carotid sinus receptors are not only sensitive to the average pressure but also to the change in the pressure $\dot{p}_{cs}$. The first approach taken here is much simpler. The model lumps the description of the afferent part and the CNS. The sympathetic and the parasympathetic activity are related to the average arterial pressure by a sigmoidal function. The description of the efferent control is based on open loop responses. Though, strikingly simple, this model of the baroreceptor mechanism

includes the main properties of the control from the baroreceptor mechanism. The computed results of the model during an 10 % acute hemorrhage, heart pacing and the computed effects of pulsation in the carotid sinus pressure will be compared with the corresponding experiments.

The *secondary goal* is to use the unified model to describe the afferent part of the above model. It appears that none of the previous models of the baroreceptor mechanism have adopted a formulation of the afferent part which embodies all of the non-linear phenomena of the firing rate listed in Section 5.3. By introducing the unified model in the mathematical formulation of the afferent part, we include all the experimentally known non-linear phenomena in the model of the baroreceptor mechanism. In particular, the model includes adaptation of the baroreceptors.

Chapter 6

A Baroreceptor Model

6.1 Introduction

It was shown in Chapter 5 that the firing rates of the carotid sinus receptors exhibit a number of non-linear phenomena. The unified model, first proposed by (Taher et al., 1988), embraces all these phenomena. Recent models of the baroreceptor mechanism tend to describe the afferent part by ordinary differential equations which embody some but not all of the non-linear phenomena (Leaning, Pullen, Carson and Finkelstein, 1983; Leaning, Pullen, Carson, Al-Dahan, Rajkumart and Finkelstein, 1983; Tham, 1988; Ursino, 1997; Ursino, 1998). In these models of the baroreceptor mechanism, the firing rates of the carotid sinus receptors are not only sensitive to the average pressure but also to the change $\dot{p}_{cs}$ in the pressure. Our *first model* of the baroreceptor mechanism uses only the average pressure whereas our *second model* adopts the unified model. The two baroreceptor models offer a description of how the sympathetic and the parasympathetic activities influence heart rate, cardiac contractility, peripheral resistance, venous compliance and the venous unstressed volume by integrating various experimental observations obtained from the literature. In addition, the models include different time delays to each of the controls. In order to allow the models to control, we will couple both models to the human circulation model established in Chapter 4.

In the *first model* of the baroreceptor mechanism the sympathetic and the parasympathetic activity are related to the average arterial pressure by a sigmoidal function, as reported by (Korner, 1971). This is described in Section 6.3.1. The formulation of the afferent part and the CNS of the *second model* is given in Section 6.3.2. It consists of the unified model (5.4) and sigmoidal relation between the firing rates and the sympathetic and parasympathetic activities.

The key element in the formulation of the efferent part is the experimentally observed sigmoidal curves relating the efferent controls to the average arterial

pressure. Section 6.2 presents a number of open loop experiments used to describe the efferent part and to estimate the involved parameters values of the baroreceptor model. The section will also present the different time delays. In Section 6.3 we will establish the general formulation of the two baroreceptor models detached from any reference to a particular cardiovascular model.

The explicit coupling between the models of the baroreceptor mechanism and the human circulation model established in Chapter 4 is described in Section 6.4. Using the *first model*, Section 6.5 compares the computed open loop responses with the corresponding experiments.

In the sections 6.8 - 6.11 we will compare a number of experiments found in the literature with the corresponding computed results of the two baroreceptor models. Using the *first model*, we will show in the sections 6.8 - 6.10 that the computed results during a 10 % acute hemorrhage and heart pacing are in favorable agreement with corresponding experiments. In addition, the first model exhibits drop and rise in the arterial pressure depending on at which pressure level a sinus pulsation is superimposed on a static carotid sinus pressure. In particular, we will also show that the control of systemic veins plays a leading role during an acute hemorrhages whereas the remaining controls appear to have a minor function. The results of the *second model* display a striking agreement with the experiments of a 10 % acute hemorrhage by (Hosomi and Sagawa, 1979) which is shown in Section 6.11.

6.2 Open Loop Descriptions of the Baroreceptor Mechanism

The key experimental results used to describe the control actions in the model of the baroreceptor mechanism, are the sigmoidal functional relations σ^b found between the effector responses (e.g. in the heart rate and in the peripheral resistance) and the average carotid sinus pressure $\bar{p}_{cs}$. The sigmoidal functions σ^b are typically obtained in vagotomized animals[1]. The carotid sinus pressure is increased in steps with the remaining hemodynamic variables free to move accordingly. The effector responses are measured $2-3$ minutes after the step change in the carotid sinus pressure. The pressure is varied until the desired pressure range is covered. Subsequently, a sigmoidal curve is drawn showing the effector responses as functions of the average pressure. This is called an *open loop response*. In general, the absolute values of the open loop responses are found from animal experiments and may differ greatly among individual species. Consequently, we report the relative

[1]In vagotomized animals the vagus is cut and the reflexes from the aortic arch receptors are eliminated.

change from the baseline value, in order to eliminate these differences. As an example, Figure 6.1 shows the sigmoidal response in the maximum of the elastance

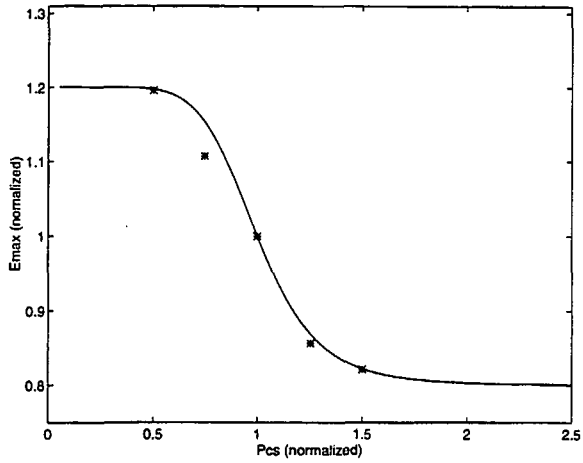

Figure 6.1: Normalized values of the computed open loop responses of the maximum elastances $E_{max,lv}$ and $E_{max,rv}$ of the left and the right ventricles as a function of the normalized average carotid sinus pressure $\bar{p}_{cs}$ superimposed on experimental data from (Suga et al., 1976) of the left ventricle ($*$). The pressures are normalized with respect to the computed steady state value (92 mmHg) and experimental data to the reported baseline values.

function of the left and the right ventricles. From the viewpoint of simplicity, we assume that the low and the high saturation are located symmetrically around the baseline value. Table 6.1 summarizes the adopted relative changes that we assume representative for the intact human.

Table 6.1: Adopted low and high saturation levels for the control of heart rate H, cardiac contractility E_{max}, peripheral resistance R_{ps}, venous unstressed volume V_{un} and venous compliance C_v. The saturation values are given relative to their baseline values.

Parameter	*Low value*	*High value*
H	0.25	1.75
E_{max}	0.8	1.20
R_{ps}	0.60	1.40
V_{un}	0.79	1.21
C_v	0.90	1.10

6.2.1 The Inotropic Effect

The inotropic effect denotes the control of the cardiac contractility, the heart's ability to pump. Several attempts have been pursued over the years to establish an index of cardiac contractility. The attempts share the same fate and have all failed (Slinker, 1996). The maximum E_{max} of the ventricular elastance function has been proposed as such an index (Suga et al., 1973). Since both ventricles of the cardiovascular model in Chapter 4 are described by a time-varying elastance function we define the maximum E_{max} of the elastance function as a measure of the cardiac contractility. A positive or negative inotropic effect corresponds then to an increase or decrease in the maximum elastance, respectively. The maximum elastance is mainly influenced by sympathetic activity but parasympathetic activity may have a weak influence (Suga et al., 1973). We follow the simplest view and exclude the parasympathetic effect on the inotropic state. Open loop results reveal that it is decreasing in the average arterial pressure and is allowed to deviate approximately 20 % from the baseline value in the absence of the aortic arch receptors (Suga et al., 1973).

6.2.2 The Chronotropic Effect

The chronotropic effect denotes the regulation of the heart rate H. The heart rate is influenced by both sympathetic and parasympathetic activity (Warner and Russel, 1969; Levy and Zieske, 1969). Experiments show that the heart rate diminishes with increasing carotid sinus pressure and can vary approximately $5-30$ % (Greene, 1986) and $3-15$ % (Bolter and Ledsome, 1976) from the baseline values after vagotomy. Experiments in normotensive humans have shown that the heart rate can increase much more (Korner, 1974). Accordingly, we allow the heart rate to vary 75 % from the baseline value in an intact human.

6.2.3 Control of the Peripheral Resistance

Vascular vessel constriction tends to increase arterial pressure whereas vessel dilation promotes a decline in the pressure. All the vascular vessels in the cardiovascular system are innervated by sympathetic activity except the capillaries (Guyton, 1991; Ganong, 1975). Experimental results show that the peripheral resistance R_{ps} decreases with increasing carotid sinus pressure $\bar{p}_{cs}$ (Greene, 1986; Cox and Bagshaw, 1975; Shoukas and Brunner, 1980) (the peripheral resistance is typically viewed as the difference between the central arterial and the central venous pressure divided by cardiac output). The peripheral resistance is shown to increase approximately $40-90$ % and decrease $30-40$ % from baseline (Greene, 1986; Cox and Bagshaw, 1975; Shoukas and Brunner, 1980). We have adopted a relative

change of 40 % from the baseline value for the systemic peripheral resistance. We ignore alterations in the peripheral resistance of the pulmonary system in agreement with experimental studies by (Shoukas, 1975; Greene, 1986) which showed no marked changes in the peripheral resistance with alterations in the carotid sinus pressure.

Autoregulation is independent of sympathetic innervation and offers local control of blood flow to the tissues. Autoregulation is not directly included in the model; neither is it mentioned in the above experimental results. Thus, autoregulation may be included in the experiments and thus in the model.

6.2.4 Control of the Venous Unstressed Volume and Venous Compliance

The veins are innervated by the sympathetic system and can mobilize a large amount of volume to other parts of the human circulatory system (Ganong, 1975; Greene, 1986; Guyton, 1991). The venous unstressed volume plays a significant role in ventricular filling (Shoukas and Sagawa, 1973; Shoukas and Brunner, 1980; Greene, 1986).

The open loop responses for the systemic unstressed volume $V_{un,s}$ are obtained from measurements of the volume ΔV shifted from the systemic system into a reservoir when the venous pressure is constant. The volume shifted is expressed by

$$\Delta V = \Delta V_{un,a} + \Delta V_{un,v} - C_a \Delta p_a, \tag{6.1}$$

where Δp_a is the concomitant change in the arterial pressure during alterations in the carotid sinus pressure. In (6.1), $\Delta V_{un,a}$ and $\Delta V_{un,v}$ are the unstressed volumes in the systemic arteries and the systemic veins, respectively. The arterial compliance C_a and the venous compliance C_v were shown to be constant in these measurements. Thus, the change in systemic unstressed volume $\Delta V_{un,s}$ is given by

$$\Delta V_{un,s} = \Delta V + C_a \Delta p_a. \tag{6.2}$$

The absolute values of $\Delta V_{un,s}$ and ΔV vary in the literature:

- (Shoukas and Sagawa, 1973) reports that $\Delta V/m = 7.5$ ml/kg during a change in pressure from $75 - 175$ mmHg, where m is body weight. Assuming that C_a is $1 - 2$ ml/mmHg (Noordergraaf, 1978) and the arterial pressure changes 100 mmHg we have to add $C_a \Delta p_a$ equal $100 - 200$ ml. This corresponds to a maximal $\Delta V_{un,s} = 725$ ml for 70 kg male.

- (Greene, 1986) states that $\Delta V/m = 9.97$ ml/kg and that $\Delta V_{un,s}/m = 20.26$ ml/kg during a change in pressure from $50 - 200$ mmHg. This corresponds to $\Delta V_{un,s} = 1120$ ml for a 70 kg male.

- (Shoukas and Brunner, 1980) reports that $\Delta V/m = 12.35$ ml/kg and can reach $\Delta V/m = 13.78$ ml/kg during a change in pressure from 50−200 mmHg. Using $\Delta V = 12.35/m$ ml/kg, this corresponds to a maximal $\Delta V_{un,s} = 1165$ ml.

We have adopted a value of $V_{un,s} = 1050$ ml.

The venous compliance can change 22 % when the carotid sinus pressure is increased from 50 − 200 mmHg (Shoukas and Brunner, 1980). In contrast, (Shoukas and Sagawa, 1973; Greene, 1986) reported no changes in total systemic venous compliance and in the arterial compliance with carotid sinus pressure. However, we allow the venous compliance to vary 22 % as given by (Shoukas and Brunner, 1980).

6.2.5 Estimation of the Distributed Time Delay

Time delays occur in the nervous control due to various biochemical and mechanical processes within the baroreceptor mechanism. The time delay may be viewed as the time from perturbation of the cardiovascular system to the time when the control is complete. The control of the heart is a quick process which amounts to a few seconds while regulation of the veins can take approximately 60 s. Arterial vessel constriction is intermediate around 10 − 15 s (Donald and Edis, 1970; Rothe, 1983; Shoukas and Sagawa, 1973; Guyton, 1991). In addition, sympathetic activity exhibits a time delay with respect to the parasympathetic activity. We ignore this detail since the strategy is to obtain a simple model. Moreover, we are interested in steady states rather than the dynamic ones during transitions. (Ottesen, 1997a) offers a more detailed discussion of this topic.

6.3 General formulation of the Baroreceptor Model

In this section we will establish the general formulation of the two baroreceptor models. Section 6.3.1 describes the first model which assumes that the sympathetic and the parasympathetic activity evolves from steady state experimental results. The approach using the unified model (5.4) is given in Section 6.3.2. Section 6.3.3 describes the efferent responses which are shared by both models. In Section 6.4 we couple the models to the human circulation model established in Chapter 4. In the description of the models, we define the average value of a variable to be the mean value over one heart period.

6.3.1 Modeling the Sympathetic and Parasympathetic Activities using a Steady State Description

We adopt a very simple approach in the modeling of the afferent part and the CNS. We assume that the sympathetic and the parasympathetic activity are described by a sigmoidal function of the averaged carotid pressure as reported by (Korner, 1971). Thus, we describe the sympathetic activity n_s and the parasympathetic activity n_p by

$$n_s(\bar{p}_{cs}) = \frac{1}{1+(\frac{\bar{p}_{cs}}{\mu})^{\nu}}, \tag{6.3}$$

$$n_p(\bar{p}_{cs}) = \frac{1}{1+(\frac{\bar{p}_{cs}}{\mu})^{-\nu}}, \tag{6.4}$$

where $\bar{p}_{cs}$ is the average of the carotid sinus pressure and the constant μ is the average of the steady state arterial pressure at the baroreceptors (i.e. the adapted pressure of the baroreceptors). The parameter ν characterizes the steepness of the curves. Figure 6.2 shows n_s and n_p as functions of the carotid sinus pressure as

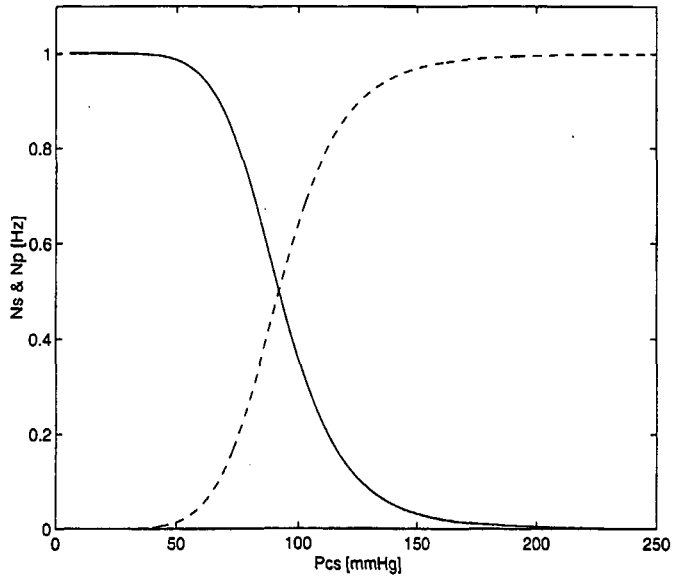

Figure 6.2: The sympathetic (full line) and the parasympathetic (dashed line) activity as predicted by the model (6.3) - (6.4).

predicted by the model. The description (6.3)-(6.4) makes it possible to study the impact of the sympathetic and parasympathetic activity on the human circulatory system and opens for the study of time-delay between the two nervous activities.

Obviously, the model ignores all pulsatile information provided by the carotid sinus pressure which does not change the average carotid sinus pressure. In essence, the model is a very simple description of its real counterpart. In particular, the model (6.3)-(6.4) predicts that a given nervous activity follows from one and only one carotid sinus pressure ignoring the dynamics which lead to this pressure level. The model (6.3)-(6.4) is justified by the complexity of the experimental data used to establish the efferent part of this baroreceptor model. The model of the efferent part is based on experiments which relate changes in effector organs to the average carotid sinus pressure and not to the complex structure of the nervous activities. In addition, we are not interested in studying the dynamic behavior during transitions but in steady states.

6.3.2 Modeling the Sympathetic and Parasympathetic Activities using the Unified Model

The model of the sympathetic n_s and the parasympathetic n_p activity, using the unified model, arises from a model of the afferent part and a model of the CNS. The two submodels are established in the two sections below.

The Model of the Afferent Part

The model of the afferent part assumes that the firing rates n of the carotid sinus receptors can be described by the model (5.4) repeated here for convenience

$$\begin{aligned}
\dot{\Delta n_1} &= k_1 \dot{p}_{cs} \frac{n(M-n)}{(M/2)^2} - \frac{1}{\tau_1}\Delta n_1, \\
\dot{\Delta n_2} &= k_2 \dot{p}_{cs} \frac{n(M-n)}{(M/2)^2} - \frac{1}{\tau_2}\Delta n_2, \\
\dot{\Delta n_3} &= k_3 \dot{p}_{cs} \frac{n(M-n)}{(M/2)^2} - \frac{1}{\tau_3}\Delta n_3,
\end{aligned} \tag{6.5}$$

where

$$n = \Delta n_1 + \Delta n_2 + \Delta n_3 - N. \tag{6.6}$$

The parameters k_1, k_2 and k_3 are weighting factors, τ_1, τ_2 and τ_3 time constants describing the resetting phenomenon, M denotes the saturation level of the firing rates and N the threshold value of the firing rate n. The model contains 8 parameters k_1, k_2, k_3, τ_1, τ_2, τ_3, M and N found from data in the literature and through curve fitting procedures. Further details of the unified model (6.5) are offered in Section 5.3.2 of Chapter 5.

Generation of the Sympathetic and Parasympathetic activities

The information processing in the CNS is complex and the explicit interaction between the firing rate n and the sympathetic activity n_s and the parasympathetic activity n_p is not available yet. Accordingly, and from the viewpoint of simplicity, we describe n_s as decreasing for increasing n by

$$n_s(\bar{n}) = \frac{1}{1 + (\frac{\bar{n}}{\mu_n})^{\nu_n}}, \tag{6.7}$$

where $\bar{n}$ is the average of the firing rates and the constant μ_n is the average of firing rates generated by the steady state carotid sinus pressure (i.e. generated by the adapted pressure at the carotid sinus receptors). The parameter ν_n characterizes the steepness of the curve. The parasympathetic activity is given by

$$n_p(\bar{n}) = 1 - n_s \tag{6.8}$$

$$= \frac{1}{1 + (\frac{\bar{n}}{\mu_n})^{-\nu_n}}. \tag{6.9}$$

Recent experiments by (Wang et al., 1993) show that the sympathetic activity n_s may decrease exponentially with the average $\bar{n}$ of the firing rates. The difference between (6.7) and (Wang et al., 1993) is that (6.7) predicts n_s to be higher for small values of $\bar{n}$ compared to the results by (Wang et al., 1993). These experiments may only provide guidance since they relate n_s to $\bar{n}$ and not to the real dynamics.

6.3.3 Formulation of the Efferent Responses

The description of the efferent responses consists of a static and a dynamic component and is common to the first and the second model. The static component amounts to the steady state responses σ^b. The dynamic component consists of a first order ordinary differential equation which introduces the temporal dynamics. The efferent responses can be described by

$$\frac{dx_i(t)}{dt} = \frac{1}{\tau_i}(-x_i(t) + \sigma_i^b(\bar{p}_{cs})), \quad i \in E = \{H, E_{max}, R_{ps}, V_{un}, C_v\}. \tag{6.10}$$

The index i denotes the particular efferent organ taken from the set E. Thus, x_i is the state variable for the efferent organ i. The time constant τ_i characterizes the transition time for the efferent response i to take full effect. The time delay is also called a distributed time delay and is distinct from a pure latency.

The sympathetic n_s and parasympathetic n_p activities follow a sigmoidal curve with changing average carotid sinus pressure $\bar{p}_{cs}$. Consequently, we assume that the function $\sigma_i^b(\bar{p}_{cs})$ can be expressed as a linear combination of n_s and n_p

$$\sigma_i^b(\bar{p}_{cs}) = \alpha_i n_s(\bar{p}_{cs}) - \beta_i n_p(\bar{p}_{cs}) + \gamma_i \ , i \in E, \tag{6.11}$$

where α_i and β_i denote the strength of sympathetic and parasympathetic activity on x_i, respectively. The constant γ_i is equal to x_i during complete denervation (i.e. $n_s = n_p = 0$). The parameter β_i is only different from zero when $i = H$. Combining (6.10) and (6.11) we obtain

$$\frac{dx_i(t)}{dt} = \frac{1}{\tau_i}(-x_i(t) + \alpha_i n_s(\bar{p}_{cs}) - \beta_i n_p(\bar{p}_{cs}) + \gamma_i) \ , i \in E. \tag{6.12}$$

In the case of the second model, (6.12) is replaced by

$$\frac{dx_i(t)}{dt} = \frac{1}{\tau_i}(-x_i(t) + \alpha_i n_s(\bar{n}) - \beta_i n_p(\bar{n}) + \gamma_i) \ , i \in E. \tag{6.13}$$

By (6.12) and (6.13) we have completed the baroreceptor model. The model consists of a number of parameters, α_i, β_i, γ_i and τ_i, each following from experimental data available in the literature. Unfortunately, firm experimental data do not exist in all cases and the amount of data seems limited. Thus, the determination of the parameter values is a balance between available experimental data found in the literature and data fitting to special topical cases as acute hemorrhage.

6.4 Baroreceptor Model and the Cardiovascular System

In order to allow the model of the baroreceptor mechanism to control the human circulatory system we have coupled the model to the cardiovascular model established in Chapter 4. The coupling of two models forms a closed negative feedback mechanism as shown in Figure 6.3. The arterial pressure p_{a1} in the first section of the cardiovascular model enters the baroreceptor model and equals the carotid sinus pressure. The baroreceptor model provides modifications of the two ventricles and the vasculature. The individual components in this model are quantified in the following sections 6.4.1 - 6.4.2. When the description below is applied to the first model, the sympathetic activity n_s and the parasympathetic activity n_p should be read as $n_s(\bar{p}_{a1})$ and $n_p(\bar{p}_{a1})$, respectively. When the second model is used n_s and n_p should be read as $n_s(\bar{n})$ and $n_p(\bar{n})$, respectively.

6.4.1 Control of the Two Ventricles

The two ventricles are modified by the inotropic and the chronotropic effects. The *inotropic effect* is given by

$$\frac{dx_{E_{max,lv}}(t)}{dt} = \frac{1}{\tau_{E_{max,lv}}}(-x_{E_{max,lv}}(t) + \alpha_{E_{max,lv}} n_s + \gamma_{E_{max,lv}}), \tag{6.14}$$

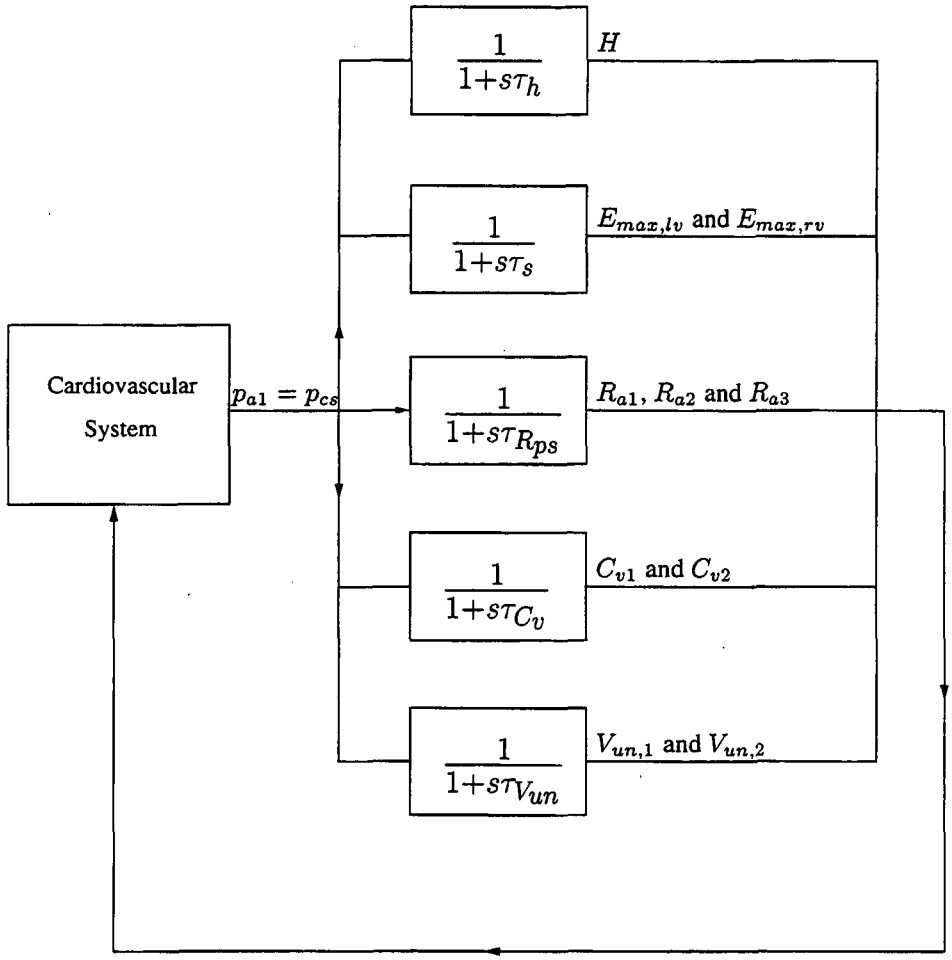

Figure 6.3: The baroreceptor model coupled to the human circulation model established in Chapter 4. The arterial pressure p_{a1} enters the baroreceptor model and equals the carotid sinus pressure. The baroreceptor model offers control of the heart rate H and the cardiac contractility represented by the maximum of the elastance functions, $E_{max,lv}$ and $E_{max,rv}$, respectively. In addition, it modifies the three arterial resistances R_{a1}, R_{a2} & R_{a3}, the venous compliances C_{v1} & C_{v2} and the two venous unstressed volumes $V_{un,2}$ & $V_{un,1}$. The parameters τ_h, τ_s, $\tau_{R_{ps}}$, τ_{C_v} and $\tau_{V_{un}}$ characterize the distributed time delay for the individual controls. The variable s is the frequency in the Laplace domain.

$$\frac{dx_{E_{max,rv}}(t)}{dt} = \frac{1}{\tau_{E_{max,rv}}}(-x_{E_{max,rv}}(t) + \alpha_{E_{max,rv}} n_s + \gamma_{E_{max,rv}}). \qquad (6.15)$$

where $E_{max,lv}$ and $E_{max,rv}$ are used in the elastance function (4.2) defined in Section 4.3.1 of Chapter 4. By (6.14)-(6.15) we neglect the possible parasympathetic influence on the cardiac contractility and follow the simplest approach.

The *chronotropic effect* is contained in

$$\frac{dx_H(t)}{dt} = \frac{1}{\tau_H}(-x_H(t) + \alpha_H n_s - \beta_H n_p + \gamma_H). \tag{6.16}$$

By (6.16) the heart rate is controlled by a linear combination of the sympathetic and the parasympathetic activity. (Ursino, 1998) applied a linear combination to control the heart period. He concluded that the non-linearity observed by (Levy and Zieske, 1969) between the heart rate and the two nervous impulses emerges from the hyperbolic relation between the heart rate H and the heart period t_h ($H = 1/t_h$). (Levy and Zieske, 1969) established a non-linear relation between heart rate and the nervous activities based on a polynomial expression in n_s and n_p. We find the formulation (6.16) perfectly suitable for the problems at hand.

6.4.2 Control of the Vasculature

The vascular efferent components involve the arterial resistances, the venous unstressed volumes and the venous compliances of the systemic circulation.

The control of the *peripheral resistance* is given by

$$\frac{dx_{R_{a1}}(t)}{dt} = \frac{1}{\tau_{R_{a1}}}(-x_{R_{a1}}(t) + \alpha_{R_{a1}} n_s + \gamma_{R_{a1}}), \tag{6.17}$$

$$\frac{dx_{R_{a2}}(t)}{dt} = \frac{1}{\tau_{R_{a2}}}(-x_{R_{a2}}(t) + \alpha_{R_{a2}} n_s + \gamma_{R_{a2}}), \tag{6.18}$$

$$\frac{dx_{R_{a3}}(t)}{dt} = \frac{1}{\tau_{R_{a3}}}(-x_{R_{a3}}(t) + \alpha_{R_{a3}} n_s + \gamma_{R_{a3}}). \tag{6.19}$$

Thus, we control the three resistances R_{a1}, R_{a2} and R_{a3} of the systemic arterial system in Figure 4.6 of Chapter 4.

The control of the *unstressed volume* involves both sections in the systemic venous system and is directed by

$$\frac{dx_{V_{un1}}(t)}{dt} = \frac{1}{\tau_{V_{un1}}}(-x_{V_{un1}}(t) + \alpha_{V_{un1}} n_s + \gamma_{V_{un1}}), \tag{6.20}$$

$$\frac{dx_{V_{un2}}(t)}{dt} = \frac{1}{\tau_{V_{un2}}}(-x_{V_{un2}}(t) + \alpha_{V_{un2}} n_s(\bar{p}_{a2}) + \gamma_{V_{un2}}). \tag{6.21}$$

where the unstressed volumes $V_{un,1}$ and $V_{un,2}$ are defined in (4.12) and (4.13), respectively, of Section 4.5 of Chapter 4.

The control of the *venous compliance* is defined by

$$\frac{dx_{C_{v1}}(t)}{dt} = \frac{1}{\tau_{C_{v1}}}(-x_{C_{v1}}(t) + \alpha_{C_{v1}} n_s + \gamma_{C_{v1}}), \tag{6.22}$$

$$\frac{dx_{C_{v2}}(t)}{dt} = \frac{1}{\tau_{C_{v2}}}(-x_{C_{v2}}(t) + \alpha_{C_{v2}} n_s + \gamma_{C_{v2}}). \tag{6.23}$$

where the compliances C_{v1} and C_{v2} are defined in the human circulation model of Figure 4.6 in Chapter 4. We have allowed the unstressed volumes and the compliances in both venous sections to be altered since the experimental data and the lumped approach do not allow an individual measure of each of the parameters. The experiments do not distinguish between alterations in the arterial unstressed volume $\Delta V_{un,a}$ and the venous unstressed volume $\Delta V_{un,v}$. Since most of the circulatory volume resides in the veins, we assume that the entire change in the unstressed volume is mediated by the veins.

6.5 Open loop Responses

Determination of the parameters values of α_i, β_i, γ_i and τ_i for an intact human evolves from a compromise between the experimental open loop responses reported in Section 6.2 and the experimental data from an acute hemorrhage by (Hosomi and Sagawa, 1979) (see Section 6.8). The reason why the latter experiments are used, is that the open loop responses only can be guiding since they are obtained in vagotomized animals. The experiments are not representative for an intact subject.

The computed open loop responses for the first model, shown in the figures 6.4 - 6.6, are obtained by varying the carotid sinus pressure p_{cs} sufficiently slowly in the model and observing the concomitant efferent responses. The parameter values of α_i, β_i and γ_i are determined from the low and the high saturation levels listed in Table 6.5. The parameter values of α_i, β_i and γ_i can be found in Table 6.7. The parameter values in Table 6.7 are also valid for the second model. The computed open loop responses of the second model will not be shown for reasons of brevity. The second model contains 9 parameters which are not included the first model. These parameters are described in Section 6.6

Figure 6.4 shows the open-loop response in cardiac contractility $E_{max,lv}$ & $E_{max,rv}$ and heart rate H superimposed on the data by (Suga et al., 1973) and (Korner, 1974; Bolter and Ledsome, 1976; Greene, 1986), respectively. The computed heart rate response for the intact human is chosen to follow the experiments by (Korner, 1974) in the central range. The experimental data by (Bolter and Ledsome, 1976; Greene, 1986) are obtained with the contribution of aortic arch eliminated and they are thus not fully representative for an intact human.

The open loop responses for the three arterial resistances R_{a1}, R_{a2} and R_{a3} are shown in Figure 6.5 superimposed on the experimental data by (Greene, 1986; Cox and Bagshaw, 1975; Shoukas and Brunner, 1980). (Cox and Bagshaw, 1975) discriminates between the resistance in the femoral and in the celiac part of the systemic arterial system. The resistance varies more in the outer part than in the more internal parts of the cardiovascular system. The lumped approach adapted

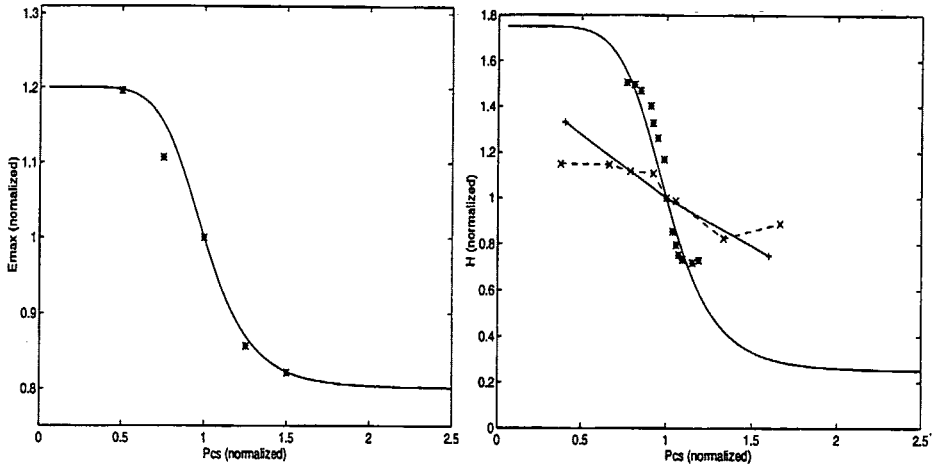

Figure 6.4: The left panel shows the computed open loop responses of the maximum elastances $E_{max,lv}$ and $E_{max,rv}$ as functions of the normalized average carotid sinus pressure $\bar{p}_{cs}$ superimposed on the experimental data from (Suga et al., 1976) (∗). The right panel displays the computed open loop responses of the heart rate H as a function of the normalized average carotid sinus pressure $\bar{p}_{cs}$ superimposed on experimental data from (Korner, 1974)(∗), (Bolter and Ledsome, 1976) (dashed, x) & (Greene, 1986) (full line, +). The pressures are normalized with respect to the computed steady state value (92 mmHg) and experimental data to the reported baseline values.

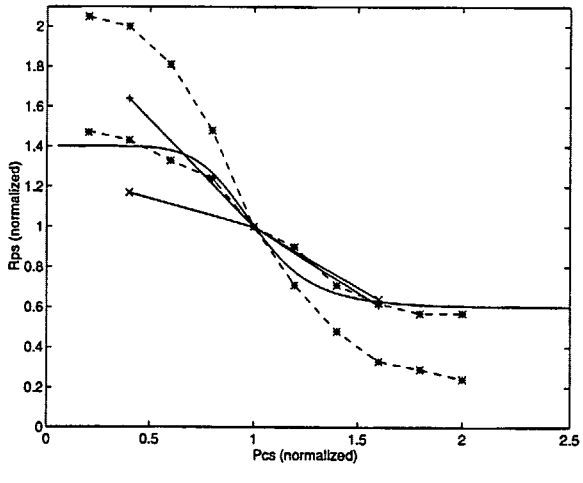

Figure 6.5: Computed open loop response for the three arterial resistances R_{a1}, R_{a2} and R_{a3} superimposed on the experimental data from (Greene, 1986) (full line, x), (Cox and Bagshaw, 1975) (dashed line, ∗) & (Shoukas and Brunner, 1980) (full line, +). The computed pressures are normalized with respect to the steady state value (92 mmHg) and the experimental data to the reported baseline values.

here does not allow such a division.

The venous unstressed volume and the venous compliance exhibit the open loop responses shown in Figure 6.6. The left panel shows the open loop response of the venous compliance superimposed on the experimental data by (Shoukas and Brunner, 1980). The right panel shows the venous unstressed volume displayed in absolute values superimposed on the absolute changes in the systemic unstressed volume by (Shoukas and Sagawa, 1973; Shoukas and Brunner, 1980).

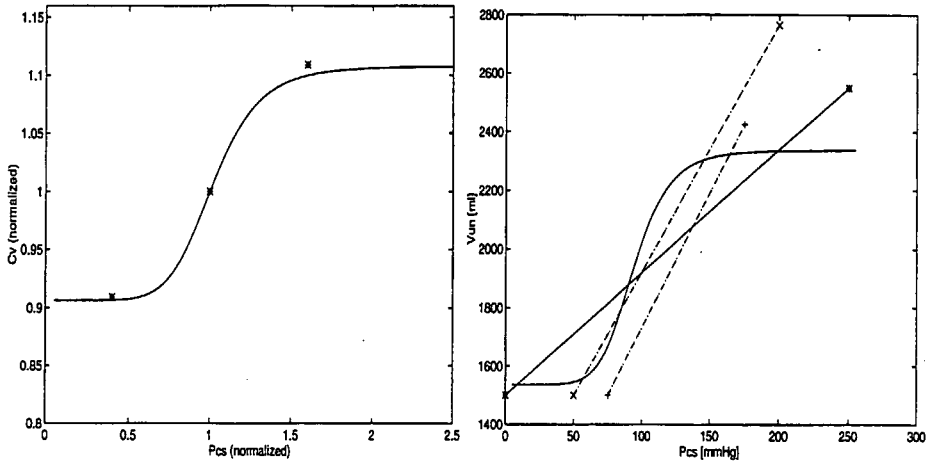

Figure 6.6: The left panel shows the computed open loop response for the venous compliances C_{v1} and C_{v2} superimposed on data from (Shoukas and Brunner, 1980) ($*$). The right panel shows the computed open loop response for the venous unstressed volume $V_{un,2}$ (full line) and the total change in computed venous unstressed volume from 0 - 250 mmHg (full line, $*$). The right panel shows also the corresponding experimental changes in the total venous unstressed volume obtained from (Shoukas and Sagawa, 1973) (dashed line, +) and (Shoukas and Brunner, 1980) (dashed line, x).

A first validation of the baroreceptor model may consist of a comparison between computed and experimental open loop responses between the carotid sinus pressure and the arterial pressure as shown in Figure 6.7. The response from the baroreceptor model appears to be more powerful than the experimental data allow. It should be kept in mind that the experimental data are measured after the aortic arch receptors are eliminated. Consequently, the two results cannot be directly compared.

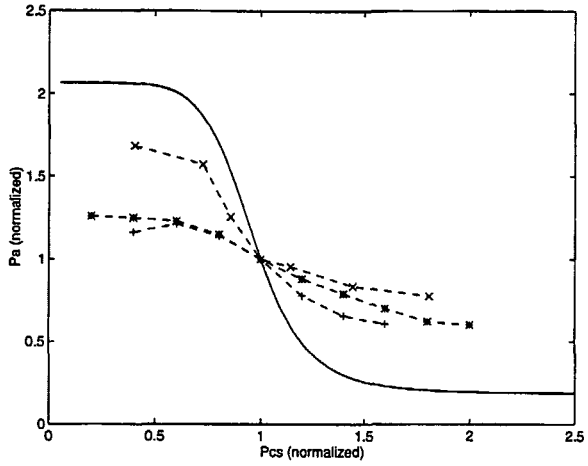

Figure 6.7: Computed open loop responses for the arterial pressure p_{a1} superimposed on experimental data by (Cox and Bagshaw, 1975) (dashed line, $*$), (Bolter and Ledsome, 1976) (dashed line, x), & (Shoukas and Brunner, 1980) (dashed line $+$). The computed pressures are normalized with respect to the steady state value (92 mmHg) and experimental data to the reported baseline values.

6.6 Parameter Values of the two Baroreceptor Models

The parameter values μ and ν, used in the generation of the sympathetic and the parasympathetic activity in the first model, can be found in Table 6.3. The parameter values of α_i, β_i and γ_i, valid for both baroreceptor models, can be found Table 6.7.

The second model contains 9 parameters k_1, k_2, k_3, τ_1, τ_2, τ_3, N, M and N_μ which are not included in the first model. These parameters are determined as follows. The parameter value of N_μ is equal the average firing rate generated by the steady state arterial pressure (the adapted pressure of baroreceptors). The value of the time constants τ_1, τ_2, τ_3 are taken from (Ottesen, 1997b) and are given in Table 5.1. The values of the weighting factors k_1, k_2, k_3 are determined from a comparison between the computed and the experimental results during an acute hemorrhage considering the physiological significance of the parameters. During the 30 s hemorrhage we assume that the slow component has the dominating role ($k_3 = 1.5$ Hz/mmHg) whereas the intermediate component plays a minor role ($k_2 = 0.5$ Hz/mmHg) and that the quick component is of no importance ($k_1 = 0$ Hz/mmHg). The parameter values can be found in Table 6.4.

6.7 Results using the First Model

In the sections 6.8 - 6.10 we compare a number of animal experiments found in the literature with the corresponding results predicted by the first model. This evaluation is carried out by computing the responses during

- *Acute hemorrhage*
- *Heart pacing*
- *Different pulsatile carotid sinus pressures*

The efferent organs are not equally important during a hemorrhage. Thus, we have performed a sensitivity analysis in order to investigate the impact the controls of H, R_{ps}, S, C_v and V_{un} have on the cardiovascular performance. This is done in Section 6.8.1.

6.7.1 Numerical Method

The set of differential equations in the model has been solved by use of a 5-6 order Runge-Kutta method with variable time steps and TOL $= 10^{-6}$. The maximum allowed time step is 10^{-3} s. All the average values are computed over one heart period by used of a trapezoidal intergration method. The computed average values in the model are calculated over the previous heart period t_h from the current time t, i.e. from $t - t_h$ to t. The human circulation model has also been tested on a fourth order Runge-Kutta method with variable time steps and TOL $= 10^{-3}$. The maximum time step was equal to 0.02 s.

6.8 Acute Hemorrhage using the First Model

An acute hemorrhage from the femoral arteries is followed by a weakening of cardiac filling and diminished arterial pressure, cardiac output, stroke volume and increased heart rate and vessel constriction. These general lines are found in the experimental results by (Hosomi and Sagawa, 1979) where 10 % of the total circulatory volume was removed via the femoral arteries in 30 s.

The experiments by (Hosomi and Sagawa, 1979) are simulated by a constant leak in the third section of the arterial systemic system. Figure 6.8 displays computed and experimental results for an intact human. The figure shows the relative changes in average arterial pressure $\bar{p}_a$, cardiac output CO, heart rate H and peripheral resistance R_{ps}. The agreement between the computed and experimental results are striking.

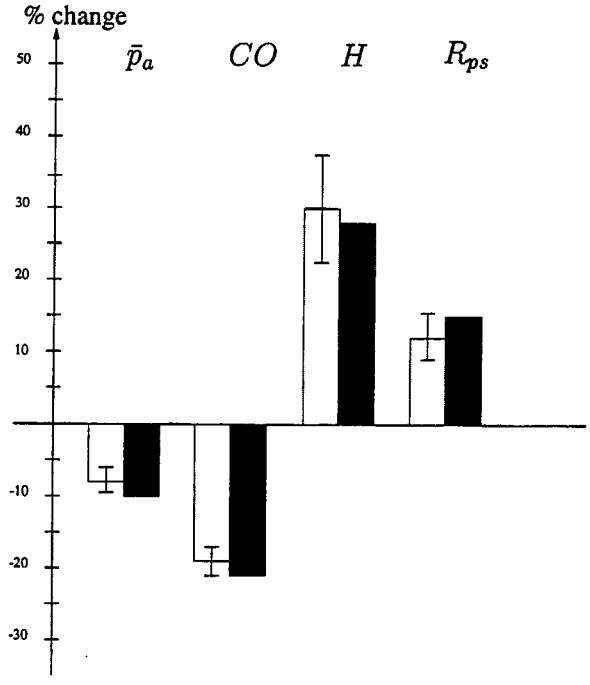

Figure 6.8: Computed (black bars) and experimental (white bars) relative changes in average arterial pressure $\bar{p}_a$, cardiac output CO, heart rate H and peripheral resistance R_{ps} during an acute 10 % hemorrhage from the femoral arteries. The experimental results are adopted from (Hosomi and Sagawa, 1979) for an intact animal. The total circulatory volume is reduced by 10 % in 30 s and the experimental data is obtained $1-2$ min after the hemorrhage is terminated. The computed results are obtained in the new steady state reached after 1 min.

The response during complete denervation is shown in Figure 6.9. Again, the computed results agree well with the experiments.

The computed results are obtained using only the average of the arterial pressure p_{a1}. This is consistent with results reported by (Kumada, Schmidt, Sagawa and Tan, 1970). They concluded that the pulsatile component of the carotid sinus pressure has only little effect compared with that of the average carotid sinus pressure during a 20 % acute hemorrhage.

6.8.1 Sensitivity results during a Hemorrhage

The control of the venous unstressed volume has a profound impact on the overall performance of the circulatory system as will become clear from Figure 6.10. Figure 6.10 shows the computed responses during acute hemorrhage for weaker control of the venous unstressed volume. The differences between experiments and computed results increase as the strength of the control is decreased except

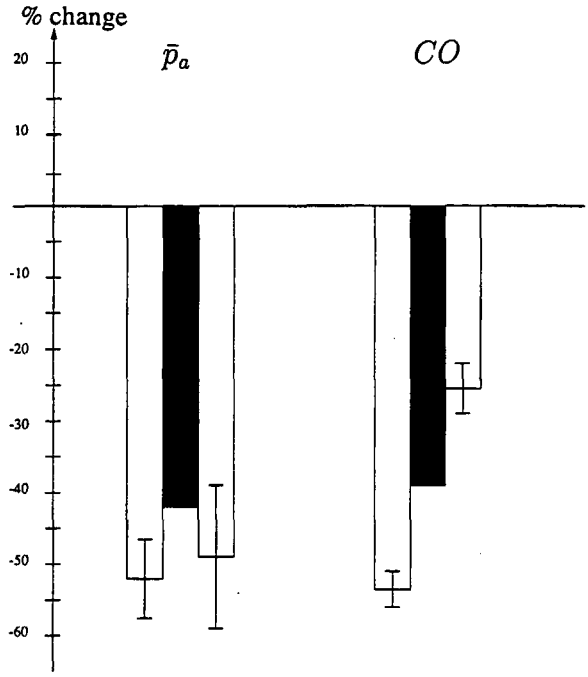

Figure 6.9: Computed (black bars) and experimental (white bars) relative changes in average arterial pressure $\bar{p}_a$ and cardiac output CO during an acute 10 % hemorrhage from the femoral arteries with complete denervation (i.e. no carotid sinus and aortic arch receptors active). The experimental results depend on the order of carotid sinus and aortic arch denervation. Aortic arch is denervated first in the left column. In the right column, the carotid sinus is denervated first. The experiments are adopted from (Hosomi and Sagawa, 1979). The total circulatory volume is reduced by 10 % in 30 s and the experimental data is obtained $1-2$ min after the hemorrhage is terminated. The computed results are obtained in the new steady state reached after 1 min.

for the response in the heart rate H. However, the response in H differs from the experiments when the control of the unstressed volume is absent. The relative changes in arterial pressure p_a, cardiac output CO, peripheral resistance R_{ps} and heart rate H increase. The computed results suggest that the impaired ventricular filling of the heart, following acute hemorrhage, can be partially compensated by active vessel constrictions in the veins. Discrepancies arise as the strength of this control is reduced while leaving the remaining regulatory strengths unaltered. This is consistent with the computed results by (Ursino et al., 1994).

In contrast to the unstressed venous volume, heart rate H, peripheral resistance R_{ps}, venous compliance C_v and cardiac contractility E_{max} play no major roles during acute hemorrhage as is evident from figures 6.11 and 6.12. Figure 6.11 displays the computed result during different strengths of heart rate control. The results show that heart rate has only a weak influence after an acute hem-

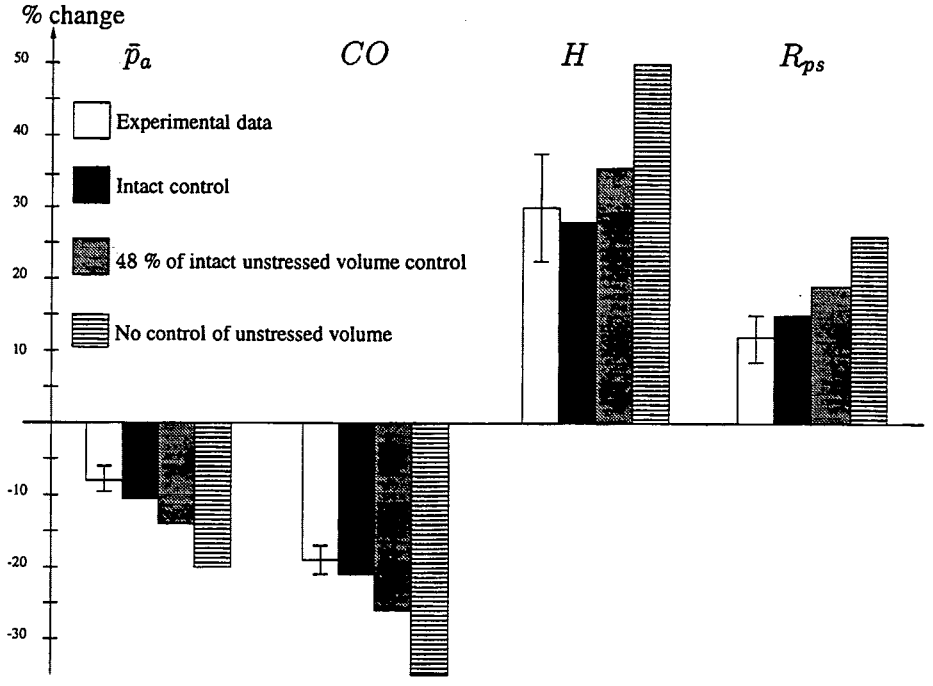

Figure 6.10: Computed and experimental (white bars) relative changes in average arterial pressure $\bar{p}_a$, cardiac output CO, heart rate H and peripheral resistance R_{ps} during an acute 10 % hemorrhage from the femoral arteries with different control strengths of the unstressed volume. The experiments are adopted from (Hosomi and Sagawa, 1979). The total circulatory volume is reduced by 10 % in 30 s and the experimental data is obtained $1 - 2$ min after the hemorrhage is terminated. The computed results are in the new steady state after 1 min.

orrhage. Figure 6.12 shows the computed results when the control of cardiac contractility E_{max}, peripheral resistance R_{ps} and venous compliance are eliminated. In particular, ignoring the control of the peripheral resistance generates an improved cardiac output but no worthwhile changes in average arterial pressure $\bar{p}_a$ and heart rate H compared with an intact human. Raising cardiac contractility E_{max} or heart rate H has only a weak impact on the circulatory response since cardiac performance cannot be much improved because of the poor ventricular filling during an acute hemorrhage. It may do the opposite and deteriorate performance further by pumping more blood out of the heart. The minor contribution from the change in venous compliance may be related to minor absolute volume changes associated with this reflex.

The computed arterial pressure p_{a1} during hemorrhage with different impairments of the efferent regulations are shown in figures 6.13 and 6.14. In essence, the two figures summarize the results stated above. The left panel of Figure 6.13 shows the pivotal role played by the baroreceptor mechanism during an acute

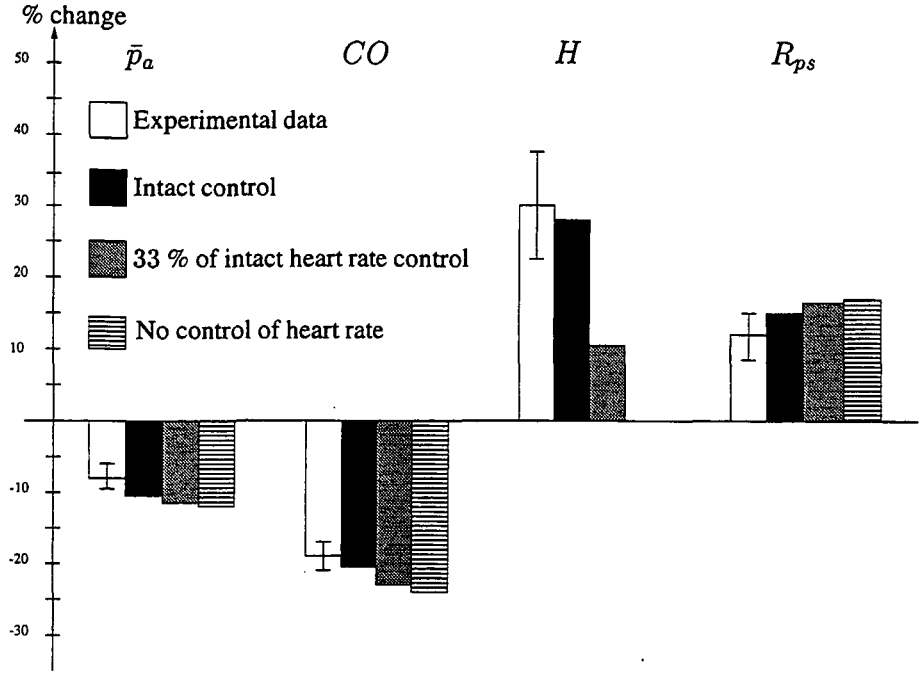

Figure 6.11: Computed and experimental (white bars) results when the regulation of the heart rate is varied in strength. The figure shows the relative changes in average arterial pressure $\bar{p}_a$, cardiac output CO, heart rate H and peripheral resistance during an acute 10 % hemorrhage from the femoral arteries with different control strengths on the heart rate. The experiments are adopted from (Hosomi and Sagawa, 1979). The total circulatory volume is reduced by 10 % in 30 s and the experimental data is obtained $1-2$ min after the hemorrhage is terminated. The computed results are obtained in the new steady state reached after 1 min.

hemorrhage. The right panel shows the arterial pressure p_{a1} when the control of cardiac contractility is absent and the computed result with intact baroreceptor mechanism. No marked difference exists between the two results. This shows the weak role played by the control of cardiac contractility, $E_{max,lv}$ and $E_{max,lv}$, after an acute hemorrhage. The impact of the venous compliance can be neglected as is evident from the left and right panel of Figure 6.14.

6.9 Heart Pacing using the First Model

Stroke volume V_s drops as heart rate H increases whereas cardiac output CO first increases, reaches a maximum and finally declines (Kumada, Azuma and Matsuda, 1967; Melbin, Detweiler, Riffle and Noordergraaf, 1982). Figure 6.15 shows the computed stroke volume V_s and cardiac output CO during heart pacing.

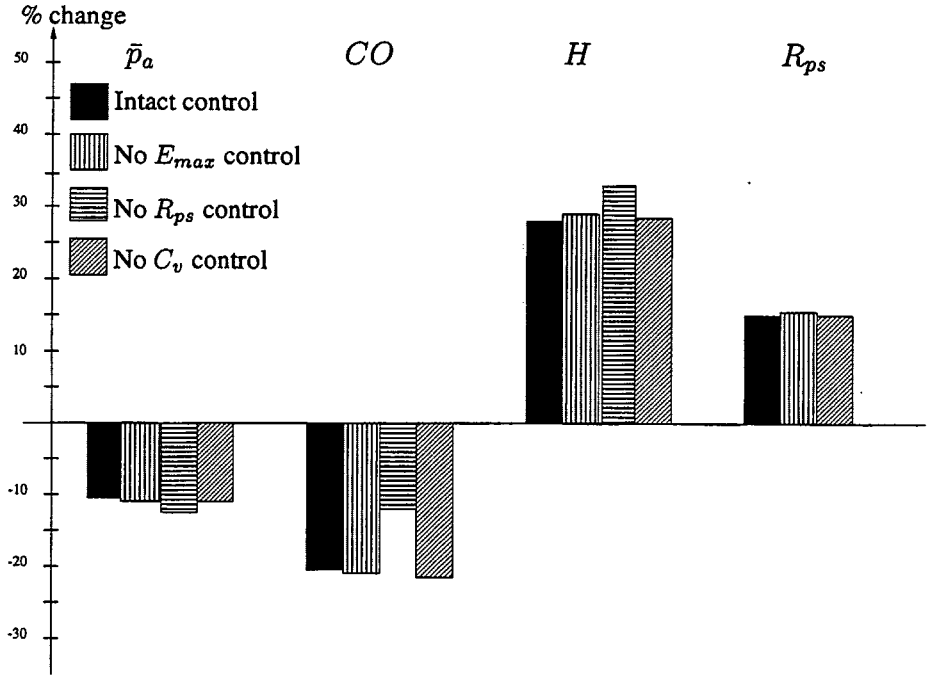

Figure 6.12: Computed results when the control of cardiac contractility E_{max}, peripheral resistance R_{ps} or venous compliance C_v are removed. The figure shows the relative changes in average arterial pressure $\bar{p}_a$, cardiac output CO, heart rate H and peripheral resistance R_{ps} during an acute 10 % hemorrhage from the femoral arteries. The computed results are obtained in the new steady state reached after 1 min.

Heart rate H is taken as the independent variable whereas the remaining effector organs are modified by the baroreceptor mechanism. The computed results show that stroke volume is consistently falling as the heart rate increases. The result is in qualitative agreement with experiments reported by (Kumada et al., 1967; Melbin et al., 1982). The computed result exhibits a reduced end-diastolic volume during the rising heart rate which contributes to the decline in stroke volume and the behavior pattern of the cardiac output during atria pacing (Kumada et al., 1967; Melbin et al., 1982).

The heart rate cannot compensate the drop in stroke volume when the heart rate exceeds approximately 2.3 Hz. Consequently, cardiac output and arterial pressure drop significantly as shown in the right panel of Figure 6.15 and in the left panel of Figure 6.16, respectively. The right panel of Figure 6.16 shows that the peripheral resistance increases when the heart rate exceeds 2.3 Hz which may decrease in stroke volume even further. The results show that the baroreceptor mechanism cannot effectively combat the drop in cardiac output when the heart rate is sufficiently high.

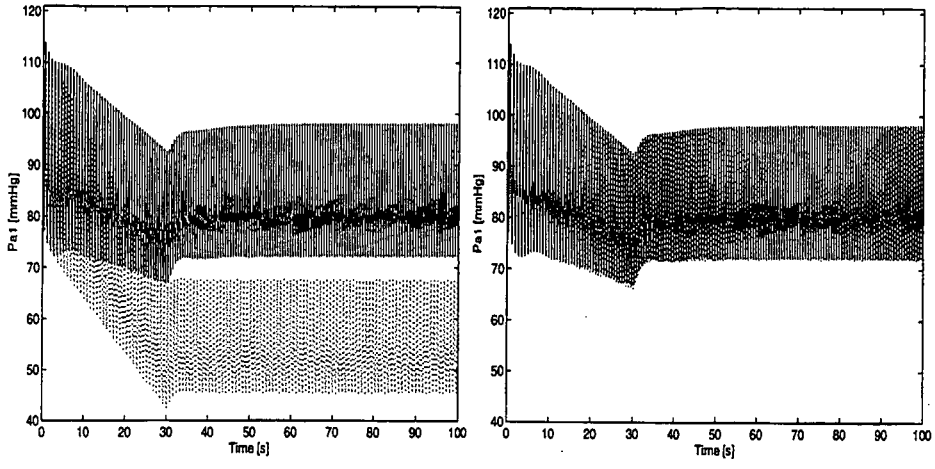

Figure 6.13: The left panel shows computed arterial pressure p_{a1} during 10 % acute hemorrhage with the entire baroreceptor mechanism active (full line) and during complete denervation (dotted line). The right panel shows the computed arterial pressure p_{a1} with the entire baroreceptor mechanism active (full line) and with no control of the cardiac contractility.

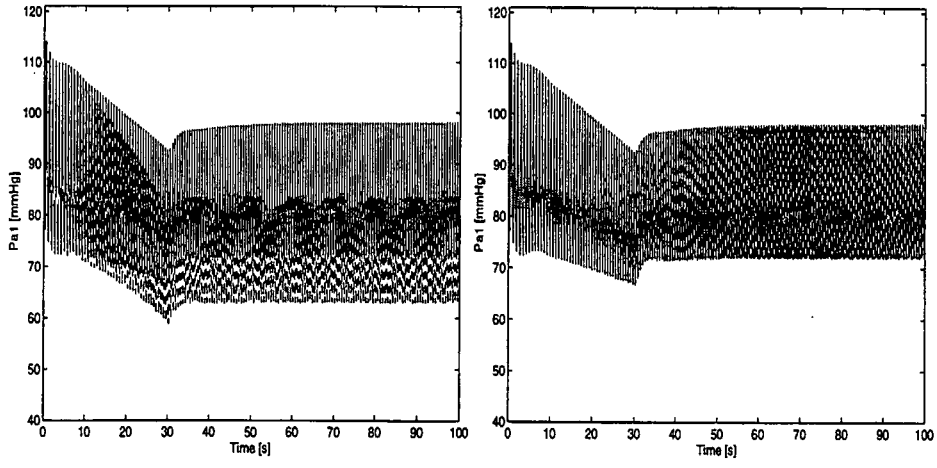

Figure 6.14: The left panel shows computed arterial pressure p_{a1} during 10 % acute hemorrhage with the entire baroreceptor mechanism active (full line) and with no control of the veins (dotted line) (i.e. no control of compliance, C_{v1} and C_{v2}, and unstressed volume, V_{un1} % V_{un2}). The right panel shows computed arterial pressure p_{a1} with the entire baroreceptor mechanism active (full line) and with no control of the venous compliance, C_{v1} & C_{v2} (dotted line).

A sudden and sustained increase in peripheral resistance lowers stroke volume and cardiac output. Figure 6.15 shows the computed results when the peripheral resistance is increased to $1.7R_{ps}$. This result agrees favorably with the experiments by (Kumada et al., 1967).

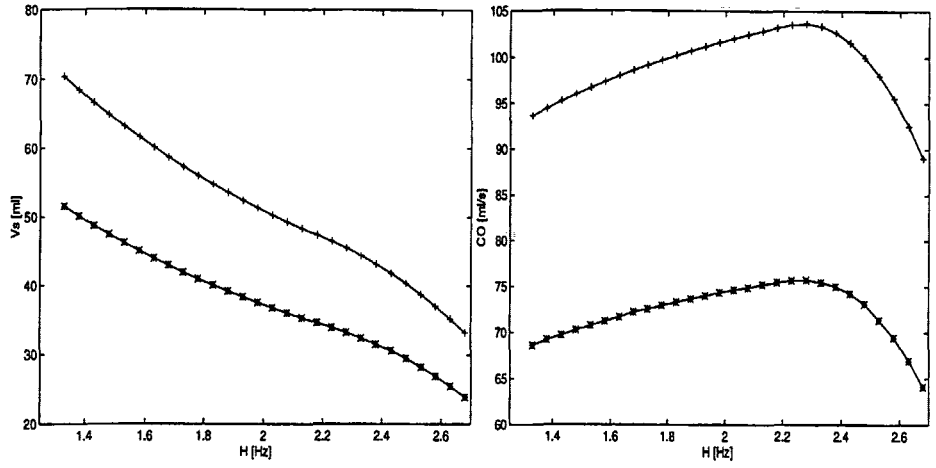

Figure 6.15: The left panel shows computed steady values of stroke volume V_s with peripheral resistance R_{ps} (+) and with a higher peripheral resistance $1.7R_{ps}$ (∗) during heart pacing. The right panel shows the corresponding computed cardiac output with the peripheral resistance R_{ps} (+) and with a higher peripheral resistance $1.7R_{ps}$ (∗) during heart pacing.

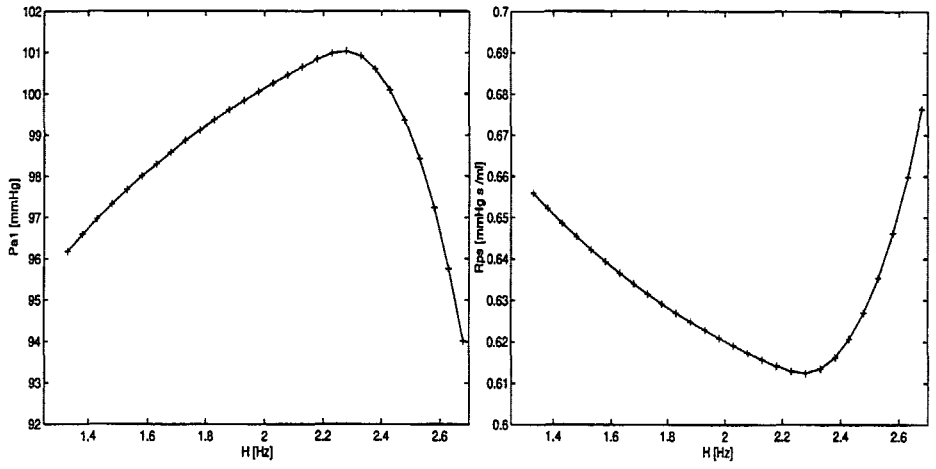

Figure 6.16: The left panel shows computed steady state values of the average of arterial pressure p_{a1} during heart pacing. The right panel shows the corresponding computed steady values for the peripheral resistance.

Experiments have shown that dV_s/dH as a function of heart rate H remains unaltered during a number of different conditions. This includes standing, awake, recumbent and during influence of various anesthetics. The curve is altered when e.g. the peripheral resistance is increased suddenly. Figure 6.17 displays the computed results superimposed on the data given by (Melbin et al., 1982). The figure shows close agreement between the computed and the experimental results when

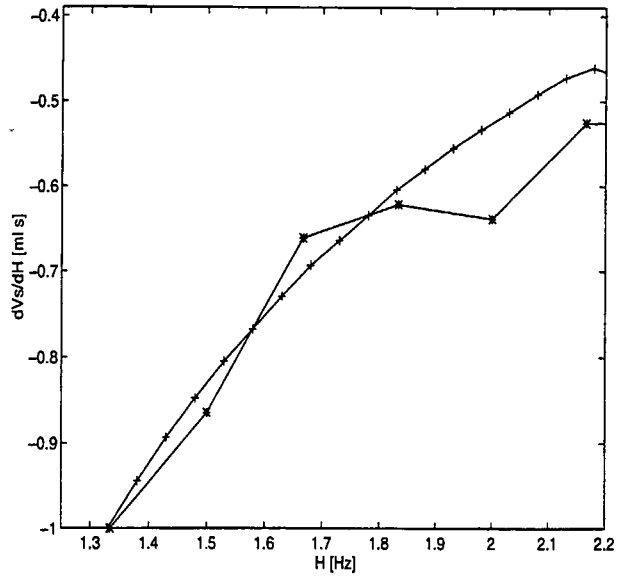

Figure 6.17: Computed dV_s/dH (+) as a function of the heart rate H superimposed on data by (Melbin et al., 1982)(∗).

heart rate runs from 1.33 Hz - 2.2 Hz. Discrepancies arise when heart rate is increased above this range. The computed dV_s/dH declines significantly when the heart rate exceeds 2.2 Hz as shown in Figure 6.18. This corresponds to an accelerated drop in the stroke volume with the heart rate. In the previous computed results, cardiac output displayed a drop when the heart rate exceeded 2.3 Hz. This fall commences at a lower heart rate than in the animal experiments. The reasons for these discrepancies may be related to the simple model of the ventricular performance. In the ventricular elastance function (4.2), the division between the active phase and the passive phase is specified by (4.11) which is a linear function of the heart period t_h. When the heart rate increases, the diastole shortens much more than the systole which implies an impaired ventricular filling (Tortora and Anagnostakos, 1990). This is included in the model. However, one reason for the discrepancy, may be, that the diastole shortens too fast, as a function of the heart rate, when (4.11) is used. In addition, autoregulation and the control from the chemoreceptors have not been included in the model which may play a role at this high value of the heart rate.

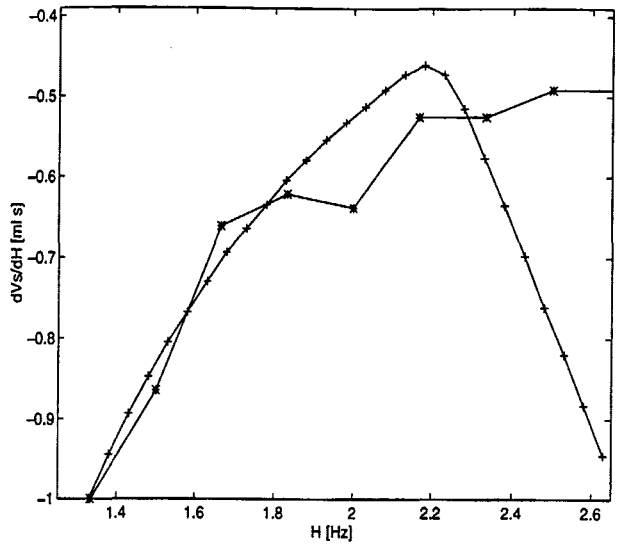

Figure 6.18: Computed dV_s/dH (+) as a function of heart rate H superimposed on data by (Melbin et al., 1982)(∗) in the heart rate range from 1.33 Hz- 2.6 Hz.

6.10 Responses to Pulsatile Carotid Sinus Pressure using the First Model

Exposing the model to different pulsatile carotid sinus pressures is a critical test of this model since it is built exclusively on steady state results and is used in a pulsatile environment. (Schmidt, Kumada and Sagawa, 1972) studied experimentally the response in the average arterial pressure, the peripheral resistance and the cardiac output to pulsations in the carotid sinus pressures in vagotomized animals. In these experiments, the carotid sinus pressure p_{cs} is taken as the independent variable (i.e. open loop) and the hemodynamic variables are altered accordingly. The carotid sinus pressure equals a static pressure $p_{cs,0}$ plus a pulsatile term $A\sin(2\pi ft)$, where the frequency $f = 2$ Hz. Thus,

$$p_{cs} = p_{cs,0} + A\sin(2\pi ft), \tag{6.24}$$

where A is the amplitude. In order to study the effects of pulsation, we replace the average pressure $\bar{p}_{cs}$ in the model of the sympathetic and parasympathetic activity, (6.3)-(6.4), by the instantaneous pressure p_{cs} in (6.24). We mimic the vagotomized condition by taking $n_p = 0$ and reduce the strength of the heart rate control from 75 % to 50 %.

The computed results are shown in the left panel of Figure 6.19. This figure shows the average of the arterial pressure p_{a1} as a function of the static pressure

$p_{cs,0}$ when the carotid sinus pressure is given by (6.24) with $A = 0$ superimposed

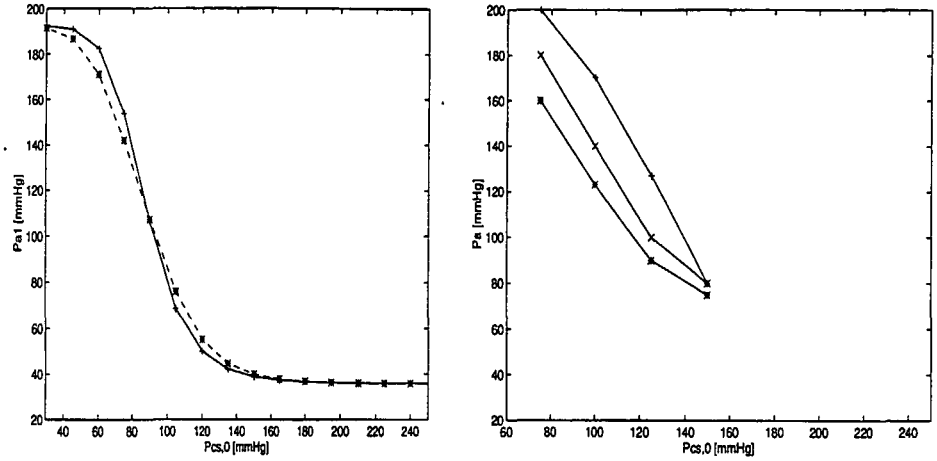

Figure 6.19: The left panel shows the computed average of the arterial pressure p_{a1} as a function of the static pressure $p_{cs,0}$ when the carotid sinus pressure is given by (6.24) with $A = 0$ (full line, +) after vagotomy. This is superimposed on the predicted pressure when $A = 25$ mmHg (dashed line, $*$). The results are obtained in the steady state. The right panel displays the corresponding experimentally obtained arterial pressure p_a, when $A = 0$ (+) in (6.24), as a function of $p_{cs,0}$. This is superimposed on the obtained arterial pressure when $A = 12.5$ (x) and when $A = 25$ ($*$). The experiments are adopted from (Schmidt et al., 1972).

on the predicted response when $A = 25$ mmHg. In these computations the static pressure $p_{cs,0}$ has been varied from 30 - 250 mmHg in steps of 15 mmHg. The displayed results are obtained in the steady state.

According to the computations, shown in the left panel of Figure 6.19, the effect of pulsation in the carotid sinus pressure is a drop in the arterial pressure when the static pressure $p_{cs,0}$ is below 90 mmHg. In contrast, the arterial pressure is unaltered when $p_{cs,0}$ is equal to 90 mmHg and when the arterial pressure is in the high and low saturation regions. When the static pressure $p_{cs,0}$ exceeds 90 mmHg the effect of pulsation in the carotid sinus pressure is a rise in the arterial pressure. The same behavior pattern is predicted in the peripheral resistance and in the cardiac output.

The right panel of Figure 6.19 shows the experimental results by (Schmidt et al., 1972). Also, the experimental results show a drop in average arterial pressure when the carotid sinus (6.24) becomes pulsatile. The effect of pulsality is a marked drop in the arterial pressure when $p_{cs,0}$ falls below 150 mmHg but the arterial pressure is practically unaltered when $p_{cs,0}$ is equal to 150 mmHg. The behavior above 150 mmHg and below 75 mmHg is not available. Thus, the computed sigmoidal behavior pattern cannot be directly compared with the experi-

ments. However, the drop in arterial pressure is clearly more pronounced in the experiments than in the computations. The experiments display also a fall in the peripheral resistance and in the cardiac output. Again, the fall in the experiments is more accentuated than in the corresponding computations.

One likely reason for the differences between the experiments and the computations may be the simple description (6.3) of the relation between the sympathetic activity and the average arterial pressure. Explicit knowledge of the processes in the CNS is not available yet but knowledge does exist about the relation between the firing rates n of the carotid sinus receptors and the carotid sinus pressure p_{cs}. This relation is not a building block in the model but is lumped into the formulation (6.3). Experimentally, the firing rates are affected by the carotid sinus pressure (6.24) in a characteristic fashion as shown by (Chapleau and Abboud, 1987). These experiments show that the firing rates n of the baroreceptors increase sigmoidally with the static carotid sinus pressure when the pressure is varied from 40 - 200 mmHg. When a pulsatile pressure is superimposed on the static carotid sinus pressure, the curve can become practically linear. Thus, the effect of pulsality in the experiments is that the firing rates rise when the average pressure is below approximately 100 mmHg and drop when the average pressure exceeds approximately 100 mmHg. The firing rates are almost unaltered for high pressures and at 100 mmHg.

Thus, the computed pressure in the left panel of Figure 6.19 is consistent with the experiments by (Chapleau and Abboud, 1987). The behavior of the computed results when the pressure is given by (6.24), can be explained from the sigmoidal curve shape of (6.3) relating the sympathetic activity n_s to the arterial pressure. The symmetry around the central point of the sigmoidal curve generates no changes in the average pressure. As the static term $p_{cs,0}$ decreases, the top portion of the pulsatile term is reduced compared to the lower part due to the bending of the sigmoidal curves. This implies a lower average value of n_s. In contrast, the lower portion of the pulsatile term is reduced, when the static term $p_{cs,0}$ is higher than the baseline value.

6.11 Acute Hemorrhage using the Unified Model

In this section we will compare the computed results of an acute hemorrhage, using the second model, with the experiments by (Hosomi and Sagawa, 1979) where 10 % of the total circulatory blood volume is removed via the femoral arteries in 30 s. The experiments are computed as explained in Section 6.8. Figure 6.20 shows the computed and the experimental relative changes in the average arterial pressure $\bar{p}_a$, the cardiac output CO, the heart rate H and the peripheral resistance R_{ps}. The figure displays a striking agreement between the computed

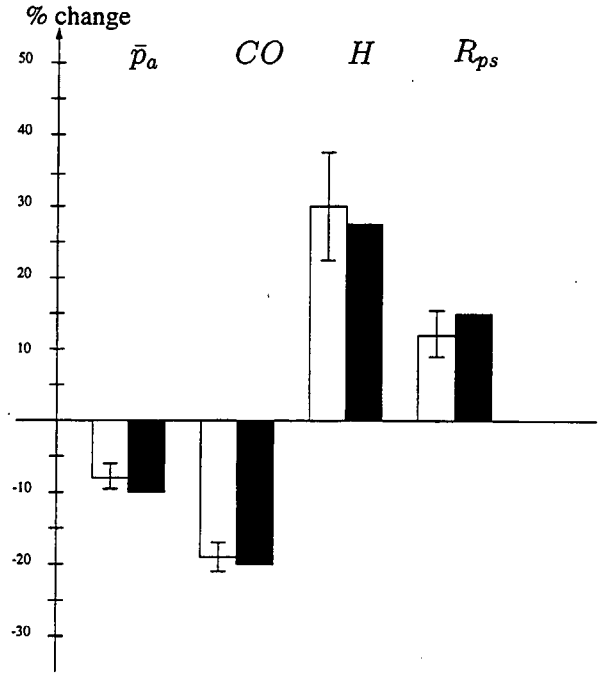

Figure 6.20: Computed (black bars) and experimental (white bars) relative changes in average arterial pressure $\bar{p}_a$, cardiac output CO, heart rate H and peripheral resistance R_{ps} during an acute 10 % hemorrhage from the femoral arteries. The experimental results are adopted from (Hosomi and Sagawa, 1979) for an intact animal. The total circulatory volume is reduced by 10 % in 30 s and the experimental data is obtained $1-2$ min after the hemorrhage is terminated. The computed results are obtained in the new steady state reached after 1 min.

and the experimental results.

Adaptation is built into the model as discussed in Section 5.3.2 of Chapter 6. The adaptation after the hemorrhage is shown in the figures 6.21 and 6.22. Figure 6.21 shows the instantaneous changes in the heart rate H and the resistance R_{a3} during and after the hemorrhage. Figure 6.22 shows the concomitant change in the average of the arterial pressure p_{a1} and the average of the firing rates n. The adaptation directs the firing rates n, the heart rate H and the resistance R_{a3} towards approximately their pre-hemorrhage values. In contrast, the arterial pressure will reach a lower value close to the pressure level obtained, if the control from the baroreceptor mechanism is absent during the hemorrhage. This is shown in Table 6.2. We stress that this adaptation results exclusively from the baroreceptors and thus that the computations exclude many other contributing mechanisms.

As seen in the figures 6.21 and 6.22, the arterial pressure p_{a1} decays faster than the decline in the heart rate, the peripheral resistance and the rise in the firing rates. The reason for this is, that the total effect on the pressure consists of a non-

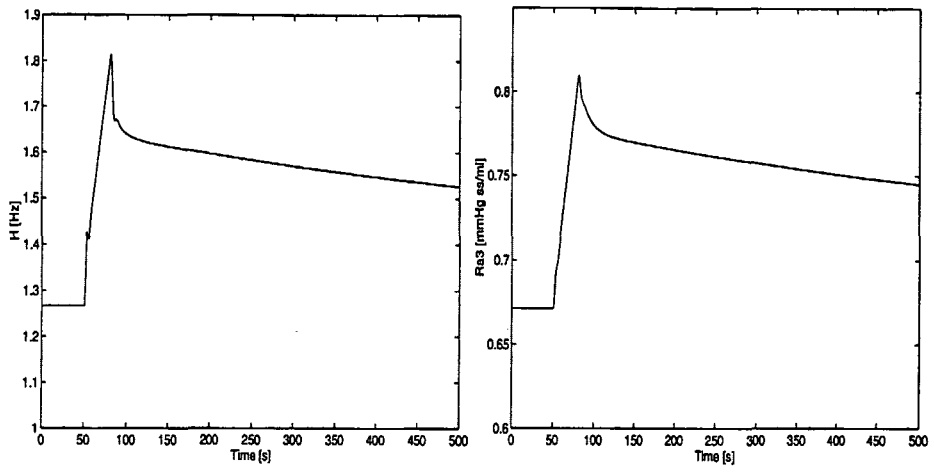

Figure 6.21: The left panel shows computed heart rate H during and after the 10 % acute hemorrhage which starts at 50 s and ends at 80 s. The right panel shows the concomitant changes in the resistance R_{a3}.

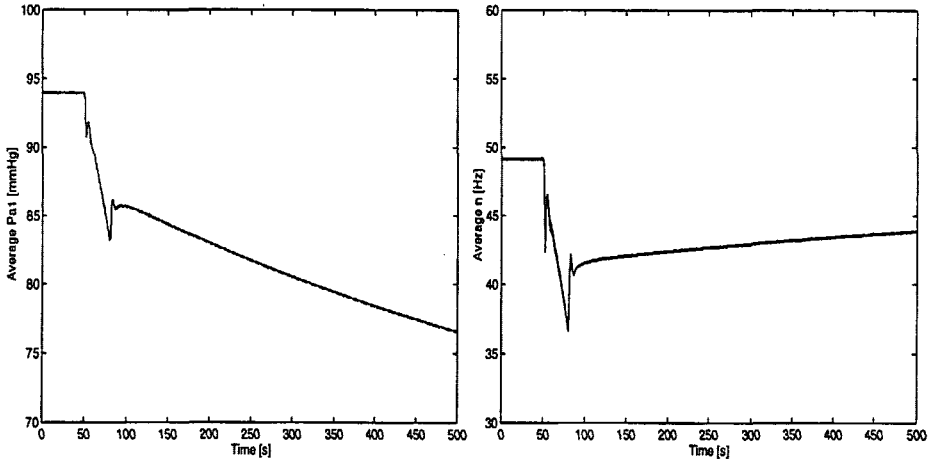

Figure 6.22: The left panel shows computed average of the arterial pressure p_{a1} during and after the 10 % acute hemorrhage which starts at 50 s and ends at 80 s. The right panel shows the concomitant changes in the average of the firing rates n.

linear interaction between the controls and is not simply the sum of the individual effects.

The figures 6.21 and 6.22 show that a knot appears in the curves of the heart rate, the arterial pressure and the firing rates in the early stage of the hemorrhage. The knot is only weakly displayed in the curve of the peripheral resistance which is due to the higher distributed time-delay. In fact, the knot is most pronounced in the efferent controls with low distributed time-delay. The knot is also observed

Table 6.2: The values of the firing rates n, the heart rate H and the peripheral resistance R_{a3} and average arterial pressure $\bar{p}_{a1}$ before the hemorrhage and after the hemorrhage when the adaptation is completed.

Parameter	*Value before*	*Value after*	*Units*
n	49.1	47	Hz
H	1.27	1.37	Hz
R_{a3}	0.67	0.70	mmHg· s /ml
$\bar{p}_{a1}$	94	63	mmHg

in the first model but less pronounced. In contrast, the knot is not observed if the bleeding is carried out in the veins instead of the third section in the cardiovascular model. When the controls from the baroreceptors are absent, the computed firing rates n and the pressure exhibit a small change in the decay rate in the early stage of the hemorrhage. We conclude therefore that the appearance of the knot depends on where the hemorrhage is carried out, and evolve from the interaction between the cardiovascular system and the baroreceptor mechanism. In the near future we will carry out animal experiments. As a part of these experiments, we will investigate if the knot appears in the real world as computed above. From this experiments we will perhaps also be able to determine if the knot is a result of the lumped element approach used to model the human circulatory system.

6.12 Summary and Discussion

Based on experimental data found in the literature and physiological principles, we established two mathematical models of the baroreceptor mechanism and allowed the models to control the human circulation model established in Chapter 4.

The two baroreceptor models differ fundamentally in their description of the afferent part and the CNS. In the first model, two sigmoidal functions relate the sympathetic activity n_s and the parasympathetic activity n_p to the average arterial pressure. By this, the model assumes that the firing rates of the baroreceptors are immune to alterations in the arterial pressure which do not generate changes in the average pressure. The second model adopts the unified model to describe the firing rates of the carotid sinus receptors. The sympathetic activity n_s and the parasympathetic activity n_p are related to the firing rates by two sigmoidal functions. In particular, the second model includes adaptation of the baroreceptors.

The mathematical description of the efferent control of the human circulation

is common to both models and offers control of heart rate, cardiac contractility, peripheral resistance, venous compliance and venous unstressed volume specified partially by the shape of the sympathetic n_s and parasympathetic n_p activity. The efferent control is composed of a static and a dynamic component. The dynamic component consists of a first order differential equation and a time constant characterizing the transition time for the efferent control to take full effect. The static component consists of a linear combination of n_s and n_p. The heart rate is assumed to be controlled by a linear combination of n_s and n_p and the remaining controls are assumed to be linear in n_s. Based on experiments, the heart rate has been described as non-linear in the n_s and n_p by (Levy and Zieske, 1969). The control from the nervous activity on the remaining effector organs are limited. We have adopted open loop responses to describe the baroreceptor mechanism. Thus, we find the linear approach perfectly suitable following our general lines of simplicity. The sympathetic activity n_s is delayed with respect to the parasympathetic activity n_p. We have omitted this feature since we are interested in the steady state rather than the dynamic behavior during transition to a new steady state. However, discrimination between n_s and n_p in our model offers access to study the effect of time-delay. Further details of time-delay can be found in (Ottesen, 1997a).

The parameter values in the model are constructed as a compromise between open loop responses and the experimental data from an acute hemorrhage by (Hosomi and Sagawa, 1979). The latter experiments are used since the open loop responses are obtained in vagotomized animals and thus not representative for the intact human. The parameter values in the control of the unstressed volume have been adjusted in order to fit the computed result to the experimental data by (Hosomi and Sagawa, 1979). This shows the pivotal role played by the control of the unstressed volume.

Despite the striking simplicity of the *first model*, we showed that principal effects of acute hemorrhage, heart pacing and pulsation of the carotid sinus pressure were included in the model.

The *first model* was shown to compute a 10 % hemorrhage of an intact human in close agreement with the corresponding experiments by (Hosomi and Sagawa, 1979) when the baroreceptor mechanism was intact and after complete denervation. Also, this is in agreement with the experiments by (Kumada et al., 1970) which show that the pulsatile term of the carotid sinus pressure has only a minor influence during an acute hemorrhage. We showed also that the control of the venous unstressed volume play a significant role in maintaining the ventricular filling during an acute hemorrhage whereas the remaining controls have a minor influence.

The computed stroke volume and cardiac output during heart pacing were in qualitative agreement with the corresponding experimental results by (Kumada et al., 1967; Melbin et al., 1982). The stroke volume was consistently falling as

the heart rate was increased whereas cardiac output first increased, reached a maximum and then declined. The latter showed that the baroreceptor mechanism cannot effectively combat the drop in cardiac output when the heart rate is sufficiently high. We showed also that an increase in the peripheral resistance caused a decrease in both the stroke volume and in the cardiac output in qualitative agreement with (Kumada et al., 1967). Experiments have shown that dV_s/dH as a function of the heart rate remains unaltered during a number of different conditions. The computed results were in close agreement with the experiments in the range from 1.33 Hz - 2.2 Hz. A discrepancy arose consisting of an accelerated drop in the stroke volume when the heart rate exceeded 2.2 Hz. We observed also a drop in the cardiac output when the heart rate exceeded 2.3 Hz. This fall starts at a lower heart rate than in the animal experiments. One reason for the difference may be the fast shortening of the diastole as defined by the elastance function which specifies the ventricular performance. In addition, autoregulation and the control from the chemoreceptors have not been included in the model which may play a role at this high value of the heart rate.

We allowed the model to be sensitive to the pulsatility of the arterial pressure and studied the effect of pulsation when the carotid sinus pressure followed (6.24). The computations showed that the effect of pulsation in the carotid sinus pressure amounts to a decrease in the average arterial pressure when the average carotid sinus pressure is below 90 mmHg and a rise in the average arterial pressure above 90 mmHg. In contrast, the average arterial pressure is unaltered when the carotid sinus pressure is equal to 90 mmHg and when it is in the high and low saturation regions. The same behavior pattern is predicted in the peripheral resistance and in the cardiac output. All obtained drops are more pronounced in the experiments by (Schmidt et al., 1972). However, the direction of the computed effects are consistent with the results in the firing rate measured by (Chapleau and Abboud, 1987). We explained the behavior in the computed results with the sigmoidal curve relating the sympathetic activity to the average arterial pressure.

How simple can a baroreceptor model be and still include the main principles of it's real counterpart ? As discussed previously in this chapter, the model of the afferent part lacks the sophistication used in previous models. In the case of the CNS, explicit knowledge is not available yet. Thus, tentative descriptions cannot be replaced by descriptive models before further experimental studies are available. However, we do have knowledge about the relation between the firing rates of the carotid sinus receptors and the arterial pressure which we have not fully used but merely lumped into the description of the sympathetic and parasympathetic activity. The sensitivity to the change in pressure $\dot{p}_{cs}$ has not been modeled. This may be one likely reason for the results we observed during pulsation in the carotid sinus pressure. According to the results of (Chapleau and Abboud, 1987), the effect of pulsation can alter the relation between the baroreceptor activity and

the arterial pressure from being sigmoidal to be practically linear. Studies of the effects of pulsation require a more advanced description of the afferent part which includes sensitivity to the change in the carotid sinus pressure $\dot{p}_{cs}$. The unified model is one approach. Alternatively, less comprehensive models can be used, as for instance the recent proposal by (Ursino, 1998), based on a high pass filter, as described in Section 5.5 of Chapter 5. In essence, including the sensitivity of the firing rates of the carotid sinus pressure to $\dot{p}_{cs}$ in the model, will broaden the range of the description of the baroreceptor mechanism.

The *second model* displayed a striking agreement between the computed and the experimental results during the 10 % hemorrhage. In addition, the model exhibited adaptation after the hemorrhage. We showed that a knot appears clearly in the curves of the arterial pressure and in the curves of the efferent controls with the lowest transient time when the hemorrhage is carried out via the third section of the cardiovascular model. The knot disappears when the hemorrhage is carried out via the veins. We concluded that the appearance of the knot depends on where the hemorrhage is carried out, and evolves from the interaction between the cardiovascular system and the baroreceptor mechanism. Future animal experiments will reveal if the knot is a real phenomena.

Two items needs to be critically addressed in the second model. The first item involves the estimation of the parameters values and the second item is related to the model of the CNS.

The unified model contains 8 parameters k_1, k_2, k_3, τ_1, τ_2, τ_3, M and N. Except the values of the weighting parameters k_1, k_2 and k_3, the remaining parameter values are adopted from (Ottesen, 1997b). He has obtained the values from literature data and through curve fitting procedures. We altered the values of the weighting factors k_1, k_2, k_3 in order to obtain a better agreement between the computed and experimental results during an acute hemorrhage. During the acute hemorrhage, we assumed that the slow component has the dominating role ($k_3 = 1.5$ Hz/mmHg) whereas the intermediate component plays a minor role ($k_2 = 0.5$ Hz/mmHg) and that the quick component is of no importance ($k_1 = 0$ Hz/mmHg). The computed results are sensitive to alterations the values of k_2 and k_3. The adaptation after the hemorrhage is accelerated when k_2 and k_3 are assigned higher values. If the acceleration is too strong the computed results will not be in agreement with the corresponding experiments. In addition, the parameter values of the unified model appears to depend on the physiological processes involved in each experiments as also pointed out by (Ottesen, 1997b). This dependence is not yet available.

The model of the CNS is a tentative description of the information processes in the CNS which is due to the lack of available data. If more experimental knowledge is provided about the relation between the firing rates and the sympathetic and parasympathetic activity in the future, the information provided by the unified

model can be better utilized. The description of CNS appears as a weak link in the baroreceptor model.

In summary, we conclude that the parameters of the unified model needs a further study. We find such a study necessary before the baroreceptor model, using the unified model, can be used further. We find that the model is not matured to a stage where it can be used in an environment as the simulator.

The control form the *mechanoreceptors* (or low pressure receptors) have been ignored. This control can combat alterations in the venous volume before activation of the baroreceptors (Guyton, 1991). The model by (Ursino, 1998) describes the control from the baroreceptors and the mechanoreceptors. His computed results suggest that the control mediated by the mechanoreceptors exhibits the major role in the first stage of an acute hemorrhage when the drop in the circulatory volume is less than $150 - 200$ ml. In this range he observed no evident fall in the arterial pressure. When the drop in the circulatory volume exceeds this level, the dominating control stems from the baroreceptor mechanism. Our model reacts only to changes in the circulatory volume which affects the arterial pressure. Thus, the control mediated by the mechanoreceptors constitutes a possible extension of the model and may be relevant in applications such as an anesthetic simulator in which a hemorrhage is a topical case. Unfortunately, the literature data on this control is very sparse. The literature offers only qualitative descriptions and no explicit dependence on the pressure changes.

The effect of *autoregulation* is omitted in the model. In fact, the model assumes the response in the efferent organs to be controlled entirely by the neural shapes of n_s and n_p. However, during an acute hemorrhage the vessel may dilate, by local controls, in order to provide blood flow to the local tissue with a high demand of oxygen as the brain. The control from the *chemoreceptors* are also ignored since they are not believed to play a major role in the short term pressure control compared with the baroreceptor mechanism. These aspects may be a part of future improvements.

6.13 Parameter Values

In this section we will give the parameter values used in this chapter.

Table 6.3: Parameter values used in the generation of the sympathetic and the parasympathetic activity in the first model given by (6.3)-(6.4) .

Parameter	*Value*	*Units*
μ	92	mmHg
ν	7	

Table 6.4: Parameter values used in the generation of the firing rate and the sympathetic and the parasympathetic activity in the second model given by (6.5)-(6.8).

Parameter	*Value*	*Units*
τ_1	0.5	s
τ_2	5.0	s
τ_3	500	s
k_1	0	Hz/mmHg
k_2	0.5	Hz/mmHg
k_3	1.0	Hz/mmHg
N	30	Hz
M	120	Hz
μ_n	49	mmHg
ν_n	7	

Table 6.5: Low and high saturation levels for each effector control given by the relative deviation from the baseline value. The baseline values of the parameters can be found in the tables 4.4 - 4.7 of Chapter 4.

Parameter	*Low value*	*High value*
H	0.25	1.75
$E_{max,lv}$	0.8	1.20
$E_{max,rv}$	0.8	1.20
R_{a1}	0.60	1.40
R_{a2}	0.60	1.40
R_{a3}	0.60	1.40
V_{un1}	0.79	1.21
V_{un2}	0.79	1.21
C_{v1}	0.90	1.10
C_{v2}	0.90	1.10

Table 6.6: Parameter values for τ_i which represents the transient time for each effector control. The parameters are explained in sections 6.3.3 and 6.4.

τ	*Value*
τ_H	2 s
τ_S	2 s
τ_R	6 s
$\tau_{V_{un}}$	20 s
τ_{C_v}	20 s

Table 6.7: The parameter values for the efferent control parameters α_i, β_i, γ_i. The values are valid for the *first model* and the *second model*. The parameters are explained in Section 6.4

Parameter	*Value*	Units
α_H	0.50	s^2
β_H	0.50	s^2
γ_H	1.0	s
$\alpha_{S_{lv}}$	1.0	mmHg·s/ml
$\gamma_{S_{lv}}$	2.0	mmHg/ml
$\alpha_{S_{rv}}$	0.21	mmHg·s/ml
$\gamma_{S_{rv}}$	0.42	mmHg/ml
$\alpha_{R_{a1}}$	0.066	mmHg·s^2/ml
$\gamma_{R_{a1}}$	0.050	mmHg·s/ml
$\alpha_{R_{a2}}$	0.14	mmHg·s^2/ml
$\gamma_{R_{a2}}$	0.11	mmHg·s/ml
$\alpha_{R_{a3}}$	0.53	mmHg·s^2/ml
$\gamma_{R_{a3}}$	0.40	mmHg·s/ml
$\alpha_{C_{v1}}$	2.6	ml· s/mmHg
$\gamma_{C_{v1}}$	14.6	ml/mmHg
$\alpha_{C_{v2}}$	14.8	ml· s/mmHg
$\gamma_{C_{v2}}$	81.3	ml/mmHg
$\alpha_{V_{un,1}}$	246.7	ml·s
$\gamma_{V_{un,1}}$	719.2	ml
$\alpha_{V_{un,2}}$	802.2	ml·s
$\gamma_{V_{un,2}}$	2338.6	ml

Chapter 7

Conclusions

The pumping heart, the human circulatory system and the baroreceptor mechanism have been the topics of this dissertation. In Section 7.1 and Section 7.2 we will give our final conclusion on the first and second part of this work, respectively.

7.1 Interaction between Ventricle and Arterial Load

In this study we addressed the interaction between the pumping heart and the receiving arterial system by describing the isolated heart and the arterial system separately. This approach is fundamentally different from previous attempts which tend to lump the description of the vascular and ventricular effects. Also, we succeeded in describing the ventricle by relating the events at the chamber level with those at the ultrastructural muscle level.

We based our investigations on the model of the isovolumic ventricular pressure established by (Mulier, 1994) which is based on the Frank mechanism. By allowing this ventricular model to eject, we showed that Starlings's two observations were embodied in the model. Consequently, we concluded that Starling's law can be reduced to the Frank mechanism and is thus disqualified as an independent law of the heart.

The ventricular model exhibits the major features of ventricular performance when coupled to a human circulation model. However, discrepancies exist between model predicted and experimentally observed pressures. The discrepancies amount to two phenomena, deactivation and hyperactivation, which we denoted the ejection effect. We related the ejection effect to alterations in the ventricular contractile properties attributable to muscle shortening during ejection. By the ejection effect, we broaden the description of the ventricle to include ejection. The pressure and flow curves were clearly more representative for the intact human than without the ejection effect. Our results suggest that the ventricular

ejection directly changes the underlying muscle contraction process and that the ventricle is influenced by alterations in the vascular parameters. Also, we showed that the ejection effect cannot be explained from smaller effects as inertial effects of ventricular blood and vascular reflections.

By the ejection effect, we have emphasized the combination of both deactivation and hyperactivation in the ventricular performance. We find hyperactivation essential in order to maintain the ventricular pressure in late systole. However, hyperactivation has not been accentuated to the same degree in earlier ventricular models as in our results although it has been experimentally observed previously. This can be related to the absence of an isovolumic ventricular model. In contrast deactivation has been included in several previous ventricular models.

We showed that the computed deactivation increases with higher ventricular outflow which follows the experiments by (Mulier, 1994). The variation in deactivation and hyperactivation are reflected in the sensitivity of the parameters of the ejection effect to alterations in the vasculature. These changes may be guided by neural, hormonal and other effects affecting the interaction between the left ventricle and the arterial load. However, we have not yet formulated this dependence mathematically.

As mentioned in the section describing alternative models to the ejection effect we emphasized that the ejection effect should be related to the cumulative effects of flow since the correction for ventricular volume is included by the Frank mechanism. Our mathematical formulation of the ejection effect depends exclusively on the instantaneous volume or solely on the ventricular outflow during ejection. These formulations of the ejection effect have only been tested against slow events during ejection. We outlined briefly a new modeling approach to the ejection effect based on shifting of energy along the time axis. This approach may be tested against experiments of withdrawal of small volumes from an otherwise isovolumic contraction. In addition, the parameter values of this approach can probably be determined from these experiments. The interesting question is if this new approach can be applied to both slow and quick phenomena.

One of the advantages of the approach taken in this dissertation is that we use a physiologically based model. The ventricular model is experimentally based and gives an excellent description of the isovolumic pressure and includes parameters which all are given physiological meaning. The model of the ejection effect was, for instance, established by expanding a parameter directly related to the ventricle's contractile state. Regarding the mathematical modeling of the ejection effect we emphasize that deactivation should be related to detachments of bonds via Hill's force-velocity relation and hyperactivation to the formation of new and cycling of crossbridge bonds.

By this study we hope that the combination of the ventricular model and the ejection effect has shed new light on the ventricular modeling.

7.2 The Cardiovascular System and the Baroreceptor Mechanism

The goal of the second part of this dissertation was to establish a human circulation model and two models of the baroreceptor mechanism of the intact human, built on experimental data and physiological arguments. These goals have been achieved.

We established a human circulation model with the ventricular performance specified by two time varying elastance functions and the vasculature described by lumped elements based partially on the architecture of (Rideout, 1991). We showed this model generates root aortic pressure and ventricular outflow curves representative for the normal human.

We divided the baroreceptor mechanism into three distinct physiological modules, the afferent part, the CNS and the efferent part. In the *first model* of the baroreceptor mechanism we lumped the first two modules and related the sympathetic activity n_s and the parasympathetic activity n_p to average arterial pressure by two sigmoidal functions. The *second model* adopts the unified model to describe the first module whereas the second module consists of two sigmoidal functions relating n_s and n_p to the firing rate n.

The description of the efferent part is common to both baroreceptor models. The models offer control of the heart rate, the cardiac contractility, the peripheral resistance, the venous compliance and the venous unstressed volume. We divided the control into a static and a dynamic component. The dynamic component consists of a first order differential equation with a time constant characterizing the transition time for the efferent controls to take full effect. We discriminated between the control from sympathetic activity n_s and the control from the parasympathetic activity n_p in the static component. We assumed that the heart rate is guided by a linear combination of n_s and n_p, and that the remaining controls are linear in n_s. We determined the corresponding parameter values from open loop responses and experimental results from an acute hemorrhage in an intact animal by (Hosomi and Sagawa, 1979).

We studied mainly the first model and computed the response of the model to an acute hemorrhage, heart pacing and to pulsations in the carotid sinus pressure. The computed response to a 10 % acute hemorrhage with the *first model* was in striking agreement with the corresponding experiments by (Hosomi and Sagawa, 1979). The model also confirmed the results by others that the control of unstressed volume plays a significant role in maintaining the ventricular filling during an acute hemorrhage. The computed effects of heart pacing was in favorable agreement with the corresponding experiments by (Kumada et al., 1967; Melbin et al., 1982) when the heart rate is below 2.2 Hz. The model confirms that

pulsality of the carotid sinus pressure can reduce the average arterial pressure but the computed drop in the arterial pressure was small compared with that of the experiments by (Schmidt et al., 1972). However, the behavior pattern was consistent with the measured baroreceptor activity by (Chapleau and Abboud, 1987).

The second model does not have the same practical scope as the first one but gives a more fundamental physiological description of the afferent part. Also, this model of the baroreceptor mechanism was shown to compute a 10 % acute hemorrhage in striking agreement with the corresponding experiment by (Hosomi and Sagawa, 1979). The model exhibited adaptation of the baroreceptor after the hemorrhage. To our knowledge this has not previously been included in a baroreceptor model.

One could argue that the validation of both models could be expanded. Indeed, a number of other experiments exist which can validate the model. Examples of these experiments include hemorrhages with weaker strength, tilting of patients, pulsation of the carotid sinus pressure with different frequencies and responses in atrial pressures. Also, computed response to heart failures and changes in the vascular parameters could have been computed. Finally, it would also have been interesting to show the impact played by the parameters in sigmoidal curves in the first model and the influence displayed by the parameters of the unified model. However, the time limitation of this project has limited the number of computations.

The ventricular performance in the human circulation model was based on the classic time-varying elastance function concept. We suspected that the description impairs the ventricular filling more than expected during heart pacing and thus plays a role in restricting the range of the heart rate change to be below 2.2 Hz. The division between the active and passive phase should be studied in greater details. The ventricular model established by (Mulier, 1994) cannot yet be applied fully to a model of the human circulation. This is due to the problems associated with changes in the heart rate and that the mathematical formulation of neural impact on the ejection effect is not yet available.

A future expansion of the first model would be to include sensitivity of the firing rates to the change in pressure. This will broaden the description of the baroreceptor mechanism to include the effect of pulsation in the carotid sinus pressure in a better way. As a first approach, we recommend the model to be expanded by a description of the firing rate based on previous attempts as described in Chapter 5. The unified model is not matured to a stage where it can be widely applied. As discussed in Section 6.12 of Chapter 6 the significance of the parameters of the unified model when used in a baroreceptor model is not fully understood. Therefore, the second model needs to be studied in greater detail before it can be used further. Also, the unified model is computationally time consuming. This disadvantage may be reduced by using only one of the three differential equations of

which the unified model is comprised.

In the near future we will perform a number of animal experiments. In these experiments we intend to perform hemorrhages with different speeds but with same drop in circulatory volume. By this we will examine the effect of the temporal dynamics. As mentioned in Section 6.11 a knot appeared in the curves of the heart rate, the arterial pressure and the firing rates in the early stage of the hemorrhage. As a part of these experiments we will try to determine its origin.

In both baroreceptor models the description of the CNS is given as a tentative formulation of the information processes in the CNS which is due to the lack of available data. A challenge for the future would be to focus on subsystems and study the relation between the firing rates and the sympathetic and the parasympathetic activities and the influence of the two nervous activities in the efferent controls.

In summary, we conclude that the *first model* of the baroreceptor mechanism exhibits the principal features of the short term pressure control during an acute hemorrhage, alterations in the peripheral resistance and changes in the heart rate in the range below 2.2 Hz when coupled to the pulsatile human circulation model established in Chapter 4. In addition, the model is computationally fast due to its simplicity. The main use of the first model is to present a model which exhibits the principal features of the short term pressure control and which can be used in an anesthesia simulator. Considering the aims listed in Section 5.6 of Chapter 5 we will conclude that we have accomplished our goal.

Appendix A

English Summary

The pumping heart has been the central topic in the first part of this dissertation. In Section A.1 we will summarize our research into the interaction between the left ventricle and the arterial load. The second part of this dissertation amounts to our study of the human circulatory system and the baroreceptor mechanism . The results in this part are summarized in Section A.2

A.1 The interaction between Ventricle and Arterial Load

The peak developed cavity pressure of the isovolumically contracting ventricle increases with the end-diastolic pressure to an upper physiological limit. This is known as the Frank mechanism and constitutes the key element in an experimentally based analytical description of the isovolumic ventricular pressure as a function of time and volume contained (Mulier, 1994). When coupled to a description of the vasculature this model of the isolated ventricle exhibits the principal features of the pumping heart. In particular, we showed that the ventricular model includes Starling's two observations and thus disqualified Starling's law as an independent law of ventricle. As we have modeled the left ventricle, Starling's law follows from the Frank Mechanism.

We uncovered, upon our more detailed analysis that discrepancies arise between model predicted and experimentally observed ventricular pressure during ejection. Measured cavity pressure tends to be lower, deactivation, during early ejection and higher, hyperactivation, during late ejection than predicted from isovolumic properties via the ventricular model. The discrepancies amount to two phenomena, deactivation and hyperactivation, identified during ejection. We termed these two phenomena the ejection effect. We interpreted the ejection effect as alterations in the contractile properties of the ventricle attributable to muscle short-

ening during ejection. This suggests that ventricular ejection directly changes the underlying muscle contraction and that the ventricle is influenced by alterations in vascular properties. Studies show that vascular reflections and inertia of blood movement alone cannot explain the two phenomena. Apparently the ejection effect consists of a number of small effects. The two phenomena should be modeled as detachment of bonds and as formation of new and cycling of crossbridge bonds, respectively.

We outlined briefly a new approach to the modeling of the ejection effect which we will follow in the near future. In this approach, the two phenomena, deactivation and hyperactivation, will be related to the shifting of energy along the time axis.

A.2 The Cardiovascular System and the Baroreceptor Mechanism

We have established a human circulation model and two models of the short term pressure control mediated by the baroreceptor mechanism based on experimental data and physiological arguments. The vasculature of the human circulation is described by lumped elements and the ventricular performance is specified by two time-varying elastance functions. In the first baroreceptor model, the sympathetic activity n_s and the parasympathetic activity n_p are related to the average arterial pressure by two sigmoidal functions. The second baroreceptor model adopts the unified model, first proposed by (Taher et al., 1988), to describe the relation between the firing rates and the carotid sinus pressures. The unified model contains all the experimentally known non-linear phenomena. Consequently, the second model includes adaptation of the baroreceptors.

The model of the efferent control is shared by both models. The model offers control of heart rate, cardiac contractility, peripheral resistance, venous compliance and venous unstressed volume. The efferent control is composed of a static and a dynamic component. The dynamic component consists of a first order differential equation with a time constant which characterizes the transient time for the control to take full effect. The static component consists of a linear combination of n_s and n_p. The heart rate is assumed to be controlled by a linear combination of n_s and n_p and the remaining controls are assumed to be linear in n_s.

The computed results of the *first model* during a 10 % acute hemorrhage, heart pacing and the computed effects of pulsation in the carotid sinus pressure are compared with the corresponding experiments. We concluded that this model contains the principle effects of the baroreceptor mechanism.

The results of the *second model* during a 10 % acute hemorrhage is also compared with the corresponding experiments. The model exhibited adaptation after the hemorrhage. We showed also that a knot appears clearly in the curves of the arterial pressure and in the curves of the efferent controls with the lowest transition times depending on where the hemorrhage is carried out, and is amplified by the interaction between the cardiovascular system and the baroreceptor mechanism. Future animal experiments may reveal if the knot is a real phenomena. We concluded that the unified model needs a further study before the range of application of this model can be broadened.

Appendix B

Dansk Resume

Det pumpende hjerte har været det centrale emne i den første del af denne ph.d. afhandling. I Afsnit B.1 giver vi et resume af vores forskning i sammenspillet mellem den venstre ventrikel og den arterielle belastning. Den anden del af afhandlingen berører vores arbejde med det menneskelige blodkredskløb og baroreceptor mekanismen. Et resume af dette arbejde findes i Afsnit B.2.

B.1 Sammenspillet mellem Ventrikel og Arteriel Belastning

Det maksimalt udviklede tryk i den isovolumetrisk kontraherende ventrikel stiger med det slutdiastolske tryk til en øvre fysiologisk grænse. Dette er kendt som Frank mekanismen og den udgør nøgleelementet i en eksperimentel baseret matematiske model for det isovolumetriske tryk som funktion af tiden og indeholdt volumen (Mulier, 1994). Denne model for den isolerede ventrikel udviser de principielle egenskaber ved det pumpende hjerte når modellen bliver koblet til en beskrivelse af det menneskelige blodkredsløb. Vi viste, at modellen indeholder Starlings to observationer, hvilket diskvalificerer Starlings lov som en uafhængig lov for ventriklen. Resultatet af modelleringen er, at Starlings lov følger fra Frank mekanismen.

Vi afslørede efter en mere detaljeret analyse, at der eksisterer uoverensstemmelser mellem model forudset og eksperimentelt observeret ventrikeltryk under udpumpning. Målt tryk er lavere i den tidlige del af udpumpningen, deaktivering, og højere i den senere del af udpumpningen, hyperaktivering, end forudset fra de isovolumetriske egenskaber indeholdt i ventrikelmodellen. Overensstemmelserne består af to fænonener, som kan identificeres under udpumpning. Vi kalder de to fænomener for udpumpningseffekten. Vi tolker udpumpningseffekten som ændringer i ventriklens kontraktionsegenskaber som skyldes muskelforkortelse un-

der udpumpning. Vores resultater foreslår, at udpumpningen direkte ændrer den underliggende muskel kontraktion, og at ventriklen er påvirket af ændringer i blodkredsløbets egenskaber. Vores arbejde viser, at udpumpningseffekten ikke kan forklares alene ved mindre effekter som inerti af blodbevægelser og reflektioner fra den arterielle belastning. Udpumpningseffekten består tilsyneladende af flere mindre effekter. De to fænomener bør modelleres som henholdsvis afkobling af tværbindinger og generering af nye og cycling af tværbindinger.

Vi afsluttede med kort skitse af en ny indfaldsvinkel til modelleringen af udpumpningseffekten som vi vil følge i den nærmeste fremtid. Denne metode relaterer deaktivering og hyperaktivering til bevægelse af energi langs tidsaksen.

B.2 Blodkredsløbet og Baroreceptor Mekanismen

Vi opstillede en model for det menneskelige blodkredsløb og to modeller af kontrollen fra baroreceptor mekanismen baseret på eksperimentelle data og fysiologiske argumenter. Det menneskelige blodkredsløb er beskrevet ved elektriske kredsløbselementer, og de to ventrikler er modelleret ved tidsvarierende elastance funktioner. Den første baroreceptor model relaterer den sympatiske aktivitet n_s og den parasympatiske aktivitet n_p til middelværdien af det arterielle tryk. Den anden baroreceptor model udnytter modellen som er blevet kaldt "the unified model". Denne model blev første gang foreslået af (Taher et al., 1988) og indeholder alle de eksperimentelt kendte ikke-lineære fænomener. Som en konsekvens indeholder modellen adaptation af baroreceptorerne.

Den matematiske beskrivelse af den efferent kontrol er fælles for begge modeller. Modellen formidler kontrol af hjertefrekvensen, den perifere modstand, kontraktiliteten, compliance på venesiden og det trykløse volume på venesiden. Beskrivelsen af den efferente kontrol er opdelt i en statisk og i en dynamisk komponent. Den dynamiske komponent består af en første ordens differential ligning med en tidskontanst, der beskriver tiden som det kræver at fuldføre en kontrol. Den statiske komponent består af en lineær kombination af n_s og n_p. Vi antager, at hjertefrekvensen er kontrolleret af såvel n_s som n_p, mens kontrollen af de resterende effektor organer er lineære i n_s.

Vi sammenlignede de beregnede resultater fra den første model med de tilsvarende eksperimentelle data under en akut 10 % blødning, hjertepacing og ved pulserende carotid sinus tryk. Vi konkluderede, at modellen indeholder de principielle effekter som er indeholdt i baroreceptor mekanismen.

De beregnede resultater fra den anden model under en akut 10 % blødning blev også sammenlignet med de tilsvarende forsøg. Denne model udviste adaptation efter blødningen. Vi viste også, at en slags knude optræder klart i kurverne for det arterielle tryk og i kurverne for de efferente kontroller med de laveste tidskonstan-

ter. Tilstedeværelsen af knuden afhænger af, hvor blødningen udføres og bliver forstærket af baroreceptor mekanismen. I den næmeste fremtid vil vi udfører en række dyreeksperimenter som måske kan afslører om knuden er et eksperimentel observerbart fænomen. Vi konkluderede, at den anden model, bygget på "the unified model", skal udsættes for et nærmere studie før den kan anvendes i en bredere forstand.

Bibliography

Abutaleb, A., Melbin, J. and Noordergraaf, A. (1986). Identification of time-varying ventricular parameters during the ejection phase, *IEEE transactions on bio-medical engineering* **33**: 370–378.

Acierno, L. J. (1994). *The History of Cardiology*, first edn, The Parthenon Publishing Group, New York.

Baan, J. (1992). Ventricular pressure-volume relation in vivo, *European Heart Journal* **13**: 2–6.

Beneken, J. (1965). *A Mathematical approach to Cardio-vascular Function*, PhD thesis, University of Utrecht.

Berger, D., Li, J., Lasky, W. and Noordergraaf, A. (1993). Repeated reflection of waves in the systemic arterial system, *American Journal of Physiology* pp. H269–H281.

Bolter, C. P. and Ledsome, J. R. (1976). The effect of cervical sympathetic nerve stimulation on canine carotid sinus reflex, *American Journal of Physiology* **230**: 1026–1030.

Bronk, D. and Stella, G. (1932). Afferent impulses in the carotid sinus nerve, *American Journal of Physiology* **1**: 113–130.

Bronk, D. and Stella, G. (1935). The response to steady pressure of single end organs in the isolated carotid sinus, *American Journal of Physiology* **110**: 708–714.

Brown, A. M. (1980). Receptors under pressure, an update on baroreceptors, *Circulation Research* **46**: 1–10.

Burkhoff, D., DeTombe, P. and Hunter, W. (1993). Impact of ejection on magnitude and time course of ventricular pressure-generating capacity, *American Journal of Physiology* pp. H899–H909.

Campell., K., Ringo, J., Knowlen, G., Kirkpatrick, R. and Schmidt, S. (1986). Validation of optional elastance-resistance left ventricle pump models, *American Journal of Physiology* **251**: H382–H397.

Cecchini, A., Tiplitz, K., Melbin, J. and Noordergraaf, A. (1982). Baroreceptor activity related to cell properties, *Proceeding of the 35th Annual Conference on Engineering in Medicine and Biology*, Vol. 24, p. 20.

Chapleau, M. and Abboud, F. (1987). Contrasting effects of static and pulsatile pressure on carotid baroreceptor activity in dogs, *Circulation Research* **61**: 648–658.

Cox, R. and Bagshaw, R. (1975). Baroreceptor reflex control of arterial hemodynamics in the dog, *Circulation Research* pp. 772–786.

Danielsen, M. (1996). Feedback mechnism of the cardiovascular system, *International Journal of Clinical Monitoring and Computing* **13**: 197–198.

Danielsen, M. and Ottesen, J. (1997). A dynamical approach to the baroreceptor regulation of the cardiovascular system, *Proceeding to the 5th International Symposium, Symbiosis '97*, pp. 25–29.

Danielsen, M., Palladino, J. and Noodergraaf, A. (1998). The left ventricular ejection effect, *in* M. Danielsen and J. Ottesen (eds), *Mathematical Modeling in Medicine*, Roskilde University Press, p. in press.

De fares, J., Hara, H., Osborn, J. and McLeod, J. (1963). Theoretical analysis and computer simulation of the circulation with special reference to the starling properties of the ventricle, *Circulatory Analog Computers* p. 91.

De Tombe, P. and Little, W. (1994). Inotropic effects of ejection are myocardial properties, *American Journal of Physiology* **266**: H1202–H1213.

Despopoulos, A. and Silbernagl, S. (1991). *Color Atlas of Physiology*, fourth edn, Georg Thieme Verlag Stuttgart, New York.

Donald, D. E. and Edis, A. J. (1970). Comparison of aortic and carotid baroreflexes in the dog, *Journal of Physiology, London* **215**: 521–538.

Ducas, J., Schick, U., Girling, L. and Prewitt, R. (1985). Effects of reduced resistive afterload on left ventricular pressure volume relationship, *American Journal of Physiology* **248**: H163–H169.

Elliott, G., Rome, E. and Spencer, M. (1970). A type of contraction hypothesis applicable to all muscles, *Nature* **226**: 417–420.

Franz, G. (1969). Non-linear rate sensitivity of carotid sinus reflex as a consequence of static and dynamic nonlinearities in baroreceptor behavior, *Annual NY Academy of Science* **156**: 811–824.

Ganong, W. (1975). *review of medical physiology*, 7th edn, LANGE Medical Publications, Los Altos, Califonia.

Greene, H. D. (1986). Changes in canine cardiac function and venous return curves by the carotid sinus baroreflex, *American Journal of Physiology* **251**: H288–H296.

Grodins, F. (1959). Intergrative cardiovascular physiology: A mathematical synthesis of cardiac and blood vessel hemodynamics, *The Quarterly Review of Biology* **34**(2): 93–116.

Guasp, F. (1980). La estructuración macroscópica del miocardio ventricular, *Revista Espñola de Cardiologio* **33(3)**: 265–287.

Guyton, A. (1955). Determination of cardiac output by equating venous return curves with cardiac response curves, *Physiological Reviews* **35**: 123–129.

Guyton, A. (1981). *Textbook of Medical Physiology*, sixth edn, Philadelphia, London, Toronto, Mexico City, Rio de Janeiro, Sydney, Tokyo: W.B. Saunders Company.

Guyton, A. (1991). *Textbook of Medical Physiology*, eight edn, Philadelphia, London, Toronto, Mexico City, Rio de Janeiro, Sydney, Tokyo: W.B. Saunders Company.

Hosomi, H. and Sagawa, K. (1979). Effect of pentobarbital anesthesia on hypotension after 10 % hemorrhage in the dog, *American Journal of Physiology* **51**: H607–H611.

Hunter, W. (1989). End-systolic pressure as a balance between opposing effects of ejection, *Circulation Research* **64**: 265–275.

Hunter, W., Janicki, J., Weber, K. and Noordergraaf, A. (1983). Systolic mechanical properties of the left ventricle, *Circulation Research* **52**: 319–327.

Jin, Z. and Qin, J. (1993). An electric model wiht time varying resistance for a pheumatic membrane blood pump, *ASAIO Journal* pp. 56–61.

Kappel, F., Lafer, S. and Peer, R. (1997). A model for the cardiovascular system under an ergometric workload, *Surveys on Mathematics for Industry* **7**: 239–250.

Kappel, F. and Peer, R. (1993). A mathematical model for fundamental regulation processes in the cardiovascular system, *Journal of Mathematical Biology* **31**: 611–631.

Korner, P. (1971). Integrative neural cardiovascular control, *Physiological Reviews* **51**: 50–51.

Korner, P. (1974). 'steady state' properties of the baroreceptor-heart rate reflex in essential hypertension in man, *Clinical and Experimental Pharmacology & Physiology* **1**: 65–75.

Kumada, M., Azuma, T. and Matsuda, K. (1967). The cardiac output-heart rate relationship under different conditions, *Japan Journal of Physiology.* **17**: 538–555.

Kumada, M., Schmidt, R., Sagawa, K. and Tan, K. (1970). Carotid sinus reflex in response to hemorrage, *American Journal of Physiology* **219**: 1373–1379.

Landgren, S. (1952). On the excitation mechanism of the carotid sinus baroreceptors, *Acta Physiology Scandiavia.* **26**: 1–34.

Leaning, M., Pullen, H., Carson, E., Al-Dahan, M., Rajkumart, N. and Finkelstein, L. (1983). Modelling a complex biological system: the human cardiovascular system-2.model validation, reduction and development, *Trans. inst. M C* **5**: 71–86.

Leaning, M., Pullen, H., Carson, E. and Finkelstein, L. (1983). Modelling a complex biological system: the human cardiovascular system-1.methodology and model description, *Trans. inst. M C* **5**: 71–86.

Levy, M. and Zieske, H. (1969). Autonomic control of cardiac pacemaker activity and atrioventricular transmission, *Journal of Applied Physiology* **27**: 465–470.

Martin, J., Schneider, A., Mandel, J., Prutow, R. and Smith, N. (1986). A new cardiovascular model for real-time applications, *Transactions* **3**: 31–65.

Melbin, J., Detweiler, D., Riffle, R. and Noordergraaf, A. (1982). Coherence opf cardiac output with rate changes, *American Journal of Physiology* **243**: H499–H504.

Milnor, W. R. (1990). *Cardiovascular Physiology*, Oxford University Press, New York.

Mulier, J. P. (1994). *Ventricular pressure as a function of volume and flow*, PhD thesis, University of Leuven.

Neumann, S. (1996). *Modeling acute hemorrhage in the human cardiovascular system*, PhD thesis, University of Pennsylvania.

Noldus, E. (1976). Optimal control aspects of left ventricular ejection dynamics, *Journal of Theoretical Biology* **63**: 275–309.

Noordergraaf, A. (1978). *Circulatory System Dynamics*, New York: Academic Press.

Noordergraaf, A. (1998). Cariodvascular concepts in antiquity, *Analysis and Assessment of Cardiovascular Function* pp. 3–12.

Olufsen, A., Larsen, H. and Danielsen, M. (1998). Sima models, documentation of the models in the sima simulator, *Technical Report: Report No: MT-89 Confidential* .

Olufsen, M. S. (1998). *Modelling the Arterial System wiht Reference to an Anesthesia Simulator*, PhD thesis, Roskilde University.

Ono, K., Uozumi, T., Yoshimoto, C. and Kenner, T. (1982). The optimal cardiovascular regulation of the arterial blood pressure, *in* T. Kenner, R. Busse and Hinghofer-Szalkay (eds), *Cardiovascular System Dynamics; Model and Measurements*, Plenum Press, pp. 119–139.

Ottesen, J. (1997a). Modelling the baroreflex-feedback mechanism with time-delay, *Journal of Mathematical Biology* **36**: 41–63.

Ottesen, J. (1997b). Nonlinearity of baroreceptor nerves, *Surveys on Mathematics for Industry* **7**: 187–201.

Ottesen, J. (1998). Compartment models of the cardiovascular system, *in* M. Danielsen and J. Ottesen (eds), *Mathematical Modeling in Medicine*, Roskilde University Press, p. in press.

Palladino, J. L. (1990). *Models of the cardiac muscle contraction and relaxation*, PhD thesis, University of Pennsylvania.

Palladino, J. L., Mulier, J. P. and Noordergraaf, A. (1996). Otto frank: Stern leader and scrupulous instrument analyst, *Journal of Cardiovascular Diagnosis and Procedures* **13**: 302.

Palladino, J. L., Mulier, J. P., Wu, F., Moser, M., Kenner, T., Baevsky, R. M. and Noordergraaf, A. (1996). Assesing the state of the circulatroy system via parameters vs. variable, *Journal of Cardiovascular Diagnosis and Procedures* **13**: 131–139.

Palladino, J. L. and Noordergraaf, A. (1997). Closed-loop circulation model based on the frank mechanism, *Surveys on Mathematics for Industry* **7**: 177–186.

Palladino, J. L., Rabbany, S. Y., Mulier, J. P. and Noordergraaf, A. (1997). A perspective on myocardial contractility, *Technology and Health Care (IOS Press)* **5**: 135–144.

Palladino, J., Mulier, J. and Noordergraaf, A. (1998). The changing views of the heart through the centuries, *in* M. Danielsen and J. Ottesen (eds), *Mathematical Modeling in Medicine*, Roskilde University Press, p. in press.

Palladino, J., Mulier, J. and Noordergraaf, A. (1998, submitted). Defining ventricular elastance, *Proceedings of the 20th Annual International Conference of the IEEE Engineering and Medicine in Biology Society, Hong Kong*.

Palladino, J. and Noordergraaf, A. (1998). Muscle contraction mechanics from ultrastructual dynamics, *Analysis and Assessment of Cardiovascular Function* pp. 3–12.

Palladino, J., Ribeiro, L. and Noordergraaf, A. (1998). Human circulatory system model based on frank's mechanism, *in* M. Danielsen and J. Ottesen (eds), *Mathematical Modeling in Medicine*, Roskilde University Press, p. in press.

Pasipoularides, A., Murgo, J., Miller, J. and Craig, E. (1987). Nonobstructive left ventricular ejection pressure gradients in man, *Circulation Research* **61**: 220–227.

Pedley, T. (1980). *The Fluid Mechanics of Large Blood Vessels*, London, New York, New Rochelle, Melbourne, Sydney: Cambridge University Press.

Peskin, C. (1976). *Partial Differential Equations in Biology*, Lecture Notes from CIMS (Courant Institute of Mathematical Sciences), New York.

Porter, P., Ryan, W., Melbin, J. and Noordergraaf, A. (1982). Features of compliacne pumping, *IEEE Frontiers of Engineering in Health Care* pp. 176–180.

Rideout, V. (1991). *Mathematical and Computer Modeling of Physiological Systems*, Medical Physics Publishing.

Robinson, J. and Sleight, P. (1980). Single carotid sinus baroreceptor adaptation in normatensive and hypertensive dogs, *Arterial baroreceptors and hypertension* pp. 45–52.

Rothe, C. F. (1983). reflex control of veins and vascular capacitance, *Physilogical Reviews* **63**: 1281–1342.

Scher, A. and Young, A. (1973). Servoanalysis of carotid sinus reflex effects on peripheral resistance, *Circulation Research* **12**: 152–162.

Schmidt, R., Kumada, M. and Sagawa, K. (1972). Cardiovascular responses to various pulsatile pressures in the carotid sinus, *American Journal of Physiology* **223**: 1–7.

Schmidt, R. and Thews, G. (1976). *Einfurung in de Physiologie des Menschen*, Springer-Verlag, Berlin, Heidelberg, New York.

Shoukas, A. A. (1975). Pressure-flow and pressure-volume relations in the entire pulmonary vascular bed af the dog determined by two-port analysis, *Circulation Research* **37**: 809–818.

Shoukas, A. A. and Brunner, M. C. (1980). Epinephrine and the carotid sinus baroreceptor reflex, *Circulation Research* **47 (2)**: 249–257.

Shoukas, A. A. and Sagawa, K. (1973). Control of total systemic vascular capacity by the carotid sinus baroreceptor reflex, *Circulation Research* **33**: 22–33.

Slinker, B. (1996). Searching for indices of contractility is counterproductive, *Studies in Health Technology and Informatics, IOS Press* **21**: 315–324.

Snyder, M. and Rideout, V. (1969). Computer simulation studies of the venous circulation, *IEEE Transactions on Bio-Medical Engineering* **16**: 325–334.

Spencer, M. and Worthington, C. (1960). A hypothesis of contraction in straited muscle, *Nature* **187**: 388–391.

Spickler, J. and Kezdi, P. (1967). Dynamic respons characteristics of carotid sinus baroreceptors, *American Journal of Physiology* **212 (2)**: 472–476.

Srinivasan, R. and Nudelman, H. (1972). Modeling the carotid sinus baroreceptor, *Biophysics Journal* **12**: 1171–1182.

Stergiopulos, N., J., M. and Westerhof, N. (1996). Determinants of stroke volume and systolic and diastolic aortic pressure, *American Journal of Physiology* **270**: H2050–H2059.

Suga, H. (1969). Time course of left ventricular pressure-volume relationship under various end-diastolic volume, *Japan Heart Journal* **10**: 509–515.

Suga, H. (1970). Time course of left ventricular pressure-volume relationship under various extents of aortic occlusion, *Japan Heart. Journal* **11**: 373–378.

Suga, H., Sagawa, H. and Shoukas, A. (1973). Load independence of the instantaneous pressure-volume ratio of the canine left ventricle and effects of epinephrine and heart rate on the ratio, *Circulation Research* **32**: 314–322.

Suga, H. and Sagawa, K. (1972). Mathematical interrelationship between instantaneous ventricular pressure-volume ratio and myocardial force-velocity relation, *Annals of Biomedical Engineering* **1**: 160–181.

Suga, H., Sagawa, K. and Kostiuk, D. (1976). Controls of ventricular contractility assessed by pressure-volume ratio, e_{max}, *Cardiovascular Research* **10**: 582–592.

Sun, Y., Beshara, M., Lucariello, R. and Chiaramida, S. (1997). A comprehensive model for right-left heart interaction under the influence of pericardium and baroreflex, *American Journal of Physiology* **272**: H1499–1515.

Taher, M. F., Cecchini, A. B., Allen, M. A., Gobran, S. R., Gorman, R. C., Guthrie, B. L., Lingenfelter, K. A., Rabbany, S. Y., Rolchigo, P. M., Melbin, J. and Noordergraaf, A. (1988). Baroreceptors responses derived from a fundamental concept, *Annals of Biomedical Engineering* **16**: 429–443.

Tham, R.-Y. (1988). *A Study of Effects of Halothane on Canine Cardiovascular System and Baroreceptor Control*, PhD thesis, University of Wisconsin-Madison. Xerographic printed by UMI Dissertation Services, A Bell & Howell Company, 1995.

Tortora, G. and Anagnostakos, N. (1990). *Principles of Anatomy and Physiology*, sixth edn, Harper and Row Publishers, New York.

Toy, S. M., Melbin, J. and Noordergraaf, A. (1985). Reduced models of arterial system, *IEEE Transactions on Biomedical Engineering, Communication* **32**: 174–177.

Ursino, M. (1997). A mathematical model of the carotid-baroreflex control in pulsatile conditions, *Surveys on Mathematics for Industry* **7**: 203–220.

Ursino, M. (1998). Modelling the interaction among several mechanism in the short-term arterial pressure control, *in* M. Danielsen and J. Ottesen (eds), *Mathematical Modelling in Medicine*, Roskilde University Press, Denmark.

Ursino, M., Antonucci, M. and Belardinelli, E. (1994). Role of active changes in venous capacity by the carotid baroreflex: analysis with a mathematical model, *American Journal of Physiology* **36(6)**: H2531–H2546.

Vaartjes, S. and Herman, B. (1987). Left ventricular internal resistance and unloaded ejection flow assessed from pressure-flow relations: A flow-clamp study on isolated rabbit hearts, *Circulation Research* **60**: 727–737.

Wang, A., Brandle, M. and Zucker, I. (1993). Influence by vagotomy on the barorecelfex sensitivty in anethetized dogs with experimental heart failure, *American Journal of Physiology* **265**: H1310–H1317.

Warberg, J. r. (1995). *Human Fysiologi*, Polyteknisk Forlag.

Warner, H. (1958). The frequency dependent nature of blood pressure regulation by carotid sinus studied with an electric analog, *Circulation Research* **6**: 35–40.

Warner, H. (1959). The use of an analog computer for analysis of control mechanisms in the circulation, *Proceeding IRE* **47**: 1913–1916.

Warner, H. and Cox, A. (1962). A mathematical model of heart rate control by sympathetic and vagus efferent information, *Journal of Applied Physiology* **17**: 349–358.

Warner, H. and Russel, R. (1969). Effect of combined sympathetic and vagal stimulation on heart rate in the dog, *Circulation Research.* **24**: 567–573.

Westerhof, N. and Stergiopulos, N. (1998). Models of the arterial tree, *in* M. Danielsen and J. Ottesen (eds), *Mathematical Modeling in Medicine*, Roskilde University Press, p. in press.

Liste over tidligere udkomne tekster tilsendes gerne. Henvendelse herom kan ske til IMFUFA's sekretariat

tlf. 46 74 22 63

217/92 "Two papers on APPLICATIONS AND MODELLING IN THE MATHEMATICS CURRICULUM"

by: Mogens Niss

218/92 "A Three-Square Theorem"

by: Lars Kadison

219/92 "RUPNOK - stationær strømning i elastiske rør"

af: Anja Boisen, Karen Birkelund, Mette Olufsen

Vejleder: Jesper Larsen

220/92 "Automatisk diagnosticering i digitale kredsløb"

af: Bjørn Christensen, Ole Møller Nielsen

Vejleder: Stig Andur Pedersen

221/92 "A BUNDLE VALUED RADON TRANSFORM, WITH APPLICATIONS TO INVARIANT WAVE EQUATIONS"

by: Thomas P. Branson, Gestur Olafsson and Henrik Schlichtkrull

222/92 On the Representations of some Infinite Dimensional Groups and Algebras Related to Quantum Physics

by: Johnny T. Ottesen

223/92 *THE FUNCTIONAL DETERMINANT*

by: Thomas P. Branson

224/92 *UNIVERSAL AC CONDUCTIVITY OF NON-METALLIC SOLIDS AT LOW TEMPERATURES*

by: Jeppe C. Dyre

225/92 *"HATMODELLEN" Impedansspektroskopi i ultrarent en-krystallinsk silicium*

af: Anja Boisen, Anders Gorm Larsen, Jesper Varmer, Johannes K. Nielsen, Kit R. Hansen, Peter Bøggild og Thomas Hougaard

Vejleder: Petr Viscor

226/92 *"METHODS AND MODELS FOR ESTIMATING THE GLOBAL CIRCULATION OF SELECTED EMISSIONS FROM ENERGY CONVERSION"*

by: Bent Sørensen

227/92 "Computersimulering og fysik"

af: Per M.Hansen, Steffen Holm, Peter Maibom, Mads K. Dall Petersen, Pernille Postgaard, Thomas B.Schrøder, Ivar P. Zeck

Vejleder: Peder Voetmann Christiansen

228/92 "Teknologi og historie"

Fire artikler af:

Mogens Niss, Jens Høyrup, Ib Thiersen, Hans Hedal

229/92 "Masser af information uden betydning"

En diskussion af informationsteorien i Tor Nørretranders' "Mærk Verden" og en skitse til et alternativ baseret på andenordens kybernetik og semiotik.

af: Søren Brier

230/92 "Vinklens tredeling - et klassisk problem"

et matematisk projekt af

Karen Birkelund, Bjørn Christensen

Vejleder: Johnny Ottesen

231A/92 "Elektrondiffusion i silicium - en matematisk model"

af: Jesper Voetmann, Karen Birkelund, Mette Olufsen, Ole Møller Nielsen

Vejledere: Johnny Ottesen, H.B.Hansen

231B/92 "Elektrondiffusion i silicium - en matematisk model" Kildetekster

af: Jesper Voetmann, Karen Birkelund, Mette Olufsen, Ole Møller Nielsen

Vejledere: Johnny Ottesen, H.B.Hansen

232/92 "Undersøgelse om den simultane opdagelse af energiens bevarelse og især deles om de af Mayer, Colding, Joule og Helmholtz udførte arbejder"

af: L.Arleth, G.I.Dybkjær, M.T.Østergård

Vejleder: Dorthe Posselt

233/92 "The effect of age-dependent host mortality on the dynamics of an endemic disease and
Instability in an SIR-model with age-dependent susceptibility

by: Viggo Andreasen

234/92 "THE FUNCTIONAL DETERMINANT OF A FOUR-DIMENSIONAL BOUNDARY VALUE PROBLEM"

by: Thomas P. Branson and Peter B. Gilkey

235/92 OVERFLADESTRUKTUR OG POREUDVIKLING AF KOKS

- Modul 3 fysik projekt -

af: Thomas Jessen

236a/93 INTRODUKTION TIL KVANTE HALL EFFEKTEN

af: Anja Boisen, Peter Bøggild

Vejleder: Peder Voetmann Christiansen
Erland Brun Hansen

236b/93 STRØMSSAMMENBRUD AF KVANTE HALL EFFEKTEN

af: Anja Boisen, Peter Bøggild

Vejleder: Peder Voetmann Christiansen
Erland Brun Hansen

237/93 The Wedderburn principal theorem and Shukla cohomology

af: Lars Kadison

238/93 SEMIOTIK OG SYSTEMEGENSKABER (2)

Vektorbånd og tensorer

af: Peder Voetmann Christiansen

239/93 Valgsystemer - Modelbygning og analyse

Matematik 2. modul

af: Charlotte Gjerrild, Jane Hansen, Maria Hermannsson, Allan Jørgensen, Ragna Clauson-Kaas, Poul Lützen

Vejleder: Mogens Niss

240/93 Patologiske eksempler.
Om sære matematiske fisks betydning for den matematiske udvikling

af: Claus Dræby, Jørn Skov Hansen, Runa Ulsøe Johansen, Peter Meibom, Johannes Kristoffer Nielsen

Vejleder: Mogens Niss

241/93 FOTOVOLTAISK STATUSNOTAT 1

af: Bent Sørensen

242/93 Brovedligeholdelse - bevar mig vel

Analyse af Vejdirektoratets model for optimering af broreparationer

af: Linda Kyndlev, Kare Fundal, Kamma Tulinius, Ivar Zeck

Vejleder: Jesper Larsen

243/93 TANKEEKSPERIMENTER I FYSIKKEN

Et 1.modul fysikprojekt

af: Karen Birkelund, Stine Sofia Korremann

Vejleder: Dorthe Posselt

244/93 RADONTRANSFORMATIONEN og dens anvendelse i CT-scanning

Projektrapport

af: Trine Andreasen, Tine Guldager Christiansen, Nina Skov Hansen og Christine Iversen

Vejledere: Gestur Olafsson og Jesper Larsen

245a+b /93 Time-Of-Flight målinger på krystallinske halvledere
Specialerapport

af: Linda Szkotak Jensen og Lise Odgaard Gade

Vejledere: Petr Viscor og Niels Boye Olsen

246/93 HVERDAGSVIDEN OG MATEMATIK - LÆREPROCESSER I SKOLEN

af: Lena Lindenskov, Statens Humanistiske Forskningsråd, RUC, IMFUFA

247/93 UNIVERSAL LOW TEMPERATURE AC CONDUCTIVITY OF MACROSCOPICALLY DISORDERED NON-METALS

by: Jeppe C. Dyre

248/93 DIRAC OPERATORS AND MANIFOLDS WITH BOUNDARY

by: B. Booss-Bavnbek, K.P.Wojciechowski

249/93 Perspectives on Teichmüller and the Jahresbericht Addendum to Schappacher, Scholz, et al.

by: B. Booss-Bavnbek

With comments by W.Abikoff, L.Ahlfors, J.Cerf, P.J.Davis, W.Fuchs, F.P.Gardiner, J.Jost, J.-P.Kahane, R.Lohan, L.Lorch, J.Radkau and T.Söderqvist

250/93 EULER OG BOLZANO - MATEMATISK ANALYSE SET I ET VIDENSKABSTEORETISK PERSPEKTIV

Projektrapport af: Anja Juul, Lone Michelsen, Tomas Højgård Jensen

Vejleder: Stig Andur Pedersen

251/93 Genotypic Proportions in Hybrid Zones

by: Freddy Bugge Christiansen, Viggo Andreasen and Ebbe Thue Poulsen

252/93 MODELLERING AF TILFÆLDIGE FÆNOMENER

Projektrapport af: Birthe Friis, Lisbeth Helmgaard, Kristina Charlotte Jakobsen, Marina Mosbæk Johannessen, Lotte Ludvigsen, Mette Hass Nielsen

253/93 Kuglepakning

Teori og model

af: Lise Arleth, Kåre Fundal, Nils Kruse

Vejleder: Mogens Niss

254/93 Regressionsanalyse

Materiale til et statistikkursus

af: Jørgen Larsen

255/93 TID & BETINGET UAFHÆNGIGHED

af: Peter Harremoës

256/93 Determination of the Frequency Dependent Bulk Modulus of Liquids Using a Piezoelectric Spherical Shell (Preprint)

by: T. Christensen and N.B.Olsen

257/93 Modellering af dispersion i piezoelektriske keramikker

af: Pernille Postgaard, Jannik Rasmussen, Christina Specht, Mikko Østergård

Vejleder: Tage Christensen

258/93 Supplerende kursusmateriale til "Lineære strukturer fra algebra og analyse"

af: Mogens Brun Heefelt

259/93 STUDIES OF AC HOPPING CONDUCTION AT LOW TEMPERATURES

by: Jeppe C. Dyre

260/93 PARTITIONED MANIFOLDS AND INVARIANTS IN DIMENSIONS 2, 3, AND 4

by: B. Booss-Bavnbek, K.P.Wojciechowski

261/93 OPGAVESAMLING
Bredde-kursus i Fysik
Eksamensopgaver fra 1976-93

262/93 Separability and the Jones Polynomial
by: Lars Kadison

263/93 Supplerende kursusmateriale til "Lineære strukturer fra algebra og analyse" II
af: Mogens Brun Heefelt

264/93 FOTOVOLTAISK STATUSNOTAT 2
af: Bent Sørensen

265/94 SPHERICAL FUNCTIONS ON ORDERED SYMMETRIC SPACES
To Sigurdur Helgason on his sixtyfifth birthday
by: Jacques Faraut, Joachim Hilgert and Gestur Olafsson

266/94 Kommensurabilitets-oscillationer i laterale supergitre
Fysikspeciale af: Anja Boisen, Peter Bøggild, Karen Birkelund
Vejledere: Rafael Taboryski, Poul Erik Lindelof, Peder Voetmann Christiansen

267/94 Kom til kort med matematik på Eksperimentarium - Et forslag til en opstilling
af: Charlotte Gjerrild, Jane Hansen
Vejleder: Bernhelm Booss-Bavnbek

268/94 Life is like a sewer ...
Et projekt om modellering af aorta via en model for strømning i kloakrør
af: Anders Marcussen, Anne C. Nilsson, Lone Michelsen, Per M. Hansen
Vejleder: Jesper Larsen

269/94 Dimensionsanalyse en introduktion
metaprojekt, fysik
af: Tine Guldager Christiansen, Ken Andersen, Nikolaj Hermann, Jannik Rasmussen
Vejleder: Jens Højgaard Jensen

270/94 THE IMAGE OF THE ENVELOPING ALGEBRA AND IRREDUCIBILITY OF INDUCED REPRESENTATIONS OF EXPONENTIAL LIE GROUPS
by: Jacob Jacobsen

271/94 Matematikken i Fysikken.
Opdaget eller opfundet
NAT-BAS-projekt
vejleder: Jens Højgaard Jensen

272/94 Tradition og fornyelse
Det praktiske elevarbejde i gymnasiets fysikundervisning, 1907-1988
af: Kristian Hoppe og Jeppe Guldager
Vejledning: Karin Beyer og Nils Hybel

273/94 Model for kort- og mellemdistanceløb
Verifikation af model
af: Lise Fabricius Christensen, Helle Pilemann, Bettina Sørensen
Vejleder: Mette Olufsen

274/94 MODEL 10 - en matematisk model af intravenøse anæstetikas farmakokinetik
3. modul matematik, forår 1994
af: Trine Andreasen, Bjørn Christensen, Christine Green, Anja Skjoldborg Hansen. Lisbeth Helmgaard
Vejledere: Viggo Andreasen & Jesper Larsen

275/94 Perspectives on Teichmüller and the Jahresbericht
2nd Edition
by: Bernhelm Booss-Bavnbek

276/94 Dispersionsmodellering
Projektrapport 1. modul
af: Gitte Andersen, Rehannah Borup, Lisbeth Friis, Per Gregersen, Kristina Vejrø
Vejleder: Bernhelm Booss-Bavnbek

277/94 PROJEKTARBEJDSPÆDAGOGIK - Om tre tolkninger af problemorienteret projektarbejde
af: Claus Flensted Behrens, Frederik Voetmann Christiansen, Jørn Skov Hansen, Thomas Thingstrup
Vejleder: Jens Højgaard Jensen

278/94 The Models Underlying the Anaesthesia Simulator Sophus
by: Mette Olufsen(Math-Tech), Finn Nielsen (RISØ National Laboratory), Per Føge Jensen (Herlev University Hospital), Stig Andur Pedersen (Roskilde University)

279/94 Description of a method of measuring the shear modulus of supercooled liquids and a comparison of their thermal and mechanical response functions.
af: Tage Christensen

280/94 A Course in Projective Geometry
by Lars Kadison and Matthias T. Kromann

281/94 Modellering af Det Cardiovaskulære System med Neural Pulskontrol
Projektrapport udarbejdet af:
Stefan Frello, Runa Ulsøe Johansen, Michael Poul Curt Hansen, Klaus Dahl Jensen
Vejleder: Viggo Andreasen

282/94 Parallelle algoritmer
af: Erwin Dan Nielsen, Jan Danielsen, Niels Bo Johansen

283/94 Grænser for tilfældighed
(en kaotisk talgenerator)

af: Erwin Dan Nielsen og Niels Bo Johansen

284/94 Det er ikke til at se det, hvis man ikke lige ve' det!
Gymnasiematematikkens begrundelsesproblem

En specialerapport af Peter Hauge Jensen
og Linda Kyndlev

Vejleder: Mogens Niss

285/94 Slow coevolution of a viral pathogen and its diploid host

by: Viggo Andreasen and
Freddy B. Christiansen

286/94 The energy master equation: A low-temperature approximation to Bässler's random walk model

by: Jeppe C. Dyre

287/94 A Statistical Mechanical Approximation for the Calculation of Time Auto-Correlation Functions

by: Jeppe C. Dyre

288/95 PROGRESS IN WIND ENERGY UTILIZATION

by: Bent Sørensen

289/95 Universal Time-Dependence of the Mean-Square Displacement in Extremely Rugged Energy Landscapes with Equal Minima

by: Jeppe C. Dyre and Jacob Jacobsen

290/95 Modellering af uregelmæssige bølger
Et 3.modul matematik projekt

af: Anders Marcussen, Anne Charlotte Nilsson, Lone Michelsen, Per Mørkegaard Hansen

Vejleder: Jesper Larsen

291/95 1st Annual Report from the project
LIFE-CYCLE ANALYSIS OF THE TOTAL DANISH ENERGY SYSTEM
an example of using methods developed for the OECD/IEA and the US/EU fuel cycle externality study

by: Bent Sørensen

292/95 Fotovoltaisk Statusnotat 3

af: Bent Sørensen

293/95 Geometridiskussionen - hvor blev den af?

af: Lotte Ludvigsen & Jens Frandsen

Vejleder: Anders Madsen

294/95 Universets udvidelse -
et metaprojekt

Af: Jesper Duelund og Birthe Friis

Vejleder: Ib Lundgaard Rasmussen

295/95 A Review of Mathematical Modeling of the Controled Cardiovascular System

By: Johnny T. Ottesen

296/95 RETIKULER den klassiske mekanik

af: Peder Voetmann Christiansen

297/95 A fluid-dynamical model of the aorta with bifurcations

by: Mette Olufsen and Johnny Ottesen

298/95 Mordet på Schrödingers kat - et metaprojekt om to fortolkninger af kvantemekanikken

af: Maria Hermannsson, Sebastian Horst,
Christina Specht

Vejledere: Jeppe Dyre og Peder Voetmann Christiansen

299/95 ADAM under figenbladet - et kig på en samfundsvidenskabelig matematisk model

Et matematisk modelprojekt

af: Claus Dræby, Michael Hansen, Tomas Højgård Jensen

Vejleder: Jørgen Larsen

300/95 Scenarios for Greenhouse Warming Mitigation

by: Bent Sørensen

301/95 TOK Modellering af træers vækst under påvirkning af ozon

af: Glenn Møller-Holst, Marina Johannessen, Birthe Nielsen og Bettina Sørensen

Vejleder: Jesper Larsen

302/95 KOMPRESSORER - Analyse af en matematisk model for aksialkompressorer

Projektrapport af: Stine Bøggild, Jakob Hilmer, Pernille Postgaard

Vejleder: Viggo Andreasen

303/95 Masterlignings-modeller af Glasovergangen
Termisk-Mekanisk Relaksation
Specialerapport udarbejdet af:

Johannes K. Nielsen, Klaus Dahl Jensen

Vejledere: Jeppe C. Dyre, Jørgen Larsen

304a/95 STATISTIKNOTER Simple binomialfordelingsmodeller
af: Jørgen Larsen

304b/95 STATISTIKNOTER Simple normalfordelingsmodeller
af: Jørgen Larsen

304c/95 STATISTIKNOTER Simple Poissonfordelingsmodeller
af: Jørgen Larsen

304d/95 STATISTIKNOTER Simple multinomialfordelingsmodeller
af: Jørgen Larsen

304e/95 STATISTIKNOTER Mindre matematisk-statistisk opslagsværk indeholdende bl.a. ordforklaringer, resuméer og tabeller
af: Jørgen Larsen

305/95 The Maslov Index:
A Functional Analytical Definition
And The Spectral Flow Formula

By: B. Booss-Bavnbek, K. Furutani

306/95 Goals of mathematics teaching

Preprint of a chapter for the forth-comming International Handbook of Mathematics Education (Alan J.Bishop, ed)

By: Mogens Niss

307/95 Habit Formation and the Thirdness of Signs

Presented at the semiotic symposium

The Emergence of Codes and Intensions as a Basis of Sign Processes

By: Peder Voetmann Christiansen

308/95 Metaforer i Fysikken

af: Marianne Wilcken Bjerregaard, Frederik Voetmann Christiansen, Jørn Skov Hansen, Klaus Dahl Jensen Ole Schmidt

Vejledere: Peder Voetmann Christiansen og Petr Viscor

309/95 Tiden og Tanken
En undersøgelse af begrebsverdenen Matematik udført ved hjælp af en analogi med tid

af: Anita Stark og Randi Petersen

Vejleder: Bernhelm Booss-Bavnbek

310/96 Kursusmateriale til "Lineære strukturer fra algebra og analyse" (E1)

af: Mogens Brun Heefelt

311/96 2nd Annual Report from the project
LIFE-CYCLE ANALYSIS OF THE TOTAL DANISH ENERGY SYSTEM

by: Hélène Connor-Lajambe, Bernd Kuemmel, Stefan Krüger Nielsen, Bent Sørensen

312/96 Grassmannian and Chiral Anomaly

by: B. Booss-Bavnbek, K.P.Wojciechowski

313/96 THE IRREDUCIBILITY OF CHANCE AND
THE OPENNESS OF THE FUTURE
The Logical Function of Idealism in Peirce's Philosophy of Nature

By: Helmut Pape, University of Hannover

314/96 Feedback Regulation of Mammalian Cardiovascular System

By: Johnny T. Ottesen

315/96 a + b "Rejsen til tidens indre" - Udarbejdelse af et manuskript til en fjernsynsudsendelse
+ manuskript

af: Gunhild Hune og Karina Goyle

Vejledere: Peder Voetmann Christiansen og Bruno Ingemann

316/96 Plasmaoscillation i natriumklynger

Specialerapport af: Peter Meibom, Mikko Østergård

Vejledere: Jeppe Dyre & Jørn Borggreen

317/96 Poincaré og symplektiske algoritmer

af: Ulla Rasmussen

Vejleder: Anders Madsen

318/96 Modelling the Respiratory System

by: Tine Guldager Christiansen, Claus Dræby

Supervisors: Viggo Andreasen, Michael Danielsen

319/96 Externality Estimation of Greenhouse Warming Impacts

by: Bent Sørensen

320/96 Grassmannian and Boundary Contribution to the -Determinant

by: K.P.Wojciechowski et al.

321/96 Modelkompetencer - udvikling og afprøvning af et begrebsapparat

Specialerapport af: Nina Skov Hansen, Christine Iversen, Kristin Troels-Smith

Vejleder: Morten Blomhøj

322/96 OPGAVESAMLING

Bredde-Kursus i Fysik 1976 - 1996

323/96 Structure and Dynamics of Symmetric Diblock Copolymers

PhD Thesis

by: Christine Maria Papadakis

324/96 Non-linearity of Baroreceptor Nerves

by: Johnny T. Ottesen

325/96 Retorik eller realitet ?

Anvendelser af matematik i det danske Gymnasiums matematikundervisning i perioden 1903 - 88

Specialerapport af Helle Pilemann

Vejleder: Mogens Niss

326/96 Bevisteori
Eksemplificeret ved Gentzens bevis for konsistensen af teorien om de naturlige tal

af: Gitte Andersen, Lise Mariane Jeppesen, Klaus Frovin Jørgensen, Ivar Peter Zeck

Vejledere: Bernhelm Booss-Bavnbek og Stig Andur Pedersen

327/96 NON-LINEAR MODELLING OF INTEGRATED ENERGY SUPPLY AND DEMAND MATCHING SYSTEMS

by: Bent Sørensen

328/96 Calculating Fuel Transport Emissions

by: Bernd Kuemmel

329/96 The dynamics of cocirculating influenza strains conferring partial cross-immunity
and
A model of influenza A drift evolution
by: Viggo Andreasen, Juan Lin and Simon Levin

330/96 LONG-TERM INTEGRATION OF PHOTOVOLTAICS INTO THE GLOBAL ENERGY SYSTEM
by: Bent Sørensen

331/96 Viskøse fingre
Specialerapport af:
Vibeke Orlien og Christina Specht
Vejledere: Jacob M. Jacobsen og Jesper Larsen

332/97 ANOMAL SWELLING AF LIPIDE DOBBELTLAG
Specialerapport af:
Stine Sofia Korremann
Vejleder: Dorthe Posselt

333/97 Biodiversity Matters
an extension of methods found in the literature on monetisation of biodiversity
by: Bernd Kuemmel

334/97 LIFE-CYCLE ANALYSIS OF THE TOTAL DANISH ENERGY SYSTEM
by: Bernd Kuemmel and Bent Sørensen

335/97 Dynamics of Amorphous Solids and Viscous Liquids
by: Jeppe C. Dyre

336/97 PROBLEM-ORIENTATED GROUP PROJECT WORK AT ROSKILDE UNIVERSITY
by: Kathrine Legge

337/97 Verdensbankens globale befolkningsprognose - et projekt om matematisk modellering
af: Jørn Chr. Bendtsen, Kurt Jensen, Per Pauli Petersen
Vejleder: Jørgen Larsen

338/97 Kvantisering af nanolederes elektriske ledningsevne
Første modul fysikprojekt
af: Søren Dam, Esben Danielsen, Martin Niss, Esben Friis Pedersen, Frederik Resen Steenstrup
Vejleder: Tage Christensen

339/97 Defining Discipline
by: Wolfgang Coy

340/97 Prime ends revisited - a geometric point of view -
by: Carsten Lunde Petersen

341/97 Two chapters on the teaching, learning and assessment of geometry
by Mogens Niss

342/97 LONG-TERM SCENARIOS FOR GLOBAL ENERGY DEMAND AND SUPPLY
A global clean fossil scenario discussion paper
prepared by Bernd Kuemmel
Project leader: Bent Sørensen

343/97 IMPORT/EKSPORT-POLITIK SOM REDSKAB TIL OPTIMERET UDNYTTELSE AF EL PRODUCERET PÅ VE-ANLÆG
af: Peter Meibom, Torben Svendsen, Bent Sørensen

344/97 Puzzles and Siegel disks
by Carsten Lunde Petersen

345/98 Modeling the Arterial System with Reference to an Anestesia Simulator
Ph.D. Thesis
by: Mette Sofie Olufsen

346/98 Klyngedannelse i en hulkatode-forstøvningsproces
af: Sebastian Horst
Vejledere: Jørn Borggren, NBI, Niels Boye Olsen

347/98 Verificering af Matematiske Modeller - en analyse af Den Danske Eulerske Model
af: Jonas Blomqvist, Tom Pedersen, Karen Timmermann, Lisbet Øhlenschlæger
Vejleder: Bernhelm Booss-Bavnbek

348/98 Case study of the environmental permission procedure and the environmental impact assessment for power plants in Denmark
by: Stefan Krüger Nielsen
Project leader: Bent Sørensen

349/98 Tre rapporter fra FAGMAT - et projekt om tal og faglig matematik i arbejdsmarkedsuddannelserne
af: Lena Lindenskov og Tine Wedege

350/98 OPGAVESAMLING - Bredde-Kursus i Fysik 1976 - 1998
Erstatter teksterne 3/78, 261/93 og 322/96

351/98 Aspects of the Nature and State of Research in Mathematics Education
by: Mogens Niss

352/98 The Herman-Swiatec Theorem with applications

by: Carsten Lunde Petersen

353/98 Problemløsning og modellering i en almendannende matematikundervisning

Specialerapport af: Per Gregersen og Tomas Højgaard Jensen

Vejleder: Morten Blomhøj

354/98 A GLOBAL RENEWABLE ENERGY SCENARIO

by: Bent Sørensen and Peter Meibom

355/98 Convergence of rational rays in parameter spaces

by: Carsten Lunde Petersen and Gustav Ryd

356/98 Terrænmodellering

Analyse af en matematisk model til konstruktion af terrænmodeller

Modelprojekt af: Thomas Frommelt, Hans Ravnkjær Larsen og Arnold Skimminge

Vejleder: Johnny Ottesen

357/98 Cayleys Problem

En historisk analyse af arbejdet med Cayley problem fra 1870 til 1918

Et matematisk videnskabsfagsprojekt af:

Rikke Degn, Bo Jakobsen, Bjarke K.W. Hansen, Jesper S. Hansen, Jesper Udesen, Peter C. Wulff

Vejleder: Jesper Larsen